# A THREE-DIMENSIONAL TWO-PHASE FIELD SCALE STREAMLINE SIMULATOR

A DISSERTATION
SUBMITTED TO THE DEPARTMENT OF PETROLEUM ENGINEERING
AND THE COMMITTEE ON GRADUATE STUDIES
OF STANFORD UNIVERSITY
IN PARTIAL FULFILLMENT OF THE REQUIREMENTS
FOR THE DEGREE OF
DOCTOR OF PHILOSOPHY

By
Roderick Panko Batycky
January 1997

*To wifey...*

*...hubby.*

I certify that I have read this thesis and that in my opinion it is fully adequate, in scope and in quality, as a dissertation for the degree of Doctor of Philosophy.

Dr. Martin J. Blunt (Principal Adviser)

I certify that I have read this thesis and that in my opinion it is fully adequate, in scope and in quality, as a dissertation for the degree of Doctor of Philosophy.

Dr. Franklin M. Orr Jr. (co-Adviser)

I certify that I have read this thesis and that in my opinion it is fully adequate, in scope and in quality, as a dissertation for the degree of Doctor of Philosophy.

Dr. Khalid Aziz

I certify that I have read this thesis and that in my opinion it is fully adequate, in scope and in quality, as a dissertation for the degree of Doctor of Philosophy.

Dr. Thomas A. Hewett

Approved for the University Committee on Graduate Studies:

# Abstract

This thesis presents the development and application of a three-dimensional, two-phase streamline simulator applied to field scale multiwell problems. The underlying idea of the streamline method is to decouple the full 3D problem into multiple 1D problems along streamlines. Fluids are moved along the natural streamline grid, rather than between discrete gridblocks as in conventional methods. Permeability effects and well conditions dictate the paths that the streamlines take in 3D, while the physics of the displacement is captured by the 1D solutions mapped along streamlines. In this work, the 1D solutions either represent tracer flow, waterflood displacements, or first-contact miscible displacements. Solutions for these mechanisms are obtained either analytically or numerically. If analytical solutions are mapped to streamlines, the final 3D results are free from numerical diffusion, but the method can only be applied to limited situations. By mapping numerical solutions to streamlines the method has been extended to changing well conditions, nonuniform initial saturations, and multiphase gravity effects.

The streamline simulator has been applied to field scale infill drilling and well conversion problems. For a 100,000 gridblock problem, the streamline simulator was over 100 times faster than an industry standard simulator. For simple 2D miscible displacements dominated by gravity, the streamline method was almost 1000 times faster than conventional methods. The speed of the streamline method also makes it well suited to the solution of large problems. Examples of $10^6$ gridblock multiwell problems are solved on a conventional workstation and require about 2 CPU days.

The large speedup factors in the streamline method are a result of decoupling fluid transport from the underlying grid. Instead fluids are moved along the natural

streamline paths. Moving fluids between gridblocks in conventional finite-difference models results in grid orientation effects and more importantly, time step limitations due to stability and/or convergence considerations. Transporting fluids along streamlines eliminates stability issues and the method is stable for any size time step. For the same displacement, the streamline simulator requires on average one to three orders of magnitude fewer time steps than a conventional finite-difference simulator.

# Acknowledgments

I feel extremely privileged to have had the opportunity to pursue a PhD at Stanford, as well as be involved in such an exciting research topic. I am deeply indebted to Martin Blunt and Marco Thiele for all of their guidance and useful discussions. Martin and Marco both played a large role in shaping this research into what you see now.

I would also like to acknowledge Lynn Orr for his support of this work, as well as the support of the SUPRIC affiliates research group. I thank the remainder of my reading committee, Khalid Aziz, Tom Hewett, and Dave Freyberg, for their many useful comments, as well as GeoQuest for providing ECLIPSE.

Finally I would like to thank my friends, my family, mom and dad, Kathryn, Rick, Andrena, and Anya, for all their friendship and encouragement. Lastly, I say "thank you" to my wife Melanie for all of the sacrifices she has made for us while I have been at Stanford.

# Contents

# List of Tables

# List of Figures

# Chapter 1

# Introduction

The main goal of any reservoir simulation method is to predict flow performance of oil recovery processes. The more realistic the reservoir model and the reservoir simulator are, the more accurate is the answer produced.

Many advancements have been made in geostatistical methods and their ability to construct realistic reservoir images. Models on the order $10^6$ to $10^7$ gridblocks are routinely generated. It is also well known that deterministic information about subsurface properties is limited, therefore present day reservoir engineers and geologists prefer a stochastic description of the reservoir. In other words, many images of the reservoir that honor hard well data can be routinely generated, each model containing millions of gridblocks.

The ability to solve large models in reservoir simulators has not kept pace with the advances in geostatistical methods. One solution to simulator improvement is based on computer hardware advances. For example, large problems are solved by domain decomposition methods on parallel machines. The size of the problem and the speed of the simulator is directly related to the number of processors and their speed. A second approach is to improve the efficiency of the simulation method itself. This is the goal of the streamline method discussed here. With some assumptions, the streamline method efficiently uses standard computer resources to model field scale displacements of large models both faster and more accurately than conventional methods.

The underlying idea of the streamline method is to decouple the governing equation of fluid motion to the full 3D problem into multiple 1D problems solved along streamlines. The solution to the pressure field dictates the paths of the streamlines in space while the physics of the displacement is captured in an appropriate 1D solution solved along each streamline. In this manner, fluids are moved along the natural streamline grid rather than between discrete gridblocks, as in conventional methods. The advantage of the streamline technique is that the stability constraint of the underlying grid is effectively decoupled from the solutions solved along streamlines. Thus, very large convective time steps can be taken with the streamline method. Furthermore, for heterogeneous systems the pressure field is a weak function of fluid properties. This implies that the pressure solution only needs to be updated a few times throughout a displacement process to accurately capture the nonlinearity in the pressure field. The ability to take large convective time steps and only update the streamline paths periodically are the primary reasons that the streamline method is orders of magnitude faster than conventional methods. Because of grid constraints, conventional methods take very small time steps resulting in recalculating the pressure field and saturation field many times – a numerically expensive process.

## 1.1 Field Scale Displacements

The application of the streamline method is presented in the context of modeling field scale displacements. The variables that influence field recovery performance, and how the streamline method can best capture these influences, are considered. Many authors have shown that correlated heterogeneity has a first-order effect on displacement predictions – see for instance [35, 42, 77]. Any simulation method that models field scale displacements must capture heterogeneity in as much detail as possible. The streamline method is well suited to honoring heterogeneity effects. However, in comparison with conventional simulation techniques, the streamline method sacrifices the ability to capture secondary displacement effects like capillary cross-flow or transverse diffusion, for an improved characterization of heterogeneity and its impact on flow.

Gravity effects can also dominate at the field scale. For example, many fields

are produced in a manner to take advantage of gravity forces to improve on field displacement efficiency. For all but the simplest displacements, gravity effects are difficult to account for with streamline methods since the gravity vector is seldom aligned with a streamline path. Gravity effects in the streamline method are modeled using an operator splitting technique, which corrects fluid positions in the vertical direction after they have been moved convectively along streamlines. Conceivably, any other mechanism that is deemed important at the field scale could be accounted for in a similar operator splitting manner and viewed as a corrective step. This work assumes that only well conditions, heterogeneity, gravity and fluid mobilities are the main forces dictating a displacement.

## 1.2 Analytical Solutions Along Streamlines

Along each streamline in 3D space, a governing 1D solution to the conservation equation exists. The solution to this equation can be obtained analytically under certain conditions. The main requirement for an analytical solution is uniform initial conditions along a streamline path. Strictly speaking, uniform initial conditions along streamlines only exist for fixed streamline paths that do not change with time. A key idea of the streamline method presented here is that streamline paths are updated to honor the changing mobility field. *Thiele et al.* [69] [70] [71] have shown that for displacements dominated by heterogeneity (and fixed well conditions), uniform initial conditions along recalculated streamline paths can be assumed without loss of solution accuracy.[1]

Permeability has a first order effect on simulation results, implying that greater resolution in permeability is desirable. Furthermore, permeability models are stochastic making it equally important to evaluate the equiprobable images of a reservoir model to predict uncertainty in a simulation forecast. Conventional simulation methods will sacrifice reservoir detail and processing of multiple reservoir images for improved speed. The result is a single forecast which is typically optimistic due to the

[1] See Chapter 2 for a detailed literature review of streamline and streamtube methods.

lack of heterogeneity detail. The streamline method however, is ideally suited to capturing the first order effects in flow simulations. As will be shown, large models can be run very quickly, making the streamline method a useful tool to process multiple realizations quickly.

Chapter 4 investigates the application of the streamline method to multiwell 3D displacements. Tracer, waterflood, and first-contact miscible (FCM) analytical solutions are mapped along the streamlines. All models are assumed to be heterogeneity dominated. Recalculating the streamline paths to honor the changing mobility field yields excellent agreement with conventional finite-difference methods, but results are generated in a fraction of the time.

## 1.3 Numerical Solutions Along Streamlines

The goal of this work is to predict field scale reservoir simulations using streamline methods. Most reservoir displacements are affected by gravity, and have well management schemes that include infill drilling and producer-injector conversions. When streamline paths are updated as a displacement proceeds, nonuniform fluid saturations exist along the recalculated streamline paths. Analytical solutions are not available for general nonuniform initial conditions. As a result, the method of Chapter 4 cannot account for gravity or changing well conditions. However, there is no restriction to the method of solution of the 1D equations mapped along streamlines.

Chapters 5 and 6 investigate the extension of the streamline method to mapping numerical solutions along streamline paths. The method is general and can be applied to homogeneous as well as heterogeneity dominated displacements. A key feature when mapping numerical solutions is that streamlines now communicate with each other at a gridblock scale. This is a result of only knowing saturation information to within a gridblock scale. Thus the numerical solutions do contain some mixing. However, the mixing in the streamline method is less than that present in conventional simulators caused by numerical diffusion.

## 1.4 Concluding Remarks

The streamline method developed in this work has been implemented in a Fortran 90 code called 3DSL (3-Dimensional StreamLines). The focus of this work is accurate modeling of field scale flow through porous media. As such, 3DSL only has simple well models, and no facility constraints. Even with these limitations, 3DSL is still a very powerful tool for modeling flow under a variety of displacement mechanisms.

# Chapter 2

# Literature Review

There are numerous examples of the use of streamlines and streamtubes to model flow in porous media, both in the petroleum and the groundwater literatures. General references include *Muskat* [57] and *Bear* [8]. Additionally, *Thiele* [68] provides a detailed literature review of streamtube methods.

A review of streamtube and streamline methods is given in the following sections. As streamtubes and streamlines are very similar, there is some overlap among the sections. Also included is a brief review of front tracking methods, which are evolving to be similar to the streamline method presented in this work. Finally, a section reviewing the impacts of reservoir heterogeneity on flow simulations is also included.

## 2.1 Streamtube Methods

*Muskat* [57] in 1937 gave an early description of the governing analytical equations that define the stream function, $\Psi$, and the potential function, $\Phi$, in simple two-dimensional domains for incompressible flow. A notable work with these definitions was by *Fay & Pratts* [29] who in 1951 developed a numerical model to predict tracer and two-phase flow in a two-well homogeneous 2D system. *Fay & Pratts* recognized that the streamlines would shift positions for two fluid problems as a displacement proceeded. To account for this, they tracked the position of the intersection of the fluid front with the instantaneous streamlines (intersection given by $\bar{\Psi}$ lines). However,

they did admit that no simple numerical method was found to track the $\bar{\Psi}$ lines. Thus, their two-phase results contained some inaccuracies.

*Higgins & Leighton* [39, 40] introduced the idea of using streamtube bundles to model multiphase displacements in porous media. Each streamtube was treated as a one-dimensional system, along which *Buckley-Leverett* [16] solutions could be mapped. In their model, the streamtube bundles were fixed throughout the displacement life. Instead, to account for a changing mobility field, the resistance within each tube was updated as a displacement proceeded. Subsequent injection volumes into streamtubes were then based on tube resistances, such that tubes with high mobility fluid (low resistance) received proportionately more injection than tubes with low mobility fluid. They showed good agreement with experimental and numerical results for mobility ratios from 1 to 800.

*Martin et al.* [52] noted that the fixed streamtube method failed for a favorable mobility ratio $M$=0.1 and gave poor results for mobility ratios greater than 100. *Martin et al.* reached a different conclusion than *Higgins & Leighton* [40] because they used greater curvature in their relative permeability curves, which in turn reduced the velocity of the Buckley-Leverett shock. Thus, the change in mobility occurred over a shorter distance increasing, the nonlinearity of the displacement. For this situation, they showed that streamtube paths behind the injection bank are relatively constant but the streamtube paths ahead of the bank change considerably. By recalculating the streamtube paths periodically, the new method worked well for $M < 1$ and for $M > 100$. However, recalculating streamline paths introduces nonuniform initial conditions along new streamlines. To overcome this problem, *Martin et al.* used a numerical approach to move saturations along updated paths, as described next.

*Martin & Wegner* [51] extended their previous method to multiwell, two-phase problems.[1] They calculated the value of the stream function ($\Psi$) numerically on a two-dimensional discretized domain. The $\Psi$ function then defined streamtubes. *Martin & Wegner* updated the streamtubes to honor the changing mobility field and mapped the original saturations to the new streamtube locations. The original saturations were then moved forward in time based on knowledge of the local saturation velocity

[1] Multiwell problems refers to more than two wells.

and the total flow rate into the tube. Because the total flow rate at the new time step was not known until the new saturation profile was known, they would iterate the procedure until the calculated flow rate no longer changed. Their mapping technique worked well since saturation velocities along streamlines were ordered from slow to fast. The method would breakdown if fronts collided (i.e.: faster saturations upstream of slower saturations). *Martin & Wegner's* method was similar to *Higgins & Leighton's* in that flow rates in tubes changed as the mobility field changed.

The advantage of all the streamline/streamtube methods discussed so far was that they were faster and more accurate than equivalent conventional finite-difference simulations. However, the method was only applicable to 2D problems for simple displacement mechanisms.

*Lake et al.* [48] combined an areal streamtube model with a finite-difference simulator to simulate a large-scale surfactant/polymer flood. The physics of the polymer displacement and layer heterogeneity were incorporated into representative 2D cross-sectional finite-difference simulations. The resulting production profiles were then mapped to areal streamtube patterns giving a hybrid 2D+2D approach.

*Emmanuel et al.* [27] and *Mathews et al.* [54] recognized that detailed reservoir descriptions of heterogeneity improved the accuracy of forecasts. Conventional simulation methods could not adequately solve the large models built to satisfy the improved reservoir descriptions. Again, they used hybrid streamtube models for this purpose. The displacement physics in this case, WAG displacements, layer heterogeneity, and gravity override, were contained in an appropriate 2D numerical simulation. The resulting fractional flow curves from the simulations were then mapped along streamtubes calculated using the method of *Martin & Wagner*. Not only did they conclude that the hybrid model was faster than conventional methods, but they found that accounting for increased heterogeneity yielded a result that matched actual field performance without history matching or adjustment of data.

*Renard* [62] developed a 2D streamtube method that included periodic regeneration of the streamtubes to account for changing well positions and changing mobility fields. *Renard* used a stepwise process to trace the streamlines that would then define streamtubes, but noted that the stepwise process was inaccurate for sharply bending

streamlines near boundaries or source/sinks. Unfortunately, *Renard* does not say how the 1D solutions were moved forward in time along streamtubes.

*Thiele et al.* [69, 70, 71] used a streamtube method to model highly nonlinear displacements in 2D cross-sections.[2] To honor the changing mobility field, *Thiele et al.* proposed periodically recalculating streamtube paths. They abandoned the idea of calculating tube resistances (*Higgins & Leighton* method) because the method failed to properly model nonlinear displacements [68]. Thus, all streamtubes contained the same flow rate for a given time step. Instead, to honor the changing mobility field, the tube sizes would change. Analytical solutions were then mapped along recalculated paths. While they admit that periodic recalculation of paths was slower than the *Higgins & Leighton* procedure, the method accurately predicted breakthrough performance for highly nonlinear displacements. *Thiele et al.* used the method to study waterflooding, FCM, and compositional displacements. The major assumption of mapping analytical solutions to recalculated paths, was that flow was governed by heterogeneity such that the streamtube paths did not change greatly from time step to time step. Additionally, because streamtube paths remained relatively fixed, very large time steps could be taken yet still capture the displacement nonlinearities. The result was a streamtube method that accurately modeled heterogeneous FCM and compositional displacements with 3 to 5 orders-of-magnitude speed-up over conventional methods.

The obvious extension of the above streamtube models is to three-dimensional systems. The key leap from 2D to 3D systems is being able to define streamtubes in 3D. As early as 1957, *Yih* [80] presented a definition of the stream function for three-dimensional incompressible flow. The 3D stream function is defined by the intersection of two sets of orthogonal stream surfaces with four intersection points defining a 3D streamtube. *Nelson* [58] extended *Yih's* method to heterogeneous systems. Both works discuss the mathematical definition of 3D stream functions and do not specifically model flow displacements. The primary difficulty of 3D streamtubes is that they become complicated geometrical objects in 3D. *Zijl* [81] and *Matanga*

[2]Nonlinear displacements are characterized by a changing velocity field as a displacement proceeds.

[55, 53] have presented 3D streamtube methods applied to simple single phase heterogeneous displacements in groundwater flow. Recently, *Hewett & Yamada* [36] have presented the theory for a semi-analytical 3D streamtube method for multiphase flow that does not rely on the construction of a 3D streamfunction.

## 2.2 Streamline Methods

The majority of published work on streamlines has been in the groundwater literature. While the applications vary, this review will only concentrate on streamline results relevant to methods of accurately predicting streamline paths in 3D space, and methods to map conservation equations to the streamlines. As already discussed, *Fay & Pratts* presented an early work in the petroleum literature that uses streamlines in 2D.

All 3D streamline methods use particle tracking ideas to define a streamline. *Shafer* [64] traced particle from sinks to sources using a Runge-Kutta technique. By keeping track of the time to travel on each streamline, *Shafer* then determined capture zones for producers based on a desired isotime surface. Shafer's method was applied to 2D heterogeneous multiwell systems. *Pollock* [61] improved on the Runge-Kutta tracing by defining a piece-wise linear interpolation of the velocity field within a gridblock. The same method was developed by *Datta-Gupta & King* [24]. The result was an algorithm which analytically defined a streamline path within a gridblock. Other interpolation schemes for gridblock velocities also exist but they are not consistent with the governing flow equation [34].

To improve on the flow physics that a streamline method could account for, *Bommer & Schecter* [11] mapped general numerical conservation equations along streamlines. The numerical solution accounted for dispersion and reaction of components along the streamline direction, while the areal streamline paths accounted for well distributions. *Bommer & Schecter's* method was 2D and streamline tracing was performed using a simple step-wise method to move between gridblocks.

*Datta-Gupta & King* [24] introduced the "time-of-flight" concept along a streamline. This idea was used by *King et al.* [44] to model FCM displacements in 2D

heterogeneous cross-sections by scaling 1D *Todd-Longstaff* [73] FCM solutions along streamlines. Rather than updating streamline paths to account for the changing mobility field, streamlines were assigned boost factors based on the overall pressure drop along a streamline. This method correctly placed high mobility fluid into the least resistant streamlines. The main focus of their work was to evaluate reservoir heterogeneity on FCM displacements. The streamline method provided a tool $10^4$ times faster than conventional high-resolution methods that would capture heterogeneity effects without sacrificing flow physics. *Datta-Gupta & King* [24] also presented a streamline model for 2D heterogeneous areal displacements of two-well tracer and waterflood problems.

Recently, the streamline method has been extended to true 3D systems by *Blunt et al.* [10] and includes longitudinal and transverse diffusion and gravity effects in FCM displacements. *Thiele et al.* [69] also present 3D streamline results and extend the method to multiwell situations as well as accounting for the changing mobility fields in multiphase displacements. These latter ideas are described and expanded on in this work. Most recently, *Peddibhotla et al.* [60] presented a 3D multiwell fixed streamline technique.

## 2.3 Front Tracking Methods and Operator Splitting

Front tracking methods are applicable to flow in porous media since the basic mass conservation equation can be written in a hyperbolic form. Front tracking amounts to discretizing a rarefaction wave into a series of shocks (fronts) with each shock speed predicted by a Rankine-Hugoniot condition. The fronts are then moved along an underlying grid based on knowing the front speed and the underlying velocity profile. An integral part of front tracking in multiple dimensions is operator splitting, whereby fronts are moved independently in each grid coordinate direction. The final front position is then the sum of the multiple movements in each direction.

The above ideas were formally presented by *Glimm et al.* [32] and applied to a 2D

quarter five-spot problem for various mobility ratios and levels of heterogeneity. The method was very accurate and exhibited little numerical diffusion or grid orientation effects. It is worth noting that prior to *Glimm, Fay & Pratts* [30] and *Martin & Wegner* [51] used simplified one-dimensional front tracking methods (moving interface) along streamlines to perform recovery calculations. Their methods were simple since they could not account for colliding fronts that would occur when upstream front velocities were higher than downstream front velocities.

Front tracking methods with gravity were presented by *Glimm et al.* [33] and *Colella et al.* [22] applied to 2D problems. Gravity was accounted for by operator splitting in the vertical direction. *Kocberber & Miller* [46] presented a novel front tracking method for three-dimensional systems that tracked fronts along grid element boundaries. The element boundaries were defined areally based on streamlines and equipotential lines and vertically based on a simple layered system. Periodically the elements would be regenerated as the fronts moved positions. Their method was applied to 2D vertical gravity displacements and areal two-well displacements, and showed minimal dispersion. *Bratvedt et al.* [12, 13] presented a similar front tracking method as that of *Glimm et al.* [33], but extended the method to full 3D systems with multiple wells. Their ideas were implemented in the commercial code `FRONTSIM`, and noted that their code was more CPU efficient and suffered from less diffusion and grid orientation effects than conventional methods.

*Bratvedt et al.* [13] also discuss a front tracking method along streamlines applied to 2D areal domains. Tracking fronts along streamlines resulted in less grid orientation effects than standard front tracking methods along grid coordinates. *Tijink et al.* [72] used the same streamline front tracking method to study areal problems of contaminant migration. Most recently, *Bratvedt et al.* [14] have presented 2D cross-sectional waterflood results of a streamline front tracking method that accounts for gravity. Gravity effects are accounted for by operator splitting such that fluids are moved convectively along streamlines then vertically due to gravity effects. This is the same method that is used in this work.

## 2.4 Streamline Methods and Heterogeneity

Heterogeneity strongly influences reservoir recovery. Because of speed, streamline/ streamtube models are ideally suited to studying heterogeneity effects.

*Hewett & Behrens* [37] used a streamtube simulator to evaluate the effect of fractal heterogeneity descriptions on flow simulations. They noted that flow results from fractal realizations showed greater channeling, earlier breakthrough, and reduced recovery than results with less heterogeneous permeability distributions. Because of the uncertainty associated with the fine scale heterogeneities, *Hewett & Behrens* additionally used the streamtube model to predict the uncertainty in recovery. The speed of the streamtube simulator allowed them to study multiple realizations of detailed models quickly.

The use of hybrid streamtube models as discussed by *Emanuel et al.* [27] and *Mathews et al.* [54] assumed that the collapsed 2D cross-sectional models mapped along streamtubes scaled linearly with displacement distance traveled. For 2D miscible and immiscible displacements *Hewett & Behrens* [35, 38] noted that linear scaling behavior did occur when flow was dominated by correlated heterogeneity. Thus the hybrid method properly modeled heterogeneity dominated flow. A related conclusion was that physical dispersion was flow length dependent (convection-dominated dispersion due to heterogeneity) and could not be accounted for by an effective dispersion coefficient within a 1D profile.

*Datta-Gupta et al.* [25] studied inverse modeling by using the 2D streamline model described by *Datta-Gupta & King* [24] to first generate type curves of tracer response for different heterogeneity indexes. The speed of the streamline model made it ideally suited to the multiple runs required to generate the type curves. Once type curves were obtained, a tracer profile could be mapped to the type curves in order to obtain heterogeneity parameters.

*Thiele et al.* [69] used the speed of the streamline method to screen multiple images under a variety of displacement mechanisms. An important conclusion was that the uncertainty due to multiple heterogeneous images was accurately captured by the streamline method in a fraction of the time required for even a single finite-difference

displacement result.

## 2.5 Concluding Remarks

Although streamline methods have been greatly extended in recent years, there are still limitations. To extend the streamline method to more general situations, a combination of novel ideas developed by several of the above authors is used. The streamline tracing method of *Pollock* [61] and *Datta-Gupta & King* [24] is used to trace analytical streamline paths in three-dimensions. After *Thiele* [68], the streamline paths are periodically recalculated to honor the changing mobility distribution. Analytical solutions are mapped to streamlines using *Thiele's* [68] approach. To generalize the streamline method to account for field situations, numerical solutions are mapped to streamlines as proposed by *Bommer & Schecter* [11]. Lastly, multiphase gravity effects are introduced in an operator splitting technique similar to that of front tracking methods [14, 33].

# Chapter 3

# Mathematical Model

## 3.1 Introduction

The streamline simulator involves two components; (i) tracing the streamline paths, and (ii) mapping 1D solutions along the streamlines. This chapter focuses on the steps required to trace the streamline paths in a 3D system for an arbitrary number of injection and production wells. Tracing streamlines requires a solution for the pressure field. Mapping of 1D solutions along streamlines, which results in determining phase distributions, is discussed in Chapters 4 and 5.

## 3.2 The Governing IMPES Equations

The streamline simulator is based on solving first for the pressure field and then for the saturation distribution. This is an IMplicit in Pressure, Explicit in Saturation method (IMPES). For conventional finite-difference methods, one advantage of an IMPES formulation over the fully-implicit formulation is that numerical diffusion due to discretization error is reduced. The trade-off is that smaller time step sizes must be taken due to stability considerations.

Here, the governing pressure and saturation equations for multiphase flow used in the streamline method are derived. The governing equation for flow of a component

$i$ with $n_p$ phases flowing in a porous medium is defined by *Lake* [49] as,

$$\sum_{j=1}^{n_p} \left\{ \frac{\partial}{\partial t}(\phi \omega_{ij} \rho_j S_j) + \nabla \cdot (\omega_{ij} \rho_j \vec{u}_j - \phi \rho_j S_j \vec{\vec{D}}_{ij} \cdot \nabla \omega_{ij}) = q_s \rho_j \omega_{ij} \right\}, \tag{3.1}$$

where $q_s$ represents a source or sink volume flow rate, $\vec{\vec{D}}_{ij}$ characterizes the component dispersivity, $\omega_{ij}$ is the mass fraction of component $i$ in phase $j$, and $\vec{u}_j$ is the phase velocity given by Darcy's Law,

$$\vec{u}_j = -\frac{\vec{\vec{K}} k_{rj}}{\mu_j} \cdot (\nabla P_j + \rho_j g \nabla D). \tag{3.2}$$

The phase pressure is $P_j$, $D$ is the depth, and $g$ is the gravitational constant. To simplify Eq. 3.1 it is assumed that the fluids are incompressible ($\rho_j$ =constant) and there is no dispersivity ($\vec{\vec{D}}_{ij}$=0) giving,

$$\sum_{j=1}^{n_p} \left\{ \frac{\partial}{\partial t}(\phi \omega_{ij} S_j) + \nabla \cdot \omega_{ij} \vec{u}_j = q_s \omega_{ij} \right\}, \tag{3.3}$$

Next, summing Eq. 3.3 over all the components and using the fact that $\sum_{i=1}^{n_c} \omega_{ij} = 1$ gives,

$$\nabla \cdot \vec{u}_t = q_s, \tag{3.4}$$

the governing volume balance equation for incompressible flow. The total velocity $\vec{u}_t$ can be defined by summing Eq. 3.2 over $n_p$ phases to give,

$$\vec{u}_t = -\vec{\vec{K}} \cdot (\lambda_t \nabla P + \lambda_g \nabla D). \tag{3.5}$$

Capillary pressure has been neglected such that $P = P_j$. The total mobility ($\lambda_t$) and total gravity mobility ($\lambda_g$) are defined as,

$$\lambda_t = \sum_{j=1}^{n_p} \frac{k_{rj}}{\mu_j}, \qquad \lambda_g = \sum_{j=1}^{n_p} \frac{k_{rj} \rho_j g}{\mu_j}. \tag{3.6}$$

Finally, combining Eq. 3.4 and Eq. 3.5 leads to the governing pressure equation for multiphase incompressible flow in porous media,

$$\boxed{\nabla \cdot \vec{\vec{K}} \cdot (\lambda_t \nabla P + \lambda_g \nabla D) = -q_s.} \tag{3.7}$$

Eq. 3.7 is elliptic and is known as a Poisson equation where the unknown is $P$. Once $P$ is defined, $\vec{u}_t$ can be determined by using Eq. 3.5.

The governing saturation equation for the IMPES method can be derived from Eq. 3.3. To simplify the problem, it is assumed that the phases are immiscible such that $\omega_{ij}$=0 for $i \neq j$ and $\omega_{ij}$=1 for $i$=$j$ giving,

$$\phi \frac{\partial S_j}{\partial t} + \nabla \cdot \vec{u}_j = q_s f_{j,s}, \tag{3.8}$$

Substituting Darcy's Law, Eq. 3.2, into Eq. 3.8 and eliminating $\nabla P$ by using Eq. 3.5 the above equation becomes,

$$\phi \frac{\partial S_j}{\partial t} + \nabla \cdot \left( \frac{k_{rj}/\mu_j}{\sum_{m=1}^{n_p} \frac{k_{rm}}{\mu_m}} \vec{u_t} + \vec{\vec{K}} \cdot g \nabla D \frac{k_{rj}/\mu_j}{\sum_{m=1}^{n_p} \frac{k_{rm}}{\mu_m}} \sum_{m=1}^{n_p} k_{rm}/\mu_m (\rho_m - \rho_j) \right) = q_s f_{j,s}. \tag{3.9}$$

Defining the standard Buckley-Leverett fractional flow term as,

$$f_j = \frac{k_{rj}/\mu_j}{\sum_{m=1}^{n_p} k_{mj}/\mu_m}, \tag{3.10}$$

and a gravity fractional flow term given by,

$$\vec{G}_j = \vec{\vec{K}} \cdot g \nabla D \frac{k_{rj}/\mu_j}{\sum_{m=1}^{n_p} \frac{k_{rm}}{\mu_m}} \sum_{m=1}^{n_p} k_{rm}/\mu_m (\rho_m - \rho_j), \tag{3.11}$$

Eq. 3.9 can be rewritten as

$$\phi \frac{\partial S_j}{\partial t} + \nabla \cdot f_j \vec{u_t} + \nabla \cdot \vec{G}_j = q_s f_{j,s}. \tag{3.12}$$

Given that $\nabla \cdot \vec{u}_t$=0 for incompressible flow, the governing saturation equation of an individual phase becomes,

$$\boxed{\phi \frac{\partial S_j}{\partial t} + \vec{u}_t \cdot \nabla f_j + \nabla \cdot \vec{G}_j = q_s f_{j,s}.} \tag{3.13}$$

The saturation equation is hyperbolic.

Eq. 3.7 and Eq. 3.13 form the governing set of nonlinear equations for the IMPES method to be used in the streamline simulator. They are nonlinear since coefficients in each equation are dependent on the unknown variables ($P$ or $S_j$). Although the

equations are closely coupled together, they are different in mathematical behavior and as such can be solved differently. This is the underlying idea of the streamline IMPES method. Unlike a conventional finite-difference IMPES method, the use of streamlines allows one to transform Eq. 3.13 into a pseudo 1D equation, as discussed in Section 3.7.

## 3.3 Solution of Pressure Equation

### 3.3.1 Numerical Representation of Pressure Equation

For the streamline method, the reservoir is divided into a Cartesian grid system, as can be done in a conventional simulation. For simplicity, a regular Cartesian grid is assumed, but it is possible to extend the method to account for local grid refinement, non-neighbor connections, or varying gridblock elevations within a given layer. The governing pressure equation (Eq. 3.7) is solved by a standard finite-difference method on the Cartesian grid. For a thorough discussion of finite-difference methods in reservoir simulation see *Aziz & Settari* [3]. The discretized form of Eq. 3.7 in 3D using a seven-point stencil on a Cartesian grid about an arbitrary gridblock at location $i, j, k$, is given by,

$$\begin{aligned}
&T_{z,k-\frac{1}{2}}P_{i,j,k-1} + T_{y,j-\frac{1}{2}}P_{i,j-1,k} + T_{x,i-\frac{1}{2}}P_{i-1,j,k} \\
&-P_{i,j,k}(T_{z,k-\frac{1}{2}} + T_{y,j-\frac{1}{2}} + T_{x,i-\frac{1}{2}} + T_{z,k+\frac{1}{2}} + T_{y,j+\frac{1}{2}} + T_{x,i+\frac{1}{2}}) \\
&T_{z,k+\frac{1}{2}}P_{i,j,k+1} + T_{y,j+\frac{1}{2}}P_{i,j+1,k} + T_{x,i+\frac{1}{2}}P_{i+1,j,k} = \\
&G_{z,k-\frac{1}{2}}D_{i,j,k-1} + G_{y,j-\frac{1}{2}}D_{i,j-1,k} + G_{x,i-\frac{1}{2}}D_{i-1,j,k} \\
&-D_{i,j,k}(G_{z,k-\frac{1}{2}} + G_{y,j-\frac{1}{2}} + G_{x,i-\frac{1}{2}} + G_{z,k+\frac{1}{2}} + G_{y,j+\frac{1}{2}} + G_{x,i+\frac{1}{2}}) \\
&+G_{z,k+\frac{1}{2}}D_{i,j,k+1} + G_{y,j+\frac{1}{2}}D_{i,j+1,k} + G_{x,i+\frac{1}{2}}D_{i+1,j,k} \\
&-q_{s,i,j,k}
\end{aligned} \tag{3.14}$$

This notation assumes that the $k$ index is in the $z$ coordinate direction, the $j$ index is in the $y$ coordinate direction, and the $i$ index is in the $x$ coordinate direction. For a block centered grid, the harmonic mean of the inter-block transmissibility is defined

as,

$$T_{z,k+\frac{1}{2}} = \frac{2\Delta x_k \Delta y_k}{\frac{\Delta z_k}{\lambda_{t,k} K_{z,k}} + \frac{\Delta z_{k+1}}{\lambda_{t,k+1} K_{z,k+1}}}, \tag{3.15}$$

where $\Delta x$, $\Delta y$, $\Delta z$ represent the gridblock dimensions. Similarly, the harmonic mean of the inter-block gravity transmissibility is defined as,

$$G_{z,k+\frac{1}{2}} = \frac{2\Delta x_k \Delta y_k}{\frac{\Delta z_k}{\lambda_{g,k} K_{z,k}} + \frac{\Delta z_{k+1}}{\lambda_{g,k+1} K_{z,k+1}}}. \tag{3.16}$$

In Eq. 3.14, $q_{s,i,j,k}$ represents a source/sink flux in the $i, j, k$ block. Injection is assumed to be positive while production is assumed to be negative.

### 3.3.2 Boundary Conditions

Boundary conditions for the solution to Eq. 3.14 are defined at wells and the no-flow boundaries of the surface of the reservoir model. The well model within the streamline simulator is simplistic relative to those found in standard finite-difference simulators. However, the model is satisfactory for testing the streamline ideas. For a detailed description of well models in finite-difference simulators see *Aziz & Settari* [3].

For any well, either pressure or total rate can be specified. The streamline simulator assumes that a well is modeled with variable density gradient in the wellbore, but no friction losses. The governing equation for a well with $n_l$ layers is given by,

$$q_s = \sum_{k=1}^{n_l} T_k^w [P_k^w - P_k], \tag{3.17}$$

where $P_k^w$ is the pressure in the wellbore and $P_k$ is the pressure in the gridblock. The well layer transmissibility, $T_k^w$, is given by,

$$T_k^w = \frac{2\pi \Delta z_k}{\ln(\frac{r_{o,k}}{r_{w,k}}) + s_k} \lambda_{t,k}^w, \tag{3.18}$$

where $s_k$ is the skin factor, $r_{o,k}$ is Peaceman's radius [59], and $r_{w,k}$ is the wellbore radius. The wellbore mobility $\lambda_{t,k}^w$ is assumed to be the gridblock mobility for production wells, and the injection phase mobility for injection wells.

Finally, for multilayer wells, each layer's well pressure is related to the well pressure of the top well gridblock completion ($k^*$). A variable density gradient wellbore is assumed giving the following relationship,

$$P_k^w = P_{k^*}^w + 0.5 \sum_{i=k^*+1}^{k} (\gamma_{i-1} + \gamma_i)(D_i - D_{i-1}) \tag{3.19}$$

where the wellbore specific gravity, $\gamma_i$, at the $i^{th}$ layer can be calculated by,

$$\gamma_i = \frac{\lambda_{g,i}}{\lambda_{t,i}}. \tag{3.20}$$

For producers $\gamma_i$ is calculated from the block properties, while for injectors $\gamma_i$ is calculated from the injection phase properties. Combining Eq. 3.17 and Eq. 3.19 gives the governing well equation,

$$q_s = \sum_{k=1}^{n_l} T_k^w [P_{k^*}^w - P_k + 0.5 \sum_{i=k^*+1}^{k} (\gamma_{i-1} + \gamma_i)(D_i - D_{i-1})]. \tag{3.21}$$

The unknown in the above equation is either $P_{k^*}^w$ for a well specified with a total rate constraint, or $q_s$ for a well specified with a pressure constraint.

### 3.3.3 Numerical Solution of Pressure Matrix

Grouping Eq. 3.14 and Eq. 3.21 and separating out the unknown gridblock pressures gives the governing set of discretized equations to be solved. In matrix form the equation set appears as

$$\mathbf{T}\vec{P} = \vec{B}, \tag{3.22}$$

where $\mathbf{T}$ contains the well and gridblock transmissibility terms from Eq. 3.14 and Eq. 3.21. For the IMPES method, $\mathbf{T}$ is a symmetric matrix. The vector $\vec{P}$ contains the unknown pressure values at all gridblocks and the unknown well pressures. The vector $\vec{B}$ contains gridblock transmissibility and gravity terms, well source or sink terms, and well terms where $P_{k^*}^w$ is defined.

Eq. 3.22 forms a linear set of equations with all saturation dependent terms evaluated at the previous time step, while $P$ is determined at the current time step. The solution to Eq. 3.22 does not require initial pressure information. However, to

uniquely define the solution, the pressure of at least one well must be defined (Dirichlet boundary condition).

Eq. 3.22 represents a large sparse linear system of equations which is solved by an iterative method. The details of the method are beyond the scope of this work. Eq. 3.22 was solved using one of two methods: conjugate gradient method (JCG from the ITPACK library [43]) or a multigrid method (AMG by GMD [66]). For all problems containing more than $\approx$ 1000 gridblocks, the multigrid solver offered superior speed compared with the conjugate gradient solver. All solutions presented in this thesis used the multigrid solver.

## 3.4 Determining the Velocity Field

Once the pressure field has been determined, the field of velocity vectors is defined in order to trace streamline paths. Darcy's Law (Eq. 3.5) applied between two pressure nodes defines the gridblock interface total Darcy velocity as,

$$u_{t,k+\frac{1}{2}} = \frac{T_{z,k+\frac{1}{2}}}{A_{k+\frac{1}{2}}}(P_{k+1} - P_k) + \frac{G_{z,k+\frac{1}{2}}}{A_{k+\frac{1}{2}}}(D_{k+1} - D_k), \tag{3.23}$$

where $A_{k+\frac{1}{2}}$ represents the cross-sectional area of the gridblock interface. To define a velocity vector at a gridblock face, the final step requires converting the Darcy velocity into an interstitial velocities ($v_t$) by dividing by gridblock porosity. The interstitial velocity is then defined at the gridblock face in a direction normal to the face.

## 3.5 Analytical Streamline Path Description

A streamline is defined as the instantaneous curve in space along which every point is tangent to the local velocity vector [8]. Tracing streamlines from injectors to producers is based on the analytical description of a streamline path within a gridblock as outlined by *Pollock* [61]. The underlying assumption is that the velocity field in each coordinate direction varies linearly and is independent of the velocities in the other directions. *Pollock's* method is attractive because it is analytical and consistent with the governing material balance equation.

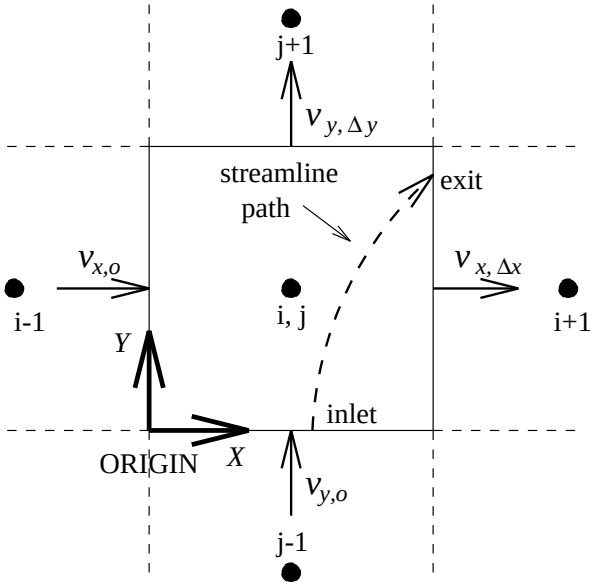


Figure 3.1: Schematic of a streamline path through a 2D gridblock of dimensions $\Delta x$ by $\Delta y$.

Consider the two-dimensional gridblock in Fig. 3.1, for which we know the interstitial velocity field and have defined a local coordinate system and origin. The total velocity in the $x$-direction, $V_x$, is defined as

$$V_x = V_{x,o} + m_x(x - x_o), \tag{3.24}$$

where $m_x$ is the velocity gradient across the gridblock and is given by

$$m_x = \frac{V_{x,\Delta x} - V_{x,o}}{\Delta x}. \tag{3.25}$$

Knowing that $V_x = dx/dt$ Eq. 3.24 can be integrated to yield the time required to reach an $x$ exit face, $\Delta t_{e,x}$ as,

$$\Delta t_{e,x} = \frac{1}{m_x} \ln \left\{ \frac{V_{x,o} + m_x(x_e - x_o)}{V_{x,o} + m_x(x_i - x_o)} \right\}, \tag{3.26}$$

where $x_i$ is the inlet position, $x_e$ is the exit position, and $x_o$ is the location of the origin – all in the $x$-coordinate direction. Similarly, the times required to reach the

exit faces in the $y$ or $z$ directions are given by

$$\Delta t_{e,y} = \frac{1}{m_y} \ln \left\{ \frac{V_{y,o} + m_y(y_e - y_o)}{V_{y,o} + m_y(y_i - y_o)} \right\}, \tag{3.27}$$

and

$$\Delta t_{e,z} = \frac{1}{m_z} \ln \left\{ \frac{V_{z,o} + m_z(z_e - z_o)}{V_{z,o} + m_z(z_i - z_o)} \right\}. \tag{3.28}$$

The correct face which the streamline exits is the face requiring the smallest value of $\Delta t_e$ calculated from Eqs. 3.26, 3.27, and 3.28. Knowing the minimum time, $\Delta t_e$, the exact exit location of the streamline is determined by rewriting Eqs. 3.26, 3.27, and 3.28 as,

$$x_e = \frac{1}{m_x}(V_{x,i} \exp\{m_x \Delta t_e\} - V_{x,o}). \tag{3.29}$$

$$y_e = \frac{1}{m_y}(V_{y,i} \exp\{m_y \Delta t_e\} - V_{y,o}). \tag{3.30}$$

$$z_e = \frac{1}{m_z}(V_{z,i} \exp\{m_z \Delta t_e\} - V_{z,o}). \tag{3.31}$$

For the trivial case of a uniform velocity across a gridblock in a given direction, $m$=0 and Eq. 3.26, for example, becomes $\Delta t_{e,x} = (x_e - x_i)/(V_{x,o})$ while Eq. 3.29 becomes $x_e = x_o + \Delta t_{e,x} V_{x,o}$.

For the situation where a flow divide exists in the $x$ direction within a gridblock (Fig. 3.2), for example, one must assure that the sign $V_x$ at the inlet location is the *same* as the sign of $V_x$ at a potential $x$ exit face. In other words, a streamline will not cross a flow divide within a gridblock. This check also avoids the possibility of calculating negative logarithms in Eqs. 3.26, 3.27, and 3.28.

## 3.6 The Time-of-Flight

The time-of-flight (TOF) is the time required to reach a distance, $s$, along a streamline based on the velocity field along the streamline. The TOF concept has been used in the ground water literature for some time as a method for calculating the capture radii of wells [64]. More recently, *King et al.* [44] and *Datta-Gupta & King* [24] have

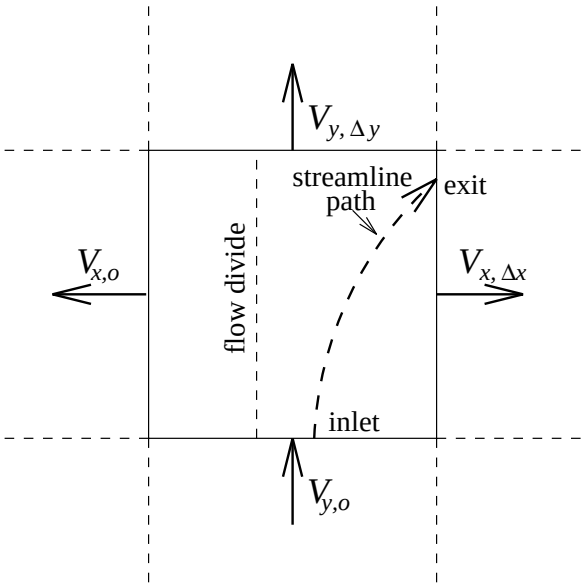


Figure 3.2: Gridblock containing a flow divide, and associated streamline path.

used the TOF concept for modeling flow in oil reservoirs. Mathematically, the time-of-flight, $\tau$, is defined as,

$$\tau(s) = \int_0^s \frac{\phi(\zeta)}{|u_t(\zeta)|} d\zeta. \tag{3.32}$$

The above integral is evaluated analytically using Eqs. 3.26 - 3.28 such that,

$$\tau = \sum_{i=1}^{n_{blocks}} \Delta t_{e,i}, \tag{3.33}$$

where $\Delta t_{e,i}$ is the calculated incremental time-of-flight through gridblock $i$.

## 3.7 Coordinate Transformation Along Streamlines

In a conventional IMPES finite-difference simulator, Eq. 3.13 is solved in its full three-dimensional form. With the streamline method, Eq. 3.13 is decoupled into multiple 1D equations that are solved along streamlines. Solving multiple 1D equations along streamlines is much faster and more accurate than solving the full 3D problem, as will be shown later.

Streamlines are launched from gridblock faces containing injectors. As the streamlines are traced from injectors to producers the time-of-flight is calculated based on Eq. 3.33. The $\tau$ information is used to transform Eq. 3.13 into multiple 1D equations.

*Blunt et al.* [10] outlined the following coordinate transform by first rewriting Eq. 3.32 as,

$$\frac{\partial \tau}{\partial s} = \frac{\phi}{|u_t|}, \tag{3.34}$$

which can further be rewritten as,

$$|u_t|\frac{\partial}{\partial s} \equiv \vec{u}_t \cdot \nabla = \phi \frac{\partial}{\partial \tau}. \tag{3.35}$$

Substituting Eq. 3.35 into Eq. 3.13 gives,

$$\boxed{\frac{\partial S_j}{\partial t} + \frac{\partial f_j}{\partial \tau} + \frac{1}{\phi}\nabla \cdot \vec{G}_j = \frac{q_s f_{j,s}}{\phi}.} \tag{3.36}$$

Eq. 3.36 is the governing pseudo 1D phase material balance equation transformed along a streamline coordinate. It is pseudo 1D since the gravity term is typically not aligned along the direction of a streamline. Chapter 4 will discuss solving Eq. 3.36 analytically and Chapters 5 and 6 will discuss solving Eq. 3.36 by a numerical method.

## 3.8 Tracing Streamlines in a 3D Multiwell Domain

Streamlines are traced from an arbitrary number of injection blocks to production blocks using the equations defined in Section 3.5. The streamline paths do not start at the center of an injection block since the velocity field cannot be approximated as piecewise linear within a gridblock containing a point source. Rather, streamlines are launched from each gridblock face containing an injector.

The number of streamlines to launch from an injection face can either be a constant for all faces, or can vary from face to face. The latter method is used within 3DSL. Streamlines are launched in proportion to the flux out of a face, such that more streamlines are launched from high flow rate injectors, while fewer streamlines are launched from low flow rate injectors. Thus more streamlines are traced through

high flow velocity regions and fewer streamlines are traced through low flow velocity regions.

The flux across each injection block face is uniform, consistent with the underlying velocity field. Since the flux is uniform, streamlines are distributed on each face in a uniform manner. One algorithm for a uniform launching pattern of an arbitrary number of streamlines is to distribute the streamlines uniformly in the horizontal coordinate direction and randomly in the vertical coordinate direction. This launching pattern allows for the intersection of a maximum number of gridblocks for a fixed number of streamlines. The flux assigned to each streamline $q^{sl}$ is simply,

$$q^{sl} = \frac{q_{face}}{n^{sl}_{face}} \tag{3.37}$$

where $q_{face}$ is the flux out of a given face, and $n^{sl}_{face}$ is the number of streamlines launched from the face.

Not every gridblock in the domain will contain a streamline for a fixed total number of streamlines launched. A missed gridblock is assigned a streamline which is then traced backwards in the velocity field towards an injector. The exact method of assigning missed gridblocks a fluid property depends on whether analytical or numerical solutions are being mapped to the streamlines. See Section 4.4 or Section 5.3 for detailed discussions on calculating missed gridblock properties.

The difference between this streamline tracing method and that proposed by *Hewett & Yamada* [36] is the location from which streamlines are launched. *Hewett & Yamada* propose launching streamlines from a closed surface some distance from an injector, then tracing each streamline back to the injector, and forward to a producer. The main reason for this latter approach was to improve on the estimate of each streamline's flux. However, computational experiments indicate that assigning a flux in this manner is no more accurate than assigning streamline fluxes based on Eq. 3.37, which is consistent with the fact that both method calculate flux using the same underlying velocity field.

## 3.9 Relation Between Streamlines and Streamtubes

However, the numerical streamline method converges as the maximum front movement is reduced to the limiting case of a single gridblock per time step between pressure solutions.

Tracing streamlines is equivalent to tracing streamtubes if one considers the relationship between a streamtube and the central streamline within a streamtube.

The volume of a streamtube $V_{st}(s)$ up to location $s$ along its central streamline is given by,

$$V_{st}(s) = \int_0^s \phi(\zeta) A(\zeta) d\zeta, \tag{3.38}$$

where $\zeta$ is a coordinate defined along the central streamline, $\phi(\zeta)$ is porosity, and $A(\zeta)$ is the cross-sectional area of the streamtube. By definition, the flux along a streamtube is a constant $q_{st} = u(\zeta)A(\zeta)$. Based on a constant flux, and using the time-of-flight information (Eq. 3.32), Eq. 3.38 becomes [36],

$$V_{st}(s) = \int_0^s \phi(\zeta) A(\zeta) d\zeta = \int_0^s q_{st} \frac{\phi(\zeta)}{u(\zeta)} d\zeta = q_{st}\tau(s). \tag{3.39}$$

Thus, the volumetric information of a streamtube is reflected in the time-of-flight information of the associated streamline. The value $q_{st}$ is equivalent to the flux assigned to each streamline as defined in the previous section (Eq. 3.37).

The advantage of using streamlines as opposed to streamtubes, is that they can be easily defined in 3D and $\tau$ is simple to evaluate compared with the integral in Eq. 3.38. One does not need to keep track of the complex geometry of a 3D streamtube. The disadvantage of using streamlines is that it is difficult to determine the boundaries of the streamtube associated with $V_{st}(s)$. Fortunately, as will be shown in Chapter 4, the calculation of gridblock properties is independent of knowing the explicit streamtube boundaries within a gridblock.

## 3.10 Chapter Summary

This chapter outlined the requirements to trace streamlines in a 3D multiwell domain. The governing mathematical equations for the IMPES method were presented with

the solution to the pressure equation following standard finite-difference methods. Based on a known pressure solution, velocities and hence streamlines could be defined. A key point was that the streamline paths are traced by an analytical method which assumes that the velocity field is piecewise linear within a gridblock. Although not discussed here, tracing a streamline path is not restricted to a regular Cartesian system. In fact, all that is required to trace streamlines is a velocity vector field. Finally, rather than solving the full 3D saturation equation, it was transformed into a series of pseudo-1D equations along streamline paths. The coordinate of interest in the transformed system is the local time-of-flight along each streamline rather than a physical space coordinate.

# Chapter 4

# Mapping 1D Analytical Solutions

## 4.1 Introduction

In the previous chapter, the method for defining streamline paths based on knowledge of the total velocity field was outlined. The governing 3D saturation equation was transformed into a pseudo-1D equation along a streamline. This chapter considers analytical solutions to the pseudo-1D equation (Eq. 3.36). First, the multiphase gravity term $G_j$ is ignored by assuming that phase densities within any given gridblock are identical (or assuming $\vec{g}$=0). This assumption results in,

$$\frac{\partial S_j}{\partial t} + \frac{\partial f_j}{\partial \tau} = 0, \tag{4.1}$$

which is a 1D hyperbolic equation. Any displacement that can be modeled by Eq. 4.1 can be mapped onto the 1D streamlines. In this chapter, tracer, waterflood, and first-contact miscible displacements will be studied. Each displacement type does, however, differ in its fractional flow function $f_j$ and the nonlinearity of the problem (coupling between pressure field and saturation field through the phase mobilities).[1]

[1]Some results in this chapter are published in *Thiele et al.* [69] and *Batycky et al.* [7].

## 4.2 Mapping an Analytical Solution to a Streamline

The reference coordinate along a streamline is the time-of-flight, $\tau$. To map an analytical solution onto a streamline, the proper scaling to the $\tau$ coordinate is required. *Higgins & Leighton* [39] mapped analytical solutions which scaled by $x_D/t_D$ to streamtubes. This is straight forward since streamtubes contain a finite volume. The dimensionless distance ($x_D$) and dimensionless time ($t_D$) can be calculated along the streamtube using,

$$x_D = \int_0^s \frac{\phi(\zeta)A(\zeta)d\zeta}{\bar{V}_p}, \tag{4.2}$$

and,

$$t_D = \int_0^t \frac{qdt}{\bar{V}_p}. \tag{4.3}$$

$\bar{V}_p$ is an arbitrary volume used for scaling streamtubes relative to each other. $\bar{V}_p$ is constant for all streamtubes and is typically defined as the average streamtube volume in a model [68].

As was discussed in Section 3.9, streamlines and streamtubes can be related to each other through the time-of-flight. The value of $x_D/t_D$ for a streamline can be derived by starting with Eq. 4.2 and Eq. 4.3. Assuming a constant flow rate, $q$, along the streamtube one gets,

$$\frac{x_D}{t_D} = \frac{\int_0^s A(\zeta)\phi(\zeta)d\zeta}{qt} = \frac{1}{t}\int_0^s \frac{A(\zeta)\phi(\zeta)d\zeta}{v(\zeta)A(\zeta)\phi(\zeta)} = \frac{1}{t}\int_0^s \frac{d\zeta}{v(\zeta)} = \frac{\tau(s)}{t}. \tag{4.4}$$

The above equation indicates that any analytical solution that is a function of $x_D/t_D$ can be correctly positioned along a streamline by knowing the value of $\tau/t$. Since properties like saturation, fractional flow, and total mobility are a unique function of $x_D/t_D$, they are also a unique function of $\tau/t$. Thus, only the time-of-flight along a streamline needs to be defined to determine fluid properties along the streamline.

Both $x_D/t_D$ and $\tau/t$ are dimensionless velocities. The $\tau/t$ value and its relationship to dimensionless velocity is illustrated in Fig. 4.1 where a Buckley-Leverett profile is mapped along a streamline. For example, Eq. 4.4 states that if the time-of-flight to a given point on a streamline is $\tau$=100 days, but the simulation time is $t$=200 days,

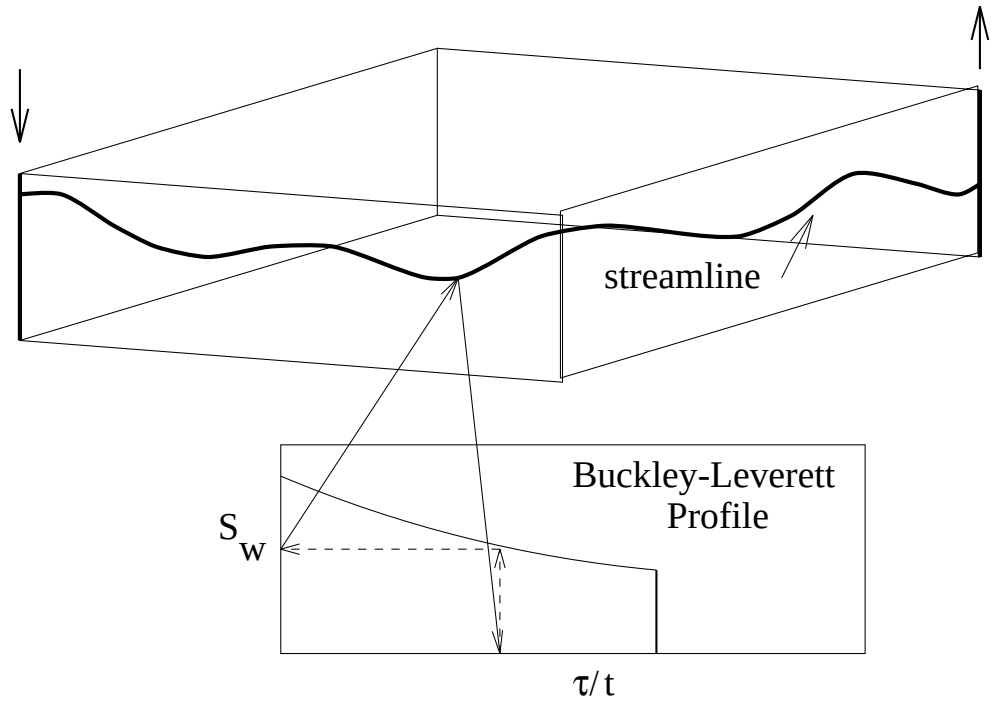


Figure 4.1: Example of mapping a Buckley-Leverett profile along a streamline based on the time-of-flight coordinate.

then the dimensionless velocity of the saturation located at $\tau$ =100 days must be $v_D$=0.5. Given the correct dimensionless velocity, the corresponding saturation with $v_D$=0.5 can be mapped onto the streamline at the desired location.

## 4.3 Calculation of Gridblock Properties

To assign gridblock properties, one could trace back from the center of every gridblock in the domain to an injector. The time-of-flight to the gridblock is then known and Eq. 4.4 could be used to calculate gridblock properties. A more efficient method is to simply trace streamlines from injectors to producers, as described in Section 3.8. The majority of gridblocks will now contain multiple streamlines.

Rather than using the relation in Eq. 4.4 to assign gridblock properties, a unique

property (saturation, mobility, or time-of-flight) must be calculated based on the multiple streamlines that pass through it. For example, the average gridblock saturation, $\bar{S}_{gb}$, is defined as

$$\bar{S}_{gb} = \sum_{i=1}^{n_{gb}^{sl}} \omega_i \bar{S}_i^{sl}, \tag{4.5}$$

where $\bar{S}_i^{sl}$ is the average saturation for the $i^{th}$ streamline and $\omega_i$ is a weighting factor for the $i^{th}$ streamline ($\sum_{i=1}^{n_{gb}^{sl}} \omega_i = 1$).

The average saturation along a single streamline in a gridblock for a given time $t$ can be defined as,

$$\bar{S}_i^{sl} = \frac{1}{\Delta\tau} \int_{\tau_{in}}^{\tau_{exit}} S_i(\tau/t) d\tau. \tag{4.6}$$

For simplicity $\bar{S}_i^{sl}$ is approximated as,

$$\bar{S}_i^{sl} \approx S_i^{sl}(\bar{\tau}/t), \tag{4.7}$$

where

$$\bar{\tau} = \frac{\tau_{inlet} + \tau_{exit}}{2}. \tag{4.8}$$

Strictly speaking, the weighting factor in Eq. 4.5 for each streamline should be the volume fraction of the associated streamtube within the gridblock. Similar to Eq. 3.39, the volume of the $i^{th}$ streamline within a gridblock is given by,

$$V_{sl}^i = \int_{\zeta_{in}}^{\zeta_{exit}} \phi(\zeta) A(\zeta) d\zeta = \int_{\zeta_{in}}^{\zeta_{exit}} q(\zeta) \tau(\zeta) d\zeta. \tag{4.9}$$

The weighting factor based on a streamtube volume fraction is given by,

$$\omega_i = \frac{\int_{\zeta_{in}}^{\zeta_{exit}} q(\zeta)\tau(\zeta) d\zeta\big|_i}{\sum_{j=1}^{n_{gb}^{sl}} \int_{\zeta_{in}}^{\zeta_{exit}} q(\zeta)\tau(\zeta) d\zeta\big|_j}. \tag{4.10}$$

As was discussed in Section 3.9, the disadvantage of using streamlines is that the associated streamtube volume within the gridblock is unknown and the integrals in Eq. 4.10 cannot be evaluated. For purposes of calculating the weighting factor only, it is assumed that the flux is independent of $\zeta$ and the flux is the same for each streamline within a gridblock. The validity of this assumption will be verified in Section 4.14. With this assumption the weighting factor reduces to,

$$\omega_i = \frac{\Delta\tau_i}{\sum_{i=1}^{n_{gb}^{sl}} \Delta\tau_i}. \tag{4.11}$$

Thus, each streamline is weighted by its time-of-flight "length" in a gridblock, relative to all of the time-of-flight "lengths" in a gridblock.[2] Although some assumptions were required to arrive at the final form for $\omega_i$, Section 4.14 illustrates that displacement results are insensitive to the manner in which $\omega_i$ is calculated. This is because gridblock properties are ultimately a function of the time-of-flight to a gridblock, the value of which can be calculated independent of any weighting factor.

Finally, based on Eq. 4.5 and Eq. 4.11, the average saturation for a gridblock is calculated as,

$$\bar{S}_{gb} = \frac{\sum_{i=1}^{n_{gb}^{sl}} \Delta\tau_i \bar{S}(\bar{\tau})_i}{\sum_{i=1}^{n_{gb}^{sl}} \Delta\tau_i}, \tag{4.12}$$

similarity the average total mobility within a gridblock is,

$$\bar{\lambda}_{tgb} = \frac{\sum_{i=1}^{n_{gb}^{sl}} \Delta\tau_i \bar{\lambda}_t(\bar{\tau})_i}{\sum_{i=1}^{n_{gb}^{sl}} \Delta\tau_i}, \tag{4.13}$$

and the average time-of-flight of a gridblock is,

$$\bar{\tau}_{gb} = \frac{\sum_{i=1}^{n_{gb}^{sl}} \Delta\tau_i \bar{\tau}_i}{\sum_{i=1}^{n_{gb}^{sl}} \Delta\tau_i}. \tag{4.14}$$

Because 3DSL is designed to solve very large models, the $\omega_i$'s are not stored for each gridblock for a given time step. Rather, the summations in Eq. 4.12, Eq. 4.13, and Eq. 4.14 are updated as streamlines are traced.

For the unique case of tracer flow and constant boundary conditions, the streamlines do not change with time. Although less accurate, Eq. 4.12 can be approximated as $\bar{S}_{gb} = S(\bar{\tau}_{gb})$ to avoid retracing streamlines (a numerically expensive process).

## 4.4 Missed Gridblocks

For the majority of simulation cases, not every gridblock will contain a streamline. For these missed gridblocks a time-of-flight must still be calculated in order to define

[2]Section 6.3 illustrates that when modeling gravity effects, circulation streamlines can occur. However, it is unclear what flux to assign to these streamlines. Since Eq. 4.11 ignores streamline fluxes it can be applied directly to gravity problems without any modifications.

a gridblock fluid property. To assign a TOF to a missed gridblock, one simply traces a streamline backwards to the nearest gridblock containing an average TOF. The missed gridblock TOF is then calculated as

$$\tau_{missed} = \bar{\tau}_{blk} + \Delta\tau_{backwards}. \tag{4.15}$$

By knowing $\tau_{missed}$, the gridblock fluid properties can then be calculated using Eqs. 4.12, 4.13, and 4.14. To eliminate a compounding error in $\tau_{missed}$ being calculated based on another missed gridblock's TOF, one simply traces back to the first gridblock containing a streamline originating from a source.

## 4.5 Calculation of Producer Fractional Flows

The flux assigned to each streamline is used to determine producer fractional flows. A producer fractional flow is given by,

$$f_p = \frac{\sum_{i=1}^{n_{arrive}} q_i^{sl} f_i^{sl}}{\sum_{i=1}^{n_{arrive}} q_i^{sl}} \tag{4.16}$$

where $f_i^{sl}$ represents the fractional flow of the $i^{th}$ streamline arriving at the producer. The denominator in Eq. 4.16 represents the producer total fluid flux, $q_s^{sl}$, determined from the arriving streamlines. For each producer, the value of this total flux can be compared against the true value of $q_s$ derived from the pressure solution. For all cases presented in this thesis, the error between $q_s^{sl}$ and $q_s$ for each producer was less than 1%.

## 4.6 Validity of Recalculating Streamline Paths

The key idea in the streamline mapping technique presented here is the method by which saturations are moved forward in time. As discussed earlier, one option is to fix the streamline paths (fixed streamtubes) for all time. The changing mobility field is accounted for by updating the resistances along streamtubes. The advantage of a fixed path method is that the pressure field is only calculated once, resulting in a

fast calculation. However, a disadvantage is that highly nonlinear displacements are incorrectly modeled leading to large errors is performance predictions [68].

A nonlinear displacement is characterized by a changing velocity field as the displacement proceeds. The level of nonlinearity is directly related to the distance over which the total fluid mobility changes. For waterfloods, the mobility change occurs over a long rarefaction wave, while for FCM displacements the mobility change occurs over a very short distance near the displacement front. As will be shown later, for heterogeneity dominated displacements, waterfloods are only weakly nonlinear while FCM displacements can be highly nonlinear.

To properly capture a displacement's nonlinearity, the alternative to fixed streamline paths is to allow the streamlines to change as the mobility field changes. This method has been used successfully by *Thiele et al.* [70, 71] to model adverse mobility FCM and compositional floods. The method is appealing since streamline paths and TOF's along the streamlines honor the changing mobility field. The major disadvantage with this method occurs when a streamline path moves from a position at time $t^n$ to a new position at time $t^{n+1}$. Consequently, the saturation profile along the new streamline will in general be nonuniform. This nonuniform condition represents the initial condition to be moved forward along the streamline at the new time step.[3] However, 1D analytical solutions only exist for uniform initial conditions. The major assumption when mapping analytical solutions to streamlines then, is to ignore the new conditions present along recalculated streamline paths and simply map a new 1D solution scaled to the new time. The validity of the assumption is based on how much the streamline paths change position from time $t^n$ to $t^{n+1}$.

Streamline paths are governed by the velocity field which, in turn, is calculated from solving the pressure equation (Eq. 3.7). If boundary conditions are constant, changes in the total mobility field ultimately determine the change in streamline paths. For unit mobility ratio displacements the streamline paths do not change, and the mapping method is exact with no assumptions. In addition, the total mobility field will change little through time for nonlinear displacements if the system is dominated by correlated heterogeneity. As a result, the uniform initial condition assumption can

[3] Chapter 5 discusses how to move these conditions forward correctly by a numerical technique.

also be applied to this latter case. *Thiele* [68] includes a thorough discussion on the validity of this method, concluding that the technique is applicable to heterogeneity dominated displacements, as will be shown here.

## 4.7 Calculation of True Time

Each time that the streamline positions are recalculated, a problem of not knowing what the true time, $T^{n+1}$, is for a displacement at the end of time step $n+1$ is introduced. This problem occurs because grid saturation information is not explicitly moved forward in time, but instead is removed and a new 1D solution scaled to $t+\Delta t$ is mapped along the new streamline positions. The old saturation information is only accounted for in the mobility terms of the pressure equation.

To determine the true time, historical information is accounted for by a volume balance on the injected phase (for example water) at the end of mapping all streamlines. This leads to an expression for the true time step size over the $n+1$ time interval as,

$$\Delta T^{n+1} = \frac{(W_{init} - W_r^{n+1} + W_I^n - W_P^n)}{Q^{n+1}(\bar{f}^{n+1} - 1)}, \tag{4.17}$$

where the average field production fractional flow is defined as $\bar{f}^{n+1} = (f^n + f^{n+1})/2$, the average of the field production fractional flows at $n$ and $n+1$, and $Q^{n+1}$ is the total injection rate during the $n+1$ time step. $W_{init}$ is the initial volume of water in the reservoir, and $W_r^{n+1}$ is the volume of water present after mapping all the new streamlines at the $n+1$ time step. Cumulative water production up to the previous time step is calculated by,

$$W_P^n = \sum_{i=1}^{n} Q^i \bar{f}^i \Delta T^i, \tag{4.18}$$

and since all injectors inject 100% water, cumulative water injection volume is simply given by,

$$W_I^n = \sum_{i=1}^{n} Q^i \Delta T^i \tag{4.19}$$

Thus, $t$ can be considered an internal time which is required for the mapping of the 1D solution to streamlines. $T$ is the true time that is external and of interest.

The true time is calculated at the end of each mapping step by applying Eq. 4.17 and then updating $T$ by $T^{n+1} = T^n + \Delta T^{n+1}$. Again, $T$ is introduced because of the mapping method used here. For the tracer case, where streamlines do not change with time, $T = t$ throughout a simulation.

## 4.8 Time Stepping

An underlying idea of the streamline method is that the streamline paths are allowed to change with time to honor the changing mobility field. To update the pressure field and move saturations forward in time from $t^n$ to $t^{n+1} = t^n + \Delta t_p^{n+1}$ the following algorithm is used,

1. Calculate the pressure field by solving Eq. 3.7 as outlined in Chapter 3. Recall that the streamline approach uses an IMPES method so the saturation field for use in Eq. 3.7 is at $t^n$ while the well boundary conditions are at $t^{n+1}$.

2. Apply Darcy's law to determine the total velocity field at gridblock faces.

3. Trace streamlines using Eqs. 3.26 - 3.31. While tracing a streamline, use Eq. 4.4 with $t$ now equal to $t^{n+1}$, map the 1D analytical solution along each streamline.

4. After tracing all streamlines and checking for missed gridblocks, use Eqs. 4.12 and 4.13 to determine the average saturation and total mobility of each gridblock.

5. Calculate the true time, $T$, that the new saturation distribution exists at.

6. Return to Step 1.

Because solutions being mapped to streamlines can scale to any time, the time stepping technique is always stable no matter the size of the time step. Instead of a Courant-Friedrichs-Lewy (CFL) condition for stability, the issue becomes, how many time steps over a fixed total time are required to capture accurately the nonlinearity of the displacement (a converged solution)? A solution is considered converged when

there is no additional change in recovery with increased number of pressure steps over a fixed simulation time. See Section 4.13 for a discussion on convergence using the streamline method when mapping analytical solutions.

## 4.9 Tracer Flow

Tracer flow is characterized by identical fluid properties between initial and injection phases. For tracer flow with constant well conditions the streamlines are fixed for all time. No approximations are made in time stepping and there are no convergence issues (nonlinearities are not present in the pressure solution). Additionally, the analytical tracing of streamline paths coupled with the mapping of a 1D analytical tracer profile will yield *exact* results. Numerical diffusion caused by averaging streamline properties within a gridblock remains confined to the gridblocks scale. When mapping analytical solutions, fluid saturations are not explicitly moved forward at each time step. Thus, the level of numerical diffusion does no grow as a displacement proceeds.

For tracer flow, the fractional flow function, $f$, is equivalent to the tracer concentration, $C$, and Eq. 4.1 becomes,

$$\frac{\partial C}{\partial t} + \frac{\partial C}{\partial \tau} = 0, \tag{4.20}$$

subject to the following initial and boundary conditions,

$$\begin{aligned} C(\tau, 0) &= C_{initial} \qquad \tau \geq 0 \\ C(0, t) &= C_{injection} \qquad t > 0. \end{aligned} \tag{4.21}$$

The solution to the above equation gives the standard tracer profile shown in Fig. 4.2 where $C_{initial}$=0 and $C_{injection}$=1. This profile contains no diffusion, however *Thiele* [68] presents streamtube solutions to tracer flow that do include longitudinal diffusion in the 1D tracer profile.

### 4.9.1 Quarter 5-Spot Tracer Case

To validate the streamline method outlined up to this point, tracer flow in a homogeneous quarter five-spot pattern is studied. Shown in Fig. 4.3 is a recovery

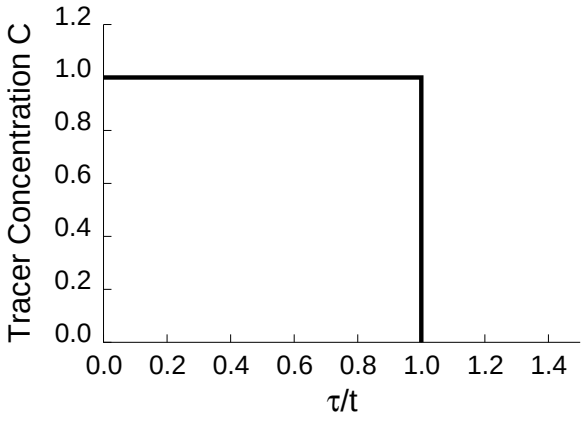


Figure 4.2: Tracer concentration profile versus dimensionless velocity.

comparison between the streamline simulator (3DSL) on a 100X100 grid and the analytical solution [56]. Similar results using streamlines were presented by *Fay & Pratts* [29] and more recently by *Datta-Gupta & King* [24]. Clearly the 3DSL results match exactly to the analytical solution. Also included in Fig. 4.3 are the results from the commercial finite-difference simulator, ECLIPSE [41], for a grid aligned parallel to the main flow direction and a grid aligned diagonal to the main flow direction. ECLIPSE shows both numerical diffusion, as illustrated by the early breakthrough times, and grid orientation effects, as illustrated by two different breakthrough profiles. Figure 4.4 is a comparison of the saturation profiles between the streamline method and ECLIPSE, at $t_D$=0.72, the moment of tracer breakthrough predicted by the analytical solution. Clearly, ECLIPSE does not capture the sharp tracer displacement front that 3DSL predicts. Also, note in Fig. 4.4 that the streamline method does show some mixing of the tracer at the leading front over the range of a single gridblock. A single gridblock represents the minimum resolution to which saturation information is known. Within these gridblocks, some streamlines carry a concentration of 1 while others carry a concentration of 0. The result is a mixed value. However, when mapping analytical solutions, these mixed compositions are not moved forward in time. Instead, a new 1D solution scaled to the new time is mapped along each streamline. Thus, the level of numerical diffusion never increases with this approach. In Chapter 5, the mixed grid compositions are moved forward at each time step and numerical

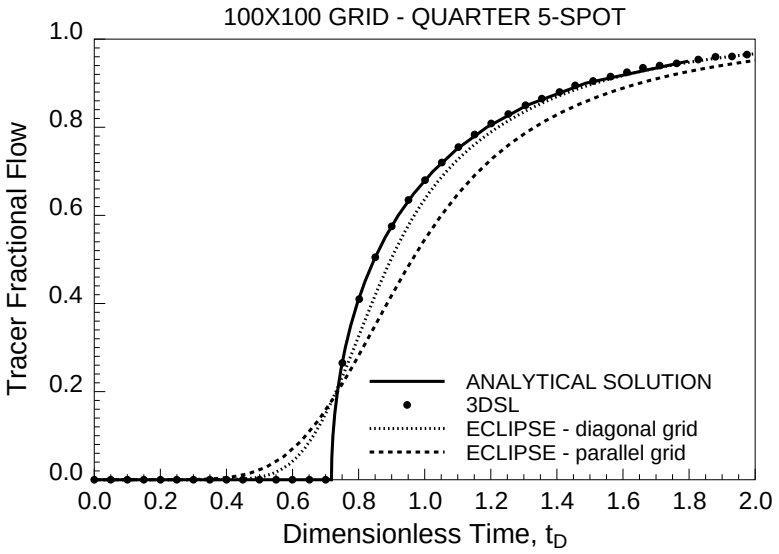


Figure 4.3: Comparison of tracer concentration at the producer in a quarter five-spot for three different methods.

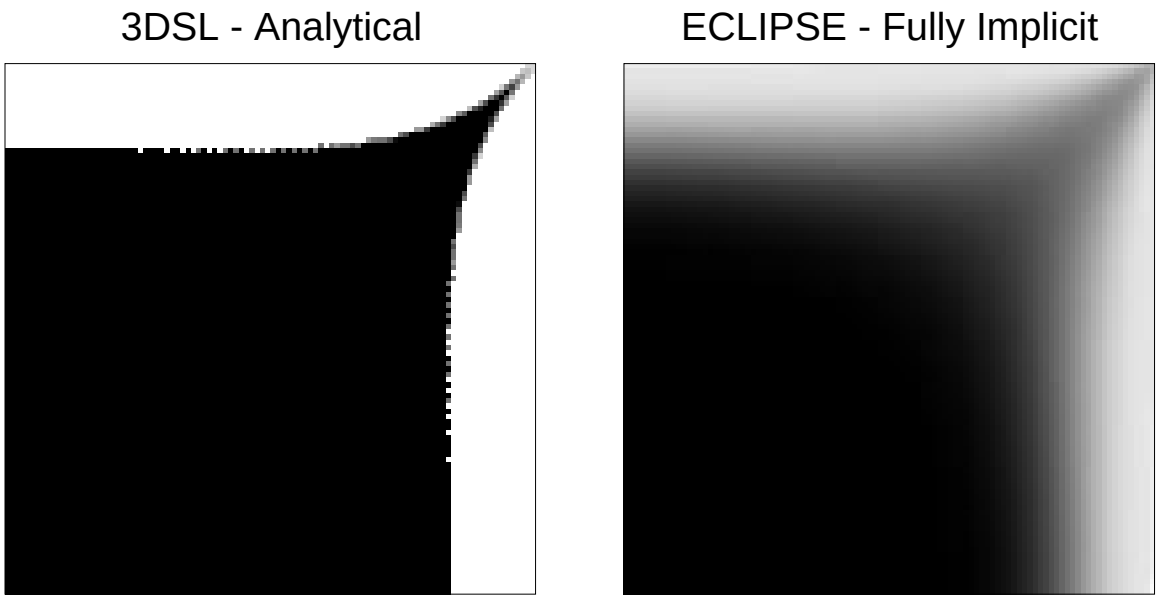


Figure 4.4: Comparison of tracer concentration distributions between two numerical method in a quarter five-spot pattern at $t_D$=0.72 - 100×100 homogeneous grid.

diffusion does grow with time as the number of convective mapping steps increase.

### 4.9.2 Sensitivity to Number of Streamlines

The results from the streamline method are dependent on the number of streamlines that are traced in a model. The greater number of streamlines that are launched in a model, the fewer number of gridblocks that are missed with the streamlines. For highly heterogeneous flows an infinite number of streamlines may be needed to trace from injectors in order to intersect all gridblocks. However, recall that any missed gridblock is assigned a saturation based on tracing streamlines backwards in the velocity field from a missed gridblock to one containing multiple streamlines (Section 4.4). As a result, launching an infinite number of streamlines is unnecessary. The number of streamlines launched does not effect the calculation of gridblock phase saturations, as shown in Fig. 4.5. However, the number of streamlines traced from injector to producer does effect the resolution of the injected phase concentration at the producer. This is because the fluid cut at a producer is calculated based on the phase flux of arriving streamlines, as discussed in Section 4.5.

### 4.9.3 Advantages of Moving Fluid Along Streamlines

With the streamline method, fluids are moved along streamline paths. In a conventional finite-difference scheme, because of the simplicity of discretizing the governing equations on a finite grid, fluids are moved between the discrete gridblocks. This section highlights the differences between the two approaches. Tracer flow is considered here since the velocity field is fixed for all time. Furthermore, since the pressure solution method is identical for both methods, the velocity field at the gridblock faces is also identical for both methods. Tracer flow highlights differences strictly due to the methods by which fluids are transported convectively in each case.

As a numerical experiment, consider a tracer slug injected into the permeability field shown in Fig. 4.6. The tracer profile mapped along the streamlines is shown in Fig. 4.7. The well pattern is a quarter five-spot with an on-trend orientation. The slug is injected from $t_D$=0 to $t_D$=0.013. Figure 4.8 compares the tracer profile

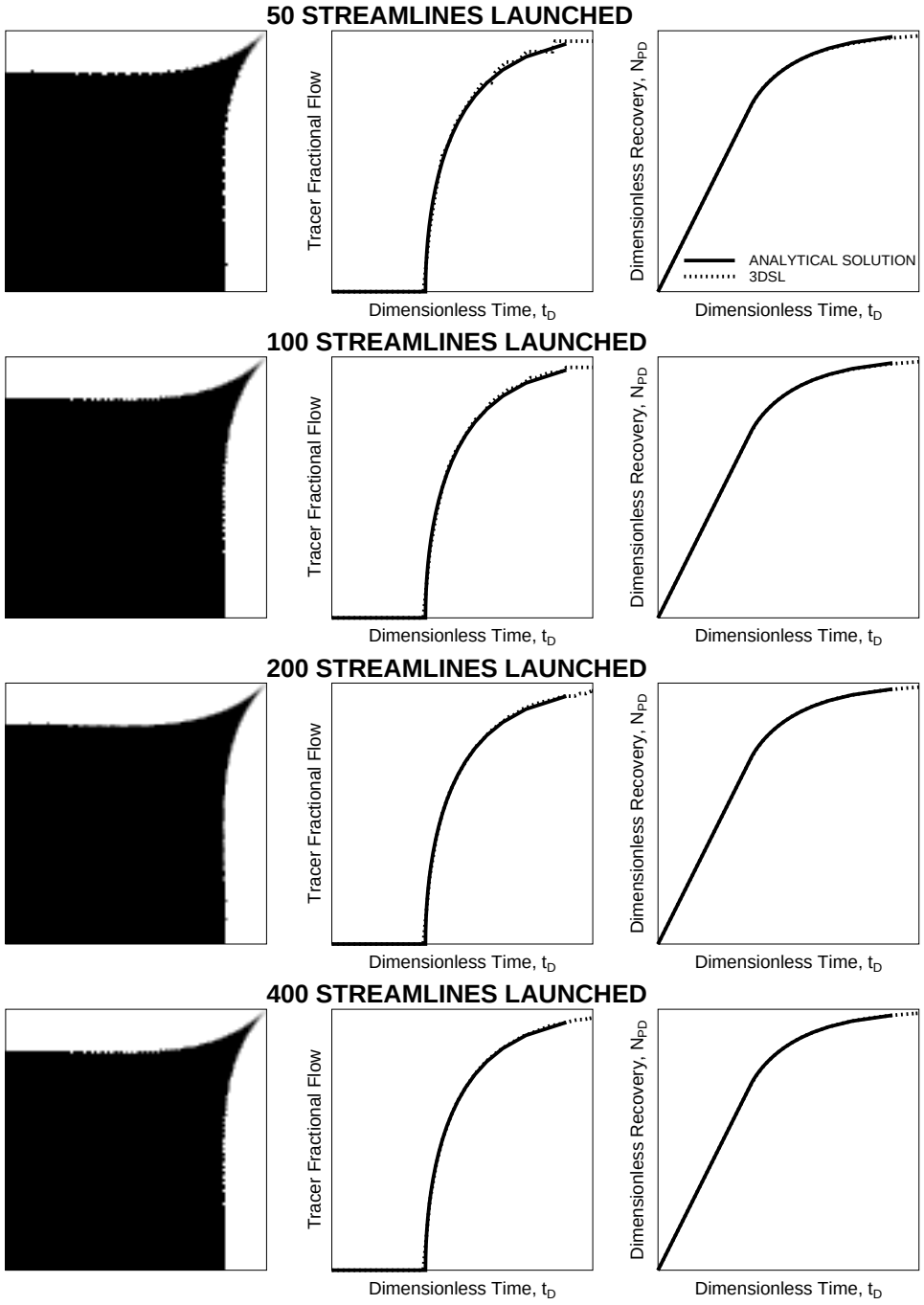


Figure 4.5: Effect of number of streamlines launched on tracer concentration distribution, resolution in tracer effluent profile, and tracer recovery calculations in a quarter five-spot pattern.

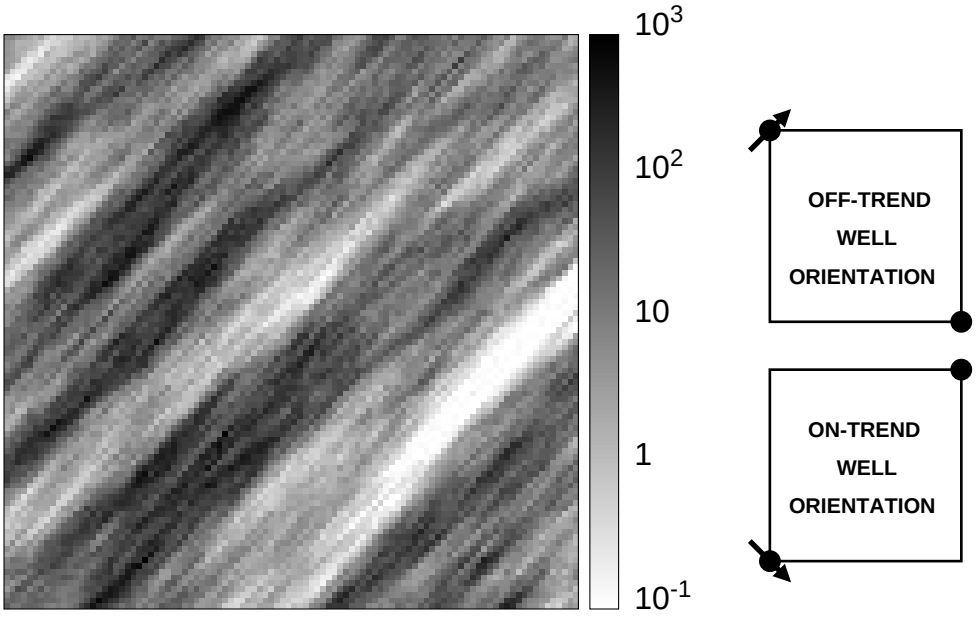


Figure 4.6: 100×100 anisotropic permeability field, and on-trend and off-trend well arrangements.

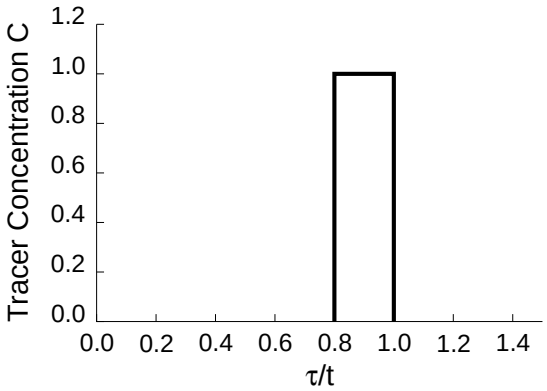


Figure 4.7: Tracer slug profile mapped along streamlines in Fig. 4.8.

between the streamline method and ECLIPSE - IMPES at the end of slug injection and at $t_D$=0.07. Two key points illustrated by Fig. 4.8 are that; 1) the streamline method correctly maintains the sharp tracer profile at the front and back of the slug, whereas ECLIPSE cannot and, 2) the center of mass $C_m$ position of the tracer slug is completely different between the two methods.

There are two sources of numerical error within ECLIPSE that lead to diffusion of the tracer. The first source is truncation error due to approximations in the time and space derivatives. This error has been quantified in one-dimensional situations (*Lantz* [50]). The second source of error is due to approximations in the path of the tracer. Shown in Fig. 4.9 is a conceptual picture of a predicted particle position at time $t_2$ for the streamline method and a conventional method. As the time step size is reduced in the conventional method, the particle path will approximate the true streamline path. However, even with an infinite number of time steps, the two paths will never be identical and will result in differences in bulk tracer movement (different centers of mass).

The streamline method is clearly more accurate, but it is also worth pointing out the difference in CPU times between the two methods. For the case shown in Fig. 4.7, ECLIPSE - IMPES required 700 seconds while the streamline method required 2 seconds (mostly I/O). Thus, another obvious advantage of moving fluids along streamlines is the significant time savings. The reason for the large speed-up factor is that very large time steps can be taken in the streamline method, since the underlying grid stability constraints are effectively decoupled from fluid movement. A fluid element can be moved from $t_1$ to $t_2$ in a single time step with the streamline method, whereas a conventional method will require many time steps to reach $t_2$. This idea is discussed further in Chapter 5.

Recall that for tracer flow, the velocity field calculated by each method was identical for all time. However, it is also worth considering a nonunit mobility ratio displacement in the context of the above discussion. Numerical diffusion will not only affect the position and concentration of an injected fluid but also incorrectly alter the velocity field. This alteration introduces compounding errors in predicting

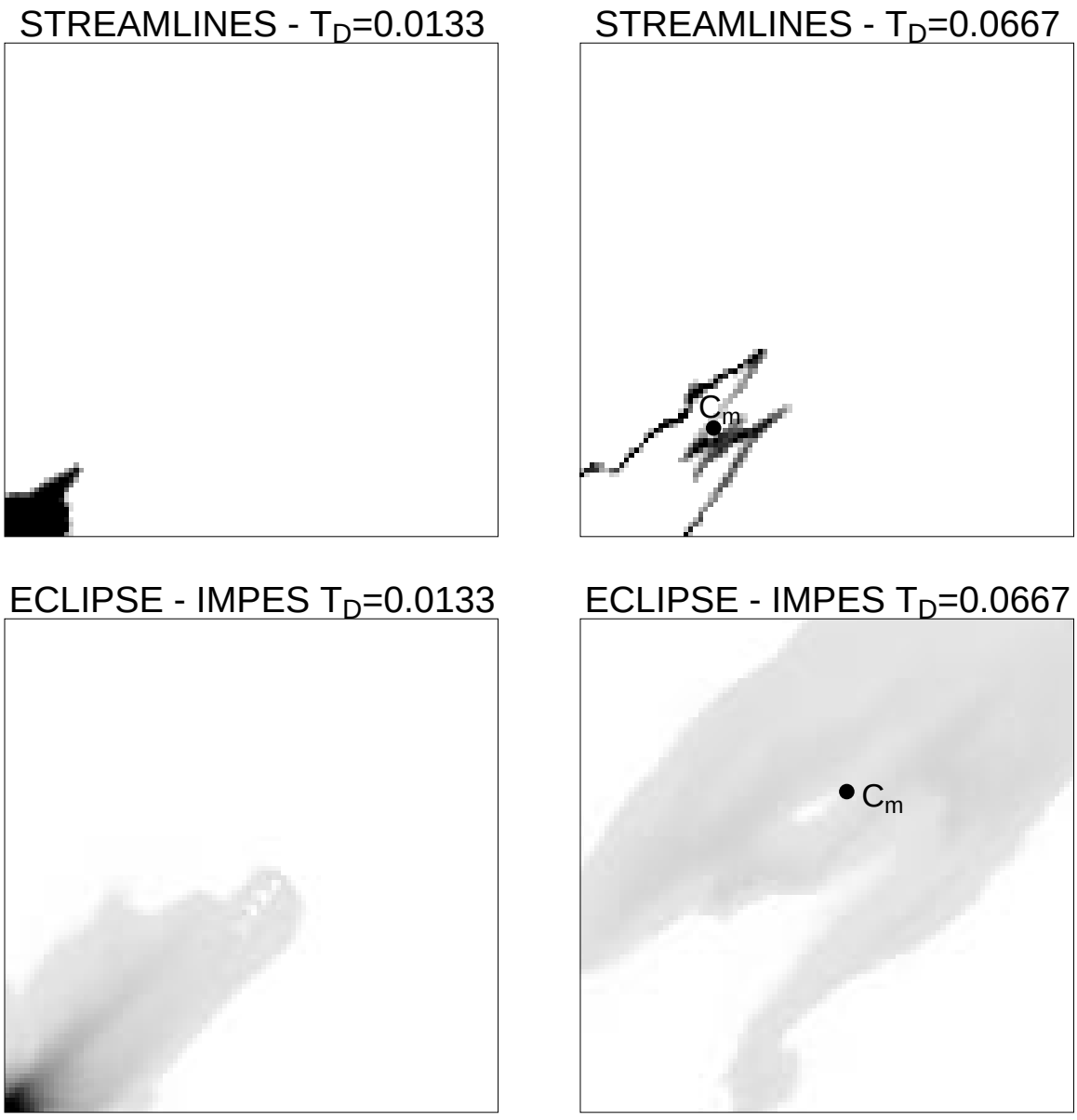


Figure 4.8: Comparison of tracer slug profile predictions between the streamline method and ECLIPSE ($C_m$ - center of mass).

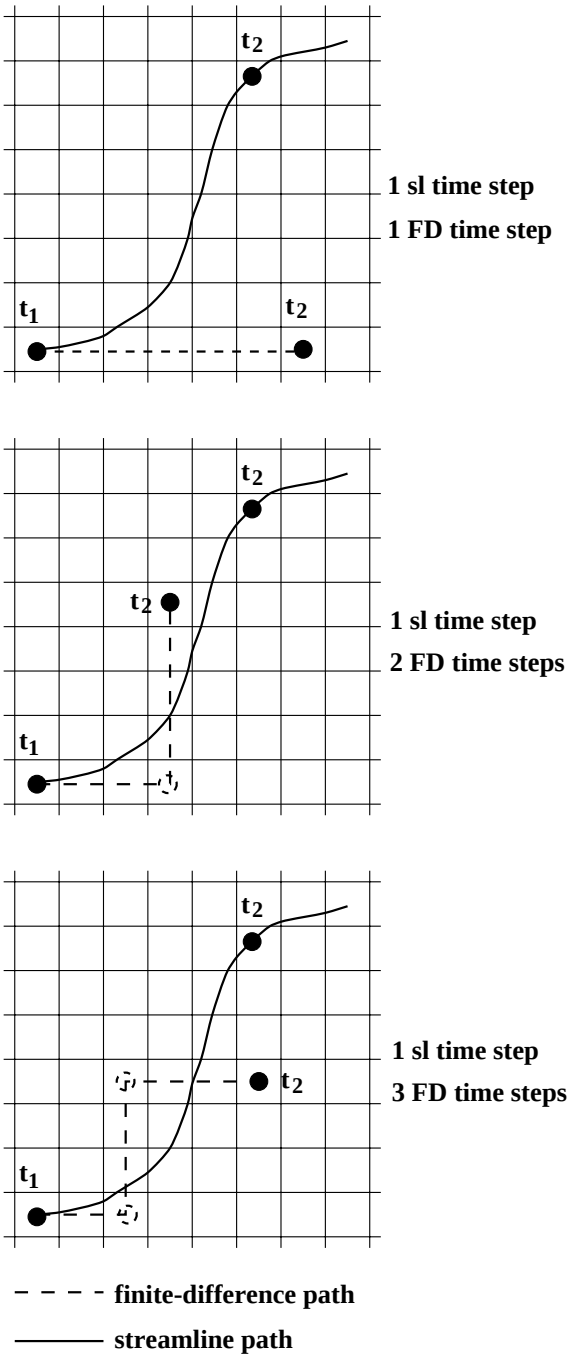


Figure 4.9: Conceptual picture illustrating the predicted particle position at time $t_2$ using the streamline method and a finite difference method.

fluid movement and helps to explain why first-contact miscible and compositional displacements are sensitive to the accuracy of numerical method used in a conventional simulator.

### 4.9.4 Quantifying Numerical Diffusion in Conventional Methods

For tracer displacements with fixed boundary conditions, the streamline method coupled with mapping the analytical tracer profile produces diffusion free results. Because of the ability to predict exact results, the streamline method can be used to quantify the level of numerical diffusion present in a conventional simulator.

Consider a tracer displacement in a two-dimensional $100 \times 100$ permeability field (Fig. 4.6). The permeability field has an anisotropy ratio of 8:1. An injector-producer pair is considered with two well arrangements in relation to the permeability orientation, on-trend arrangement and off-trend arrangement. Both 3DSL and ECLIPSE were run to $t_D$=2.0 for each well orientation, with the resulting saturation profiles at breakthrough shown in Fig. 4.10 and the recovery profiles shown in Fig. 4.11.

A comparison of saturation profiles indicates that there is numerical diffusion within ECLIPSE for both models. However, the diffusion has a greater effect on predicted recovery for the on-trend well model than for the off-trend well model. To explain the differences in recovery matches, one must consider diffusion as a secondary recovery mechanism. Within ECLIPSE, there is both longitudinal and transverse diffusion, while the streamline method contains neither. Transverse diffusion will tend to enhance recovery, while longitudinal diffusion will reduce recovery. Thus, for the on-trend model where flow is primarily longitudinal, transverse diffusion is significant enough to result in improved recovery. However, for the off-trend model where flow paths are highly tortuous between the injector and producer (Fig. 4.10), the magnitude of transverse convective flow is greater than any transverse diffusion that may be present; thus no improvement in recovery.

The important conclusion from this numerical experiment is that the level of numerical diffusion and its impact on recovery is directly related to the heterogeneity

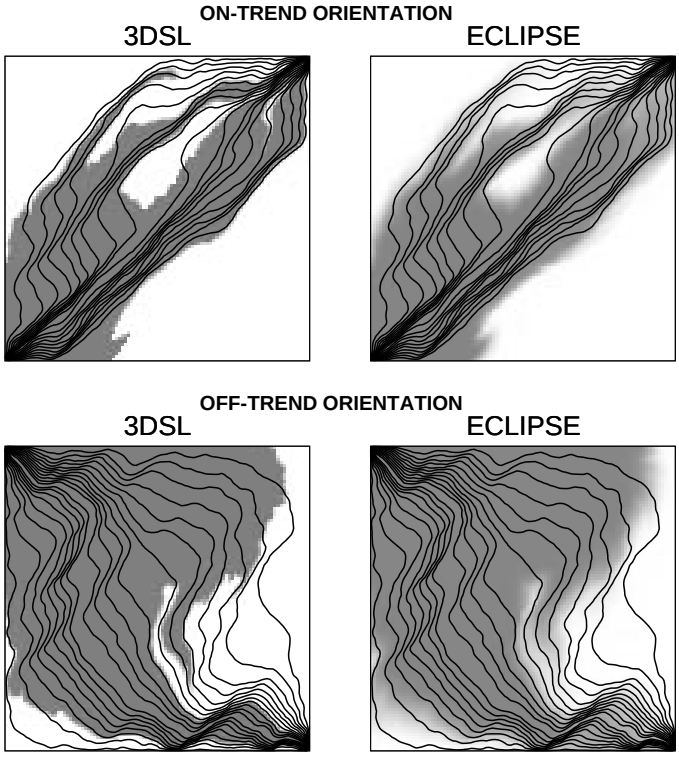


Figure 4.10: Comparison of tracer distributions for on-trend and off-trend models, between 3DSL and ECLIPSE.

distribution and flow orientation. For waterflooding, diffusion effects on recovery will be minor. However, in first-contact miscible displacements, numerical diffusion can be large. Diffusion can incorrectly alter the underlying mobility field and hence have a large impact on displacement predictions. This will be shown in Section 4.12.2.

### 4.9.5 Particle Tracking to Model Tracer Flow

Clearly, the streamline method is well suited to modeling tracer displacements. The computation time is significantly reduced and numerical diffusion is eliminated. In order to avoid numerical diffusion, particle tracking has been used to model flow of pollutants in water (tracer flow) in the ground water industry. See *Kinzelbach* [45], *Uffink* [76], *Tompson & Gelhar* [74] or *Tompson et al.* [75] for a detailed discussion

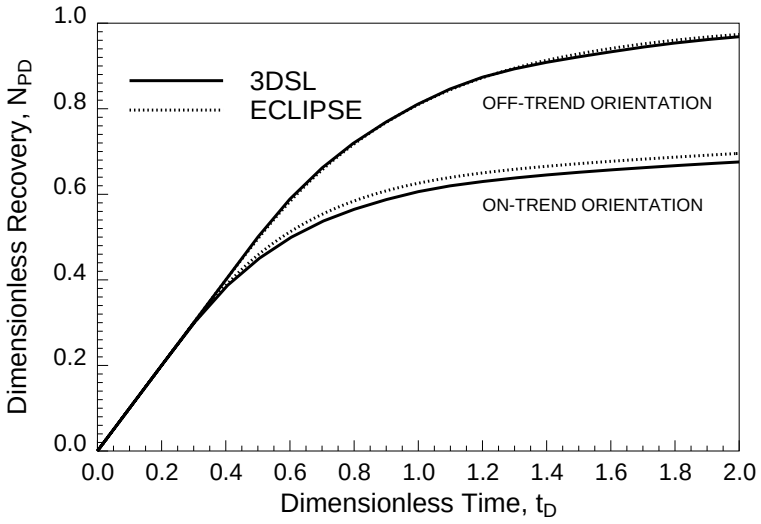


Figure 4.11: Comparison of recovery profiles for on-trend and off-trend models, between 3DSL and ECLIPSE.

of contaminant modeling using particle tracking. In both the streamline method and particle tracking, transport occurs along streamlines. Particle tracking does eliminates numerical diffusion and grid orientation effects. However, tracking individual particles can lead to fluctuations in computed cell concentrations if the number of particles in a gridblock is small. Furthermore, complex accounting issues occur in order to track particle positions through time and space. On the other hand, the streamline method transports concentrations along streamlines which eliminates fluctuations in cell concentrations. Additionally, the accounting process is more straight forward since time stepping only requires knowledge of the previous cell concentrations and not the previous streamline paths.

## 4.10 Definition of Speed-up Factors

The ability to take large time steps with the streamline method translates into short execution times relative to conventional methods. A key idea to convey is "How much faster is the streamline method compared to conventional methods, and how is the

speed-up measured?" For practical purposes, the speed-up factor of interest, and the convention in this thesis, is based on the actual CPU time required by each simulator. However, given the inefficiencies in the 3DSL matrix solvers compared to the ECLIPSE matrix solver, quoted speed-up factors are assumed to be pessimistic. Note that all CPU results are for a single processor run time on a DEC Alpha workstation with 256 MB of memory.

Speed-up factors are also sensitive to whether ECLIPSE results are obtained using a fully-implicit scheme or the IMPES scheme. The IMPES method requires more time steps but results in less numerical diffusion. Thus, the trade-off is time versus accuracy. In this and subsequent chapters, it is made clear which ECLIPSE method is being used in the speed-up factor calculations.

In addition to actual CPU times, the number of time steps and the number of matrix solves throughout a displacement are also quoted when comparing simulator performance. For 3DSL, the number of time steps corresponds to the number of convective steps taken (number of times 1D solutions are mapped along streamlines), while the number of times the pressure field is recalculated corresponds to the number of matrix solves. For ECLIPSE, the number of time steps corresponds to the number of times the nonlinear equation set is solved (the number of times the saturation solution is moved forward). However, the iterative solver required to invert the nonlinear equation set is typically called multiple times. Thus, the number of matrix solves for ECLIPSE reflects the number of times that the iterative solver is called.

## 4.11 Immiscible Two-Phase Displacements

Immiscible two-phase displacements can be modeled using the streamline method with an appropriate two-phase immiscible one-dimensional solution, such as the Buckley-Leverett solution [16]. The key difference between an immiscible two-phase displacement and tracer flow is the changing total mobility field. Eq. 3.7 is now nonlinear since $\lambda_t$ changes with time. As discussed in Section 4.6, the streamline paths are recalculated to honor the changing mobility field. Although nonuniform saturation conditions are present along recalculated streamline paths, the conditions are ignored

and a new 1D solution scaled to the new time is mapped. This is a reasonable assumption for displacements dominated by heterogeneity since streamline positions change little throughout a displacement.

### 4.11.1 1D Immiscible Two-Phase Solution

The governing 1D immiscible two-phase solution mapped along streamlines is the Buckley-Leverett solution. For this solution, Eq. 4.1 becomes

$$\frac{\partial S_w}{\partial t} + \frac{\partial f_w(S_w)}{\partial \tau} = 0, \tag{4.22}$$

with the following initial and boundary conditions,

$$\begin{aligned} S_w(\tau, 0) &= S_{w,initial} \qquad \tau \geq 0 \\ S_w(0, t) &= S_{w,injection} \qquad t > 0. \end{aligned} \tag{4.23}$$

The fractional flow function is now given by,

$$f_w(S_w) = \frac{k_{rw}(S_w)/\mu_w}{k_{rw}(S_w)/\mu_w + k_{ro}(S_w)/\mu_o} \tag{4.24}$$

Assuming simple Corey-type [23] relative permeability curves of the form $k_{rw} = (S_w)^2$ and $k_{ro} = (1 - S_w)^2$ and a fluid viscosity ratio of $\mu_o/\mu_w = 10$, the resulting Buckley-Leverett profiles to map along streamlines are shown in Fig. 4.12.

It is worth observing that although the total mobility ratio changes from 0.1 to 1.0, there is a long rarefaction wave over which this change occurs. *Thiele* [68] noted that as a result, waterflooding displacements are only weakly nonlinear and require only a few pressure solves throughout a displacement life to capture this nonlinearity.

### 4.11.2 3D Five-Spot Displacements

The 1D profile shown in Fig. 4.12 is used to model a waterflood displacement in a five-spot pattern initially at 100% oil saturation. The model contains 50,000 gridblocks ($50 \times 50 \times 20$), with a producer completed in the upper ten layers in each corner of the model and a central injector located in the lower ten layers of the model. Three

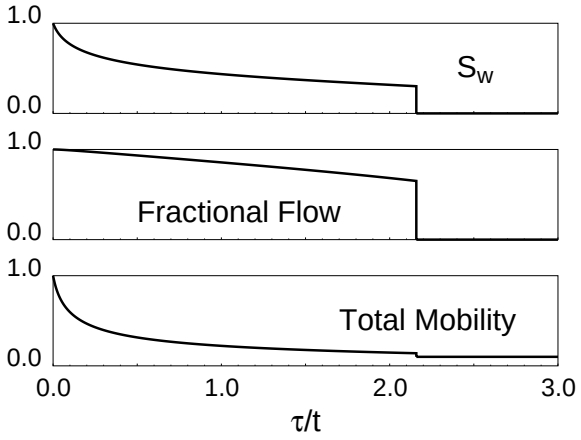


Figure 4.12: Buckley-Leverett profiles for water saturation, water fractional flow, and total mobility as a function of $\tau/t$.

| Permeability Field | Correlation Length | | | Horiz. Rotation wrt. $x$-axis |
|---|---|---|---|---|
| | $\lambda_{c,x}$ | $\lambda_{c,y}$ | $\lambda_{c,z}$ | |
| Model 1 | 0.3 | 0.03 | 0.1 | $45^o$ |
| Model 2 | 0.4 | 0.4 | 0.1 | $0^o$ |
| Model 3 | 0.4 | 0.1 | 0.8 | $45^o$ |

Table 4.1: Correlation length parameters used to build geologic models for results in Fig. 4.13.

different permeability models with different correlation lengths were constructed using sequential Gaussian simulation [26]. The model properties are summarized in Table 4.1[4] and the resulting 3D permeability fields are shown in Fig. 4.13.

The oil recovery curves for the three permeability models are shown in Fig. 4.14 and compared with ECLIPSE fully implicit solutions. For each case, 5,000 streamlines were used in 3DSL. A comparison of individual well watercuts for each model is also shown in Fig. 4.14. The agreement in recoveries for the three different permeability fields is excellent. Agreement is also excellent on a per well basis, although numerical diffusion in ECLIPSE does tend to delay breakthrough at the two off-trend producers

[4]For a rotated coordinate systems the longest model distance along the rotated coordinate axis is used, when calculating $\lambda_c$.

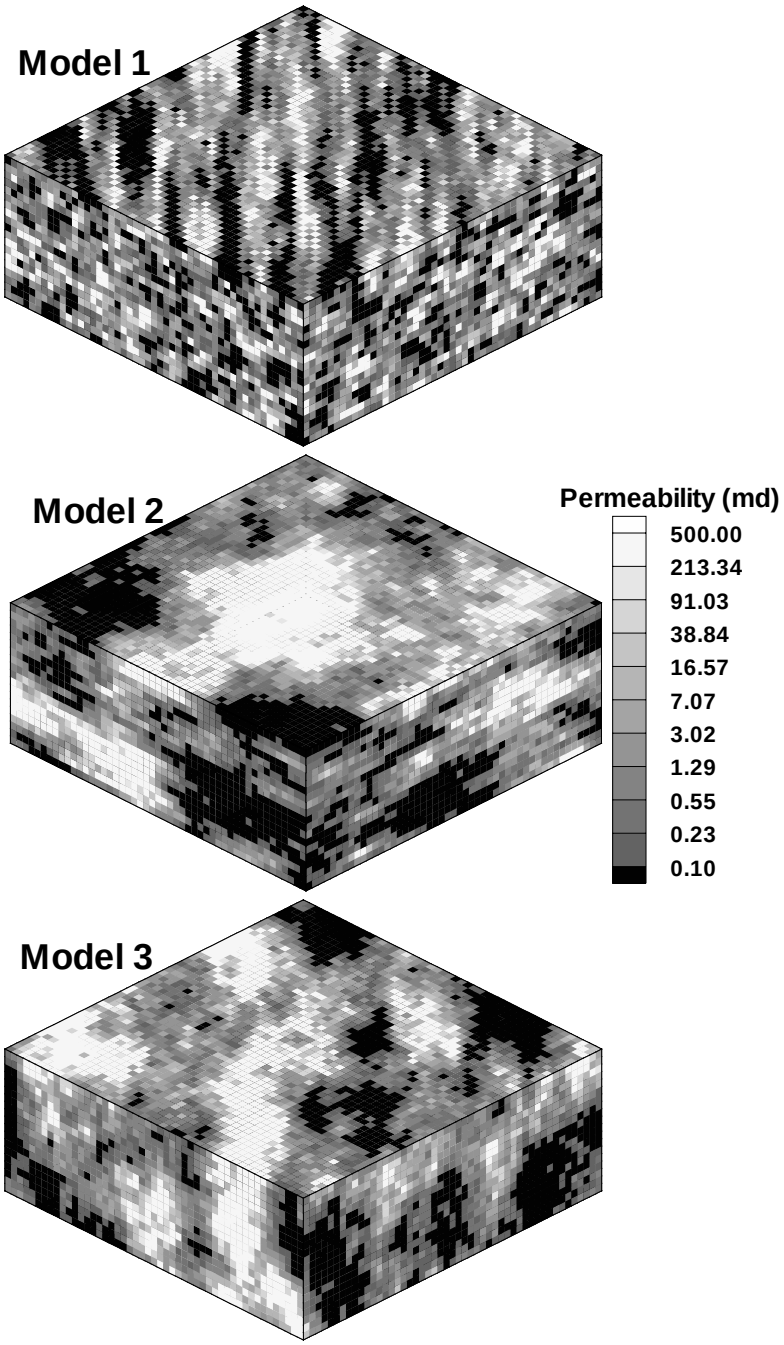


Figure 4.13: Three permeability models with different permeability correlation structures (summarized in Table 4.1).

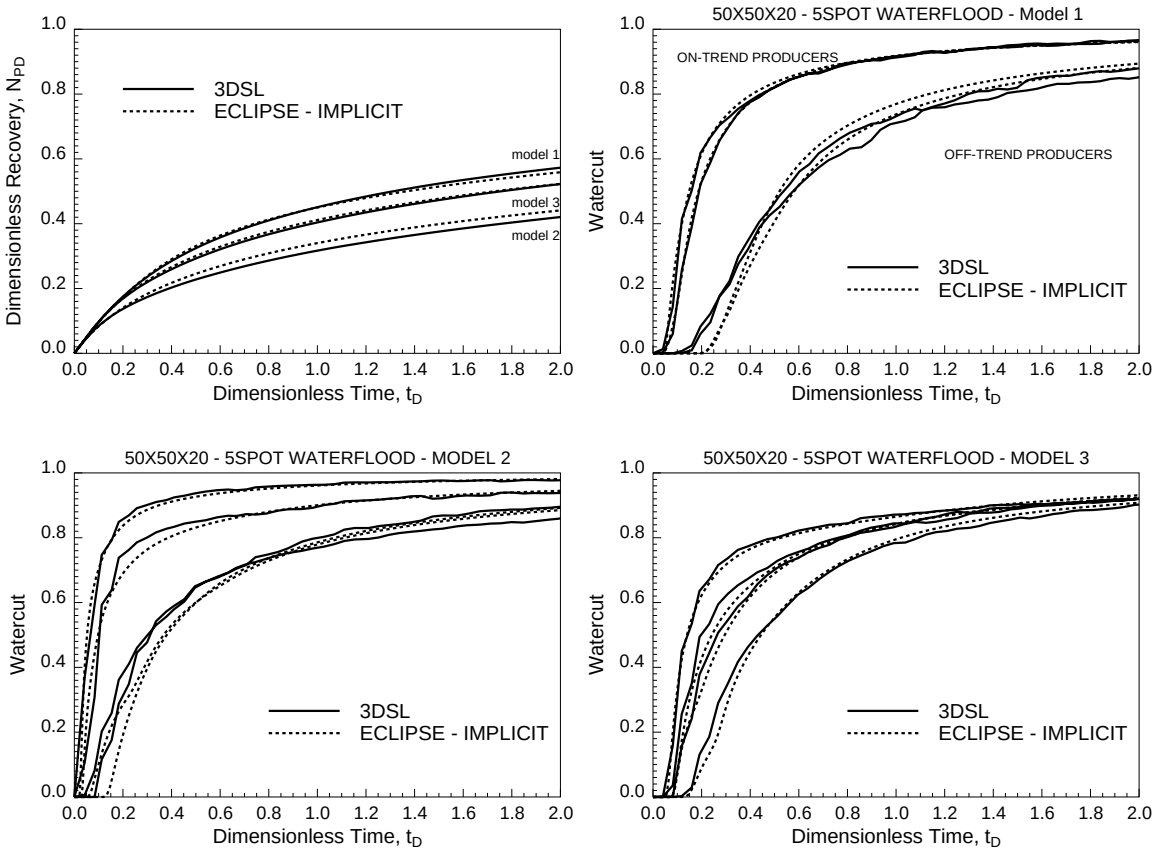


Figure 4.14: Field oil recovery and individual well watercut responses in a full five-spot pattern for three different permeability models.

for model 1. Table 4.2 summarizes simulator performance for each method on each model. The speed-up factor, based on CPU time, for the streamline method over ECLIPSE is between 25–50. The primary reason for these large speed-ups is due to the fact that ECLIPSE required approximately 25 times more matrix solves than 3DSL.

One could argue that the true timing comparison should be between the streamline method and ECLIPSE - IMPES since 3DSL is an IMPES simulator. Model 2 results were also generated using the IMPES method and showed no change in recovery. However, ECLIPSE run time increased to 2370 minutes, a speed-up factor of 110.

| Model | 3DSL | | | ECLIPSE - implicit | | | |
|---|---|---|---|---|---|---|---|
| | CPU (min) | Time Steps | Pressure Solves | CPU (min) | Time Steps | Matrix Solves | Speed-up Factors |
| 1 | 20 | 50 | 25 | 1062 | 206 | 663 | 53 |
| 2 | 22 | 50 | 25 | 600 | 182 | 340 | 27 |
| 3 | 20 | 50 | 25 | 959 | 187 | 599 | 48 |

Table 4.2: Comparison of simulator performance parameters between the streamline method and ECLIPSE for 3 different waterflood 5-spot models.

Since waterflooding is highly stable and numerical diffusion is minimal, the more accurate IMPES formulation in ECLIPSE did not alter the recovery predictions for these problems.

## 4.12 First-Contact Miscible Displacements

First-contact miscible (FCM) displacements are considerably more difficult to model than 2-phase immiscible displacements. The large mobility contrast between the solvent and the oil makes the problem highly nonlinear, while instabilities in the displacement front lead to substantial numerical diffusion in conventional methods. This numerical diffusion can, in turn, incorrectly alter the mobility field and ultimately the displacement behavior. Because of the limitations in conventional methods, other numerical schemes have been proposed for modeling FCM displacements. *Araktingi & Orr* [1] [2] used particle tracking to model flow in two-dimensional heterogeneous cross-sections. *Tchelepi & Orr* [67] developed a hybrid particle tracking/finite-difference method for three-dimensional systems. *Christie & Bond* [18] developed a high order numerical method that used a flux correcting transport (FCT) algorithm for modeling FCM displacements. All methods used non-conventional techniques to improve the calculation of inter-gridblock component fluxes.

The streamline method can also be used to model FCM displacements, however mapping 1D analytical solutions along streamlines does restrict application. Recall

that the method requires flow to be dominated by heterogeneity. Furthermore, there is no interaction between streamlines neighboring in space or between the calculated composition distributions in time, implying that explicit viscous fingering cannot be modeled.

### 4.12.1 1D First-Contact Miscible Solution

*Thiele* [68] presents a detailed discussion on the appropriate 1D solution to map along streamlines, based on the scale at which a FCM displacement occurs. Because of the assumptions inherent in mapping analytical solutions along streamlines, the primary interest is field scale displacements. As such, the *Todd & Longstaff* [73] solution along each streamline will be used, which assumes that viscous fingering occurs at a sub-streamtube scale.

*Todd & Longstaff* [73] noted that accurate predictions of field scale FCM displacements could be made by accounting for viscous fingering in an averaged 1D sense even though the detailed fingering phenomena is a 2D or 3D process. The averaged 1D results show linear scaling of concentrations with distance. The Todd & Longstaff model includes this linear scaling feature and also includes a mixing parameter ($\omega$) to account for the level of fingering between solvent and oil at the gridblock scale. For FCM displacements Eq. 4.1 can be rewritten as,

$$\frac{\partial C_s}{\partial t} + \frac{\partial f(C_s)}{\partial \tau} = 0, \tag{4.25}$$

with the following initial and boundary conditions,

$$\begin{aligned} C_s(\tau, 0) &= C_{s,initial} \qquad \tau \geq 0 \\ C_s(0, t) &= C_{s,injection} \qquad t > 0. \end{aligned} \tag{4.26}$$

The fractional flow, $f$, of solvent concentration, $C_s$, predicted in the Todd & Longstaff model is given by,

$$f(C_s) = \frac{C_s}{C_s + \frac{1-C_s}{M^{1-\omega}}}, \tag{4.27}$$

where the mobility ratio is simply the viscosity ratio between oil and solvent, $M = \mu_o/\mu_s$. Due to mixing of the solvent and oil, the effective phase mobilities are given

by,

$$\mu_{oe} = \mu_o^{1-\omega}\mu_m^{\omega} \qquad \mu_{se} = \mu_s^{1-\omega}\mu_m^{\omega}, \tag{4.28}$$

where the effective mixture viscosity $\mu_m$ is defined by a quarter power mixing rule,

$$\mu_m = (\frac{C_s}{\mu_s^{1/4}} + \frac{1-C_s}{\mu_o^{1/4}})^{-4}. \tag{4.29}$$

Equation 4.28 is used in calculating the total mobility ($\lambda_t$) related to a specific solvent concentration. By setting $\omega$=1 (complete mixing at the gridblock scale) the result is a highly unstable piston-like displacement whereas $\omega$=0 (no mixing) gives the equivalent two-phase displacement with straight-line relative permeabilities.

*Thiele* [68] studied the effect of the mixing parameter on displacement results in comparison with high-order numerical results. Although only one permeability field was used, he concluded that $\omega$ closer to 1 yielded recoveries similar to the numerical results. A special case of the Todd & Longstaff model is *Koval's* [47] model which assumes the mixing parameter is a unique function of mobility ratio only,

$$\omega = 1 - 4\frac{ln(0.78 + 0.22M^{1/4})}{lnM}. \tag{4.30}$$

*Thiele* [68] found that Koval's model mapped along streamlines gave acceptable results when compared with high resolution finite-difference simulations.

Shown is Fig. 4.15 is a 1D FCM profile using Koval's model for $M$=10 ($\omega$=0.725). Again, the total mobility varies from 0.1 to 1.0 as in the waterflood example, but now the change in mobility (the nonlinearity) occurs over a much shorter dimensionless velocity range. This can be interpreted, all else being equal, as the streamline method requiring a greater number of pressure solves for FCM displacements than for waterflood displacements, to capture the nonlinearity accurately.

### 4.12.2 2D Displacement With Different Numerical Methods

Before studying FCM results from the streamline method, one question to ask is, "What is the correct solution to compare against?" As discussed earlier, conventional methods have difficulty modeling FCM displacements. The BP FCT code [19] is designed specifically for miscible displacements in 2D cross-sectional models and

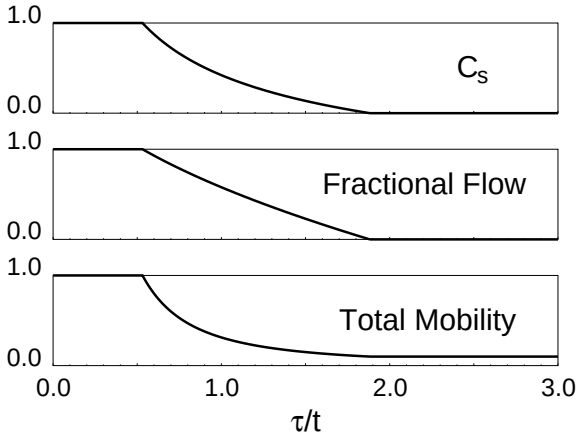


Figure 4.15: FCM Koval model profiles for gas saturation, gas fractional flow, and total mobility as a function of $\tau/t$.

provides a reference to compare against. However, for 3D multiwell problems the only alternative is to compare with ECLIPSE. The purpose of this section is to determine if ECLIPSE can accurately model 2D FCM displacements before examining 3D displacements.

*Thiele* [68] presents FCM results from the BP FCT code for a mildly heterogeneous 125×50 permeability field that will represent the reference solution. For comparison purposes, the following methods are considered; (1) the streamline method with Koval's solution, (2) ECLIPSE fully implicit single point upstream (SPU) weighting scheme, and (3) ECLIPSE fully implicit two-point upstream weighting scheme. The two-point upstream weighting technique provides a better estimate of interblock fluxes than the SPU scheme and thus a more accurate answer containing less numerical error.

Shown in Fig. 4.16 is a comparison of oil recovery predicted by the four methods. Saturation profiles of the solvent at $t_D$=0.3 for each method are shown in Fig. 4.17. The presence of numerical diffusion in the SPU scheme can be clearly seen in Fig. 4.17 in comparison with the two-point scheme and the BP FCT scheme. The increased level of diffusion improves transverse sweep and results in an overly optimistic recovery, compared with the other methods. Figure 4.16 highlights that by using the

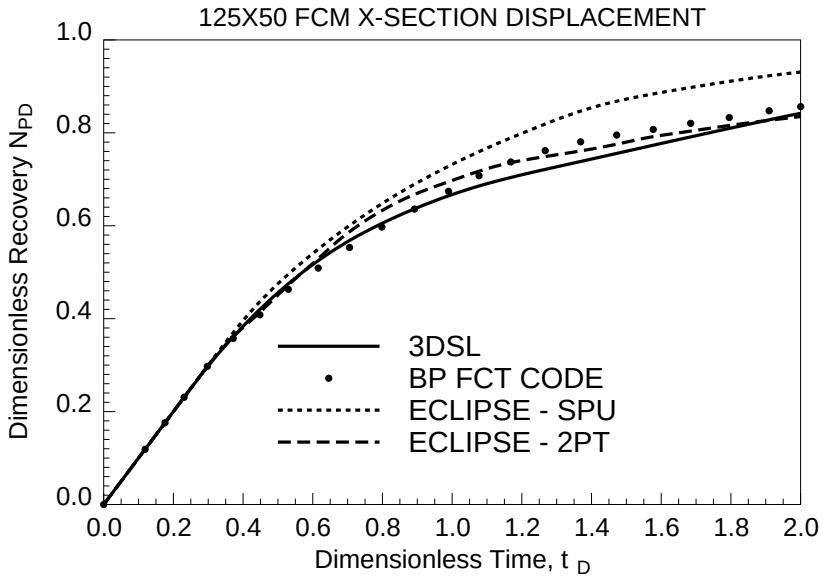


Figure 4.16: Oil recovery for a 2D FCM displacement by 4 numerical methods.

two-point upstream scheme in ECLIPSE, the method can give accurate recovery predictions. It is worth noting for this size problem the two-point upstream scheme was about 5 times slower than the SPU scheme.

### 4.12.3 3D First-Contact Miscible Displacements

The three 50×50×20 permeability fields (Fig. 4.13) used in modeling waterflood displacements are used here for modeling FCM displacements. The well configuration is a 5-spot arrangement with a central injector in the lower 10 gridblocks, and a producer in the upper 10 gridblock of each corner. The fluid mobility ratio is $M$=10 and Koval's model was used for the streamline results. Fully implicit ECLIPSE results were also generated for each permeability field using the two-point upstream weighting method. A summary of recovery curves and individual producer GOR's for each model is shown in Fig. 4.18.

Field recoveries match well for model 3 but less so for models 1 and 2. The difference in matches is due to different levels of numerical diffusion in each model. As

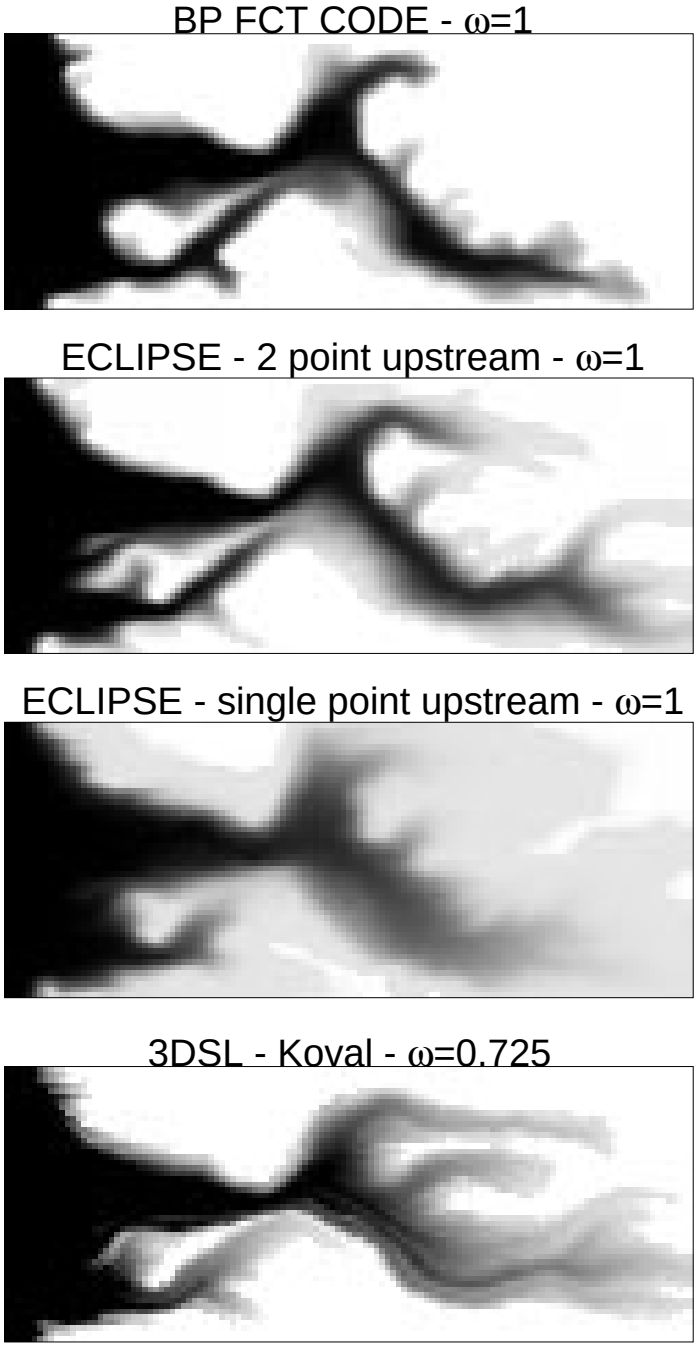


Figure 4.17: Solvent profile in a 125×50 heterogeneous FCM displacement, for four different numerical methods at $t_D$=0.3.

| Model | 3DSL | | | ECLIPSE - implicit | | | |
|---|---|---|---|---|---|---|---|
| | CPU (min) | Time Steps | Pressure Solves | CPU (min) | Time Steps | Matrix Solves | Speed-up Factors |
| 1 | 34 | 50 | 50 | 3980 | 326 | 1327 | 117 |
| 2 | 37 | 50 | 50 | 2361 | 336 | 860 | 64 |
| 3 | 33 | 50 | 50 | 4370 | 362 | 1085 | 132 |

Table 4.3: Comparison of simulator performance parameters between the streamline method and ECLIPSE for 3 different FCM 5-spot models.

was shown in Section 4.9.4, different reservoir heterogeneity characteristics can result in different levels of numerical diffusion. These diffusion effects are amplified in FCM displacements. For model 1, numerical diffusion in ECLIPSE results in delaying breakthrough to the off-trend producers which in turn leads to higher recovery predictions over the streamline method. Finally, note in models 1 & 2 that the individual well GOR profiles predicted by both methods, although not matching, show similar characteristics. The ECLIPSE results appear to be shifted in time relative to the streamline results.

The simulator run time performance results are summarized in Table 4.3. For these 50,000 gridblock models, the streamline method was about 100 times faster than ECLIPSE. As Fig. 4.18 shows, the streamline results also have less numerical diffusion. It is worth noting that the level of numerical diffusion in ECLIPSE could be reduced by using the IMPES method. However, due to the increase in time steps required, the speed-up factor would be three orders of magnitude [70], implying many days per simulation.

## 4.13 Convergence

As discussed in Section 4.8, there is no stability criterion for the streamline method, and any desired time step size between pressure solves ($\Delta t_p$) can be taken. However,

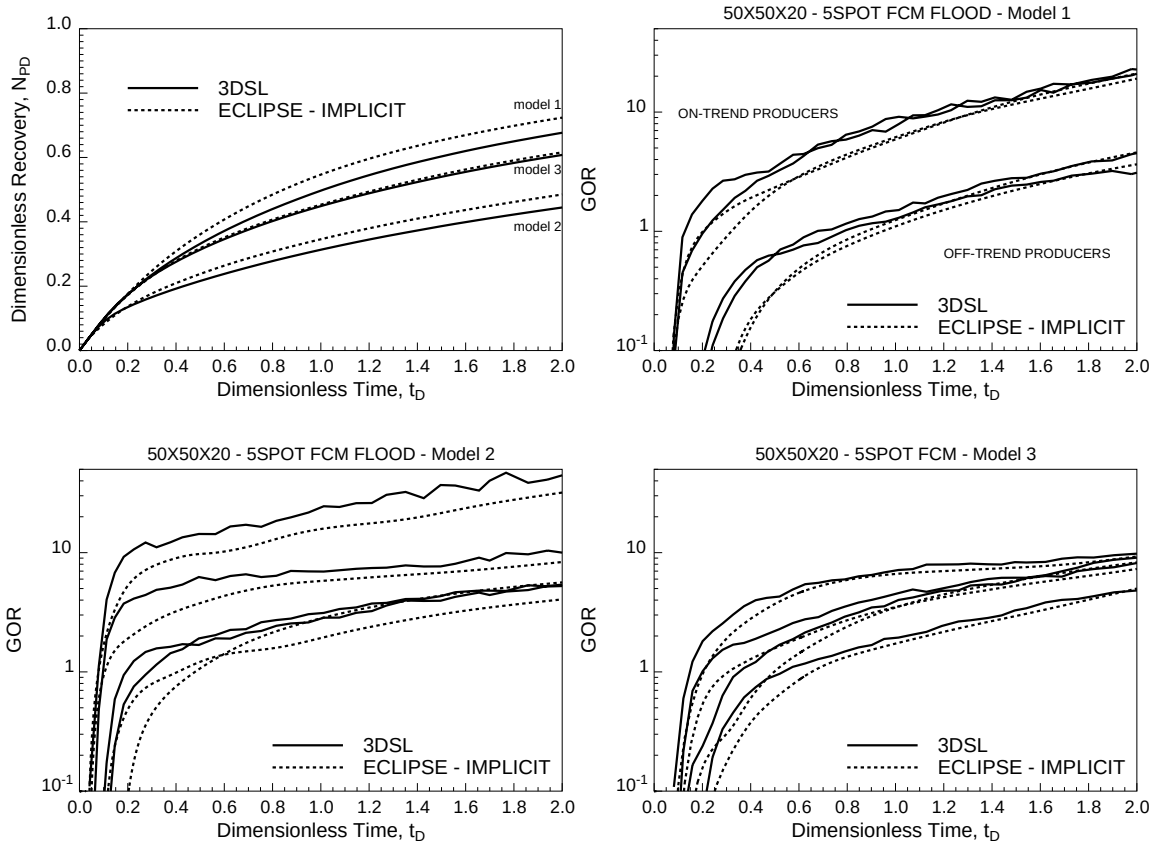


Figure 4.18: Field oil recovery and individual well GOR responses in a full five-spot pattern FCM displacement for three different permeability models.

when modeling nonlinear displacements, the nonlinearity is accounted for by updating the pressure field. The number of updates is dependent on the strength of the nonlinearity which in turn is a function of the mobility ratio, the displacement type, and the level of heterogeneity. Figures 4.19 and 4.20 illustrate the convergence in recovery of the streamline method as the number of pressure solves increases for two different displacement mechanisms. The reservoir model is Model 1 used in the previous sections. These figures show that about 10 pressure solves result in a converged solution for the waterflood, while about 25 pressure solves result in a converged solution for the FCM displacement, over two pore volumes injected. As expected, the more nonlinear problem required a greater number of pressure solves to capture the

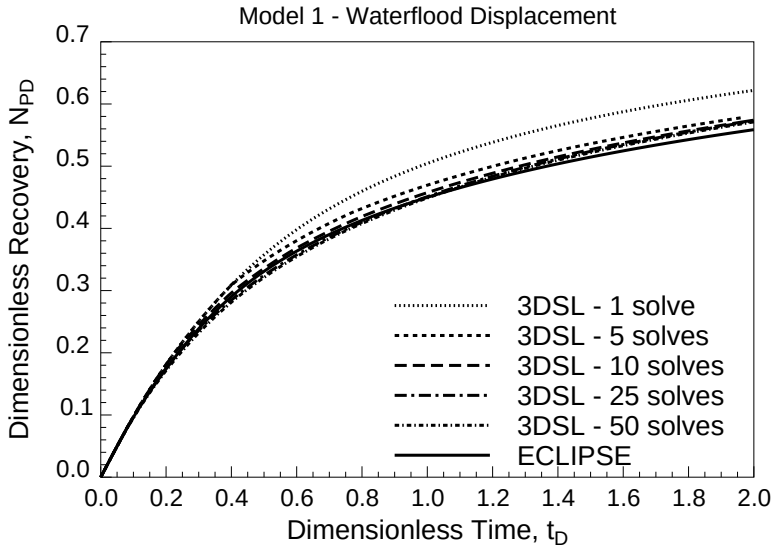


Figure 4.19: Convergence of waterflood displacement recovery as the number of pressure solves for the streamline method are increased.

nonlinearity. Recall that ECLIPSE required 206 pressure solves for the waterflood and 326 for the FCM displacement.

The fact that the streamline method can produce converged solutions using an order of magnitude fewer pressure solves implies that the displacements are only a weak function of the changing fluid distribution (weakly nonlinear). In other words, for heterogeneity dominated displacements, the total mobility field is a greater function of the permeability distribution than the fluid distribution. A displacement that is only weakly nonlinear leads to streamline paths that remain relatively constant as a displacement proceeds. Thus, the required assumption of uniform initial conditions along streamline paths, in order to map analytical solutions, is valid for heterogeneity dominated displacements.

## 4.14 Sensitivity to Streamline Weighting Factor

In Section 4.3, it was assumed that average gridblock properties could be determined based on weighting each streamline's property within a gridblock by its $\Delta\tau_i$ only. The

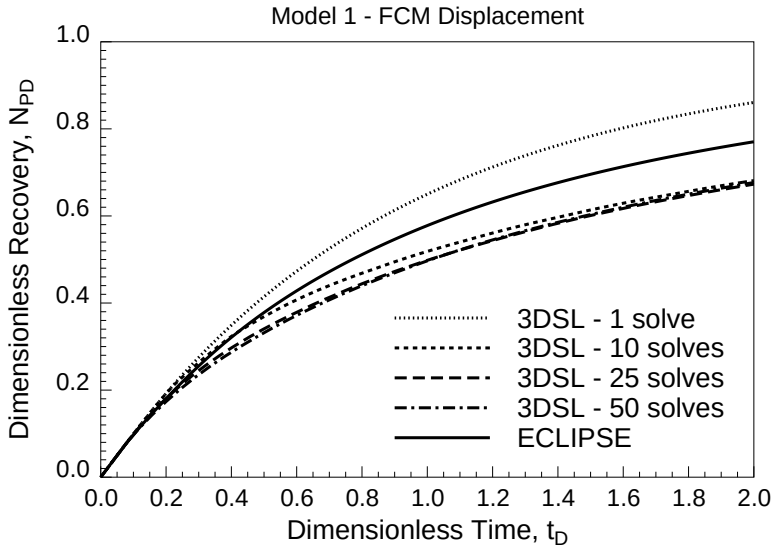


Figure 4.20: Convergence of first-contact miscible displacement recovery as the number of pressure solves for the streamline method are increased.

flux or volume associated with each streamline within a gridblock was ignored, giving the definition for the weighting factor in Eq. 4.11.

In this section, the 125×50 cross-sectional model FCM displacement used in Section 4.12.2 is considered here in the context of four different weighting methods. As the displacement proceeds, the nonlinearity of a FCM displacement will magnify small differences, if any, due to the method of calculation of gridblock properties. The following four cases for studying the effect of $\omega_i$ on displacement performance are considered.

**Case 1** Standard method used for all cases in this thesis. The weighting factor is calculated using the definition of Eq. 4.11. A total of 250 streamlines are launched from the 50 injection block faces. The number of streamlines launched from each face is determined such that each streamline in the model carries approximately the same flux.

**Case 2** A total of 250 streamlines are launched from the 50 injection block faces. The number of streamlines launched from each face is determined such that

each streamline in the model carries approximately the same flux. However, the weighting factor now includes the streamline flux,

$$\omega_i = \frac{q_i^{sl}\Delta\tau_i}{\sum_{i=1}^{n_{gb}^{sl}} q_i^{sl}\Delta\tau_i}. \tag{4.31}$$

**Case 3** Five streamlines are launched from each of the 50 injection block faces. The total number of streamlines remains 250, but the flux assigned to each streamline can vary considerably. The weighting factor includes the streamline flux and is described by Eq. 4.31.

**Case 4** Five streamlines are launched from each of the 50 injection block faces. The weighting factor does not include the streamline flux, but instead is described by Eq. 4.11.

The recovery results for the four cases described above are presented in Fig. 4.21. Solvent saturation profiles at $t_D$=0.25 for each case are shown in Fig. 4.22. There are no differences in recoveries or saturation profiles between the four cases. Clearly, the choice of weighting factor has no effect on the final solution – calculated gridblock properties are the same for each choice. This is expected since gridblock properties are a function of the streamline properties which in turn are a function of the time-of-flight. Ultimately, since the time-of-flight along each streamline in a gridblock is independent of the weighting factor, gridblock properties are also independent of the weighting factor. Furthermore, in the context of the convergence results of Section 4.13, the number of times a pressure field is updated to capture a displacements non-linearity, has a greater impact on displacement predictions than the type of weighting factor used.

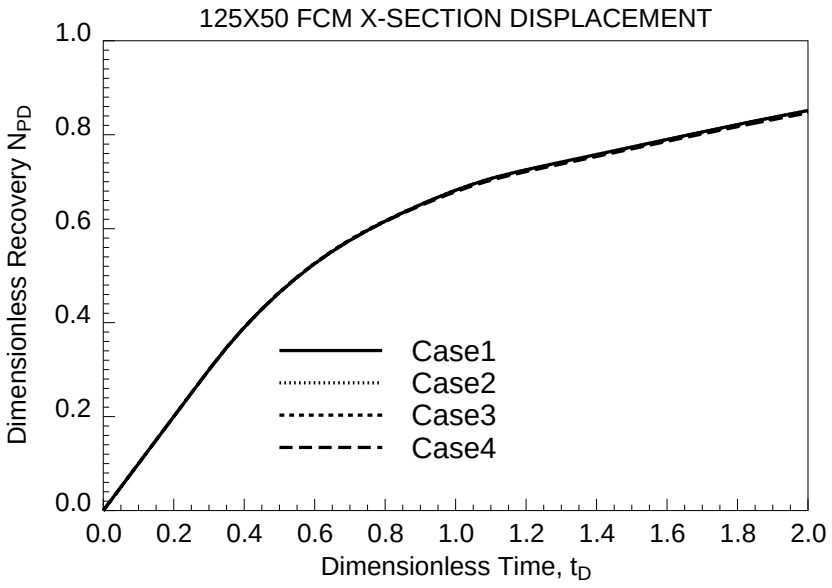


Figure 4.21: Sensitivity of solvent recovery to type of weighting factor method used to determine average gridblock properties.

## 4.15 Gravity Effects

Gravity effects can be accounted for with the streamline method presented in this chapter. Streamlines follow the total velocity field rather than individual phase velocities; thus only gravity effects in FCM displacements for $\omega = 1$ can be modeled.[5] *Blunt et al.* [10] provide a thorough discussion on modeling gravity effects when mapping analytical solutions to the streamlines. They provide detailed comparisons of the streamline method to the BP FCT research code for ten two-dimensional heterogeneous fields. In order to properly compare against the FCT code they also added a small amount of longitudinal and transverse dispersion to the streamline method to replicate numerical dispersion in the FCT code.[6] The authors noted that for unit mobility ratio ($M = 1$) displacements, the streamline method gave acceptable results

[5]For $\omega$=1 the phase properties are identical at the gridblock scale and Eq. 4.1 can be used to describe the movement of phases.

[6]Transverse dispersion is added by retracing streamline paths multiple times with a random component added to the tracing algorithm.

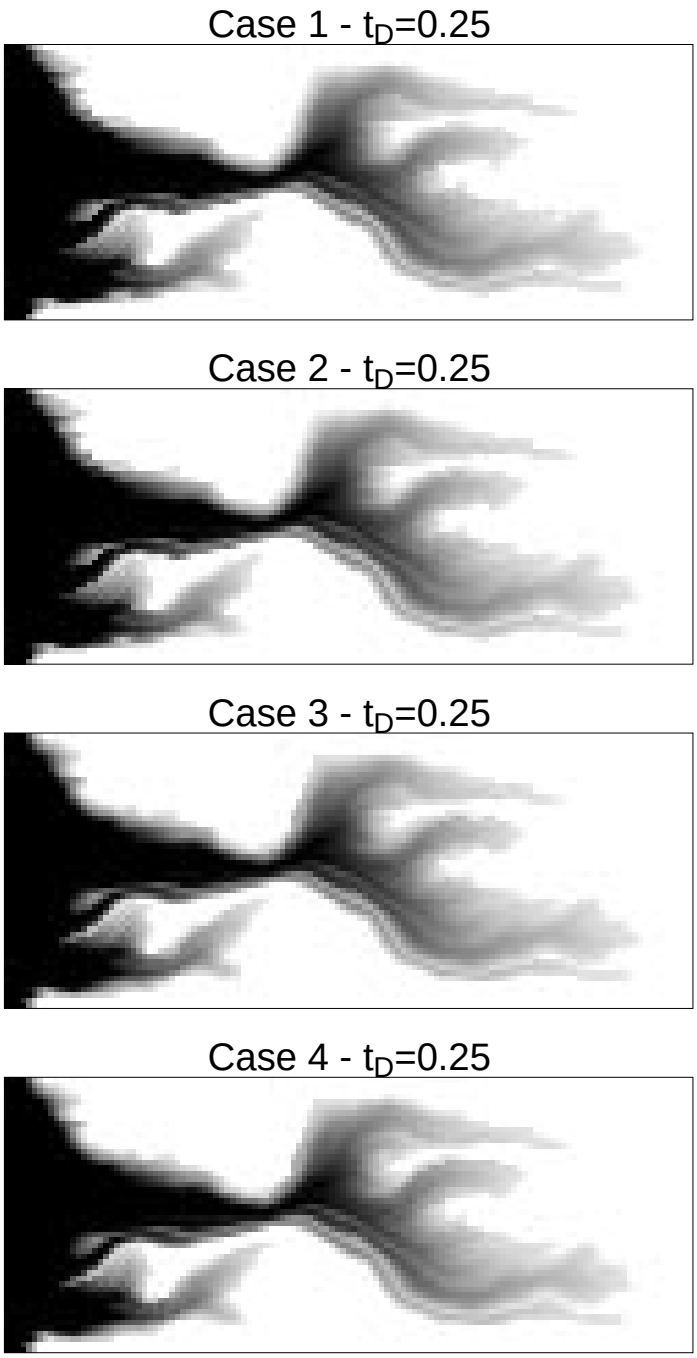


Figure 4.22: Solvent profile in a 125×50 heterogeneous FCM displacement, using four different streamline weighting factor methods to calculate average gridblock properties.

for $N_g < 2$. The method was also applied to non-unit mobility ratio ($M > 1$) first-contact miscible displacements. For $M < 10$ the streamline method gave acceptable results for $N_g < 1$. Additionally, they noted that the streamline method was 100 to 150 times faster than the FCT results. This was due to the fact that the streamline method required 20-40 time steps per pore volume injected, whereas the conventional method required 2000-3000 times steps per pore volume injected.

*Blunt et al.* [10] comment that the method works best for cases where the principal flow directions are dominated more by heterogeneity than by gravity. Although not discussed in their paper, one difficulty with accounting for gravity even in single phase displacements is that for large gravity forces, circulation cells occur. Thus, a streamline rather than joining injectors to producers, can become a loop with no beginning or end. The difficulty now is that there are no analytical solutions to map to a closed domain without a starting boundary. This problem can be overcome by mapping numerical solutions to streamlines. Rather than redo work already presented by *Blunt et al.* [10] subject to the above limitations, gravity effects using the streamline method will be accounted for by a numerical approach and will be discussed in Chapter 6.

## 4.16 Field Applications

The examples given in the previous sections all demonstrate that the streamline method is fast and accurate for heterogeneity dominated displacements. This section illustrates some practical uses of the streamline method due to its speed.

### 4.16.1 Million Gridblock Waterflood

The ability to solve large models ($10^6$ gridblocks) is important since it allows for increased resolution of the permeability field. This is especially important if permeability is considered to have a dominant effect on displacement performance. Additionally, large models increase the number of gridblocks between wells and allow for greater resolution of displacement fronts. For large models it is important to limit

the number of times needed to solve for the pressure and saturation fields, since this represents the majority of CPU time. The decoupling of heterogeneity from fluid flow makes the streamline method well suited to solve large problems specifically because of the reduction in the number of time steps required.

To illustrate the use of the streamline method on a large model, consider a fine scale 1.16 million gridblock (220×220×24) permeability field (Fig. 4.23). The field was created using the sequential Gaussian simulation method in GSLIB [26]. The permeability field has an anisotropic structure with an on-trend correlation length of $\lambda_c = 0.6$, off-trend $\lambda_c = 0.05$, and a vertical correlation length of $\lambda_c = 0.6$. Imposed on the model was a single 5-spot well pattern with a central injector in the lower 12 layers and a producer in the upper twelve layers in each corner. Using the 1D profile in Fig. 4.12, a fine scale waterflood displacement was generated with the streamline method in 50 hours on a standard workstation. Because of time and memory constraints, ECLIPSE implicit results were generated on an upscaled 72,000 gridblock (110×110×6) model and required 23 hours. For reference, upscaled streamline results were also generated and required 0.75 hours. Note that simple geometric upscaling of absolute permeabilities was used, with no upscaling of relative permeabilities. Permeability histograms for each field are shown in Fig. 4.24. The upscaling process reduced the standard deviation in the distribution from 102 $mD$ to 70 $mD$ and, more importantly, reduced the concentration of high permeability values.

Figure 4.25 provides a visual comparison of the water saturation in the five-spot at $t_D$=0.2 for each model. Because of the absence of numerical diffusion, both streamline cases show water breakthrough at all four producers, not just the on-trend producers as with ECLIPSE. Also, both streamline solutions show resolution to a single gridblock scale.

Figure 4.26 compares the oil recovery of the three cases. Note that there is a greater change in recovery due to upscaling than due to the choice of simulation method. For this problem, having the ability to capture all of the first order influences (due to permeability) outweighs the approximations in mapping analytical solutions to the streamlines. The upscaled finite difference solution overestimates recovery by 5% as compared with the fine scale results.

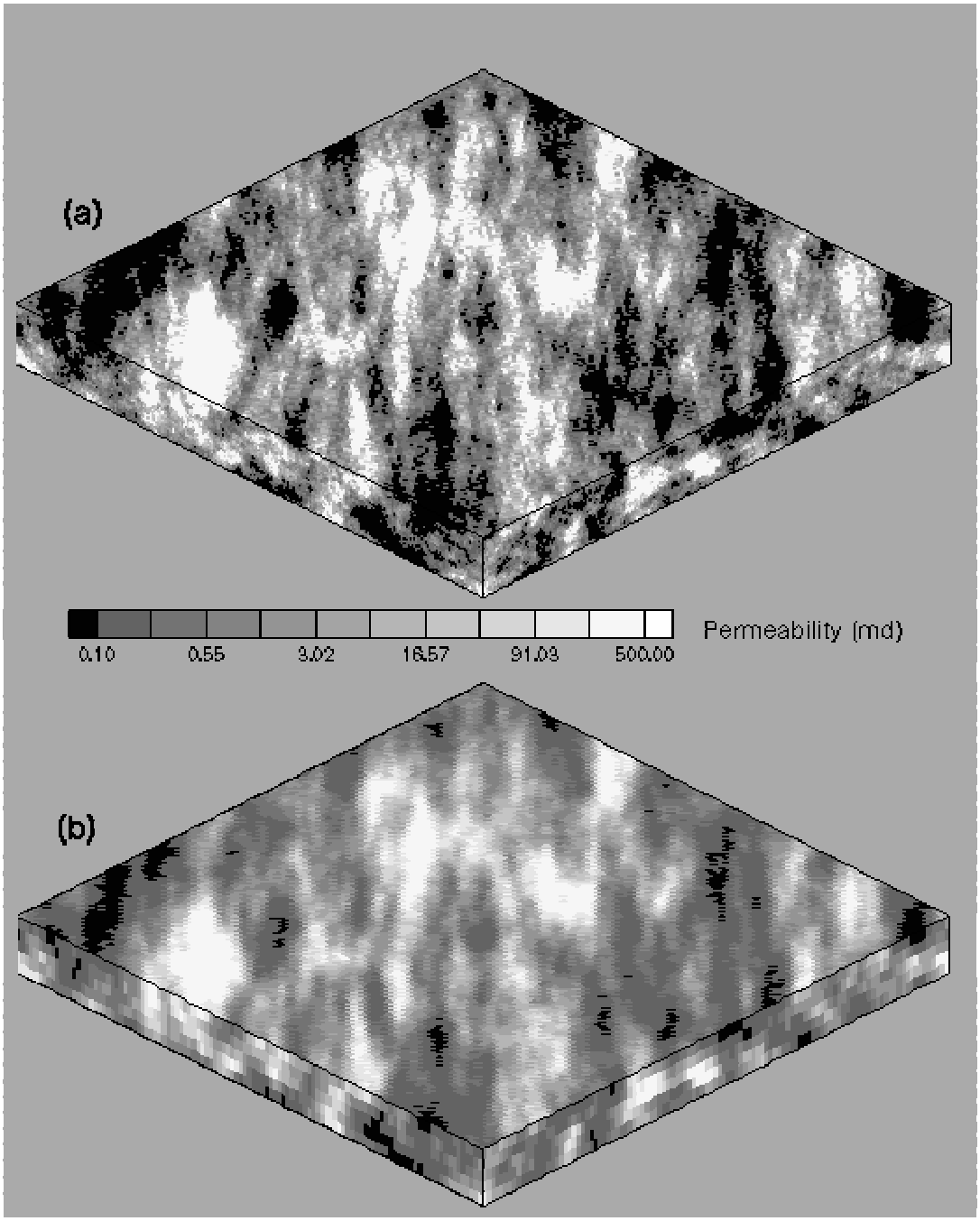
(a)
0.10
0.55
3.02
16.57
91.03
500.00
Permeability (md)
(b)

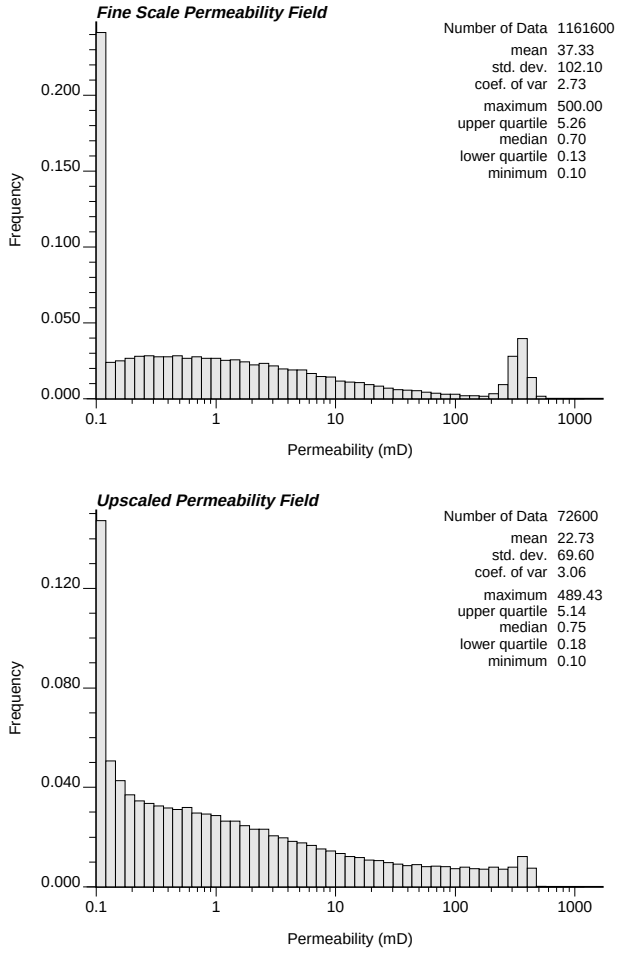


Figure 4.24: Histograms of fine scale million gridblock permeability field and upscaled 72,600 gridblock permeability field.

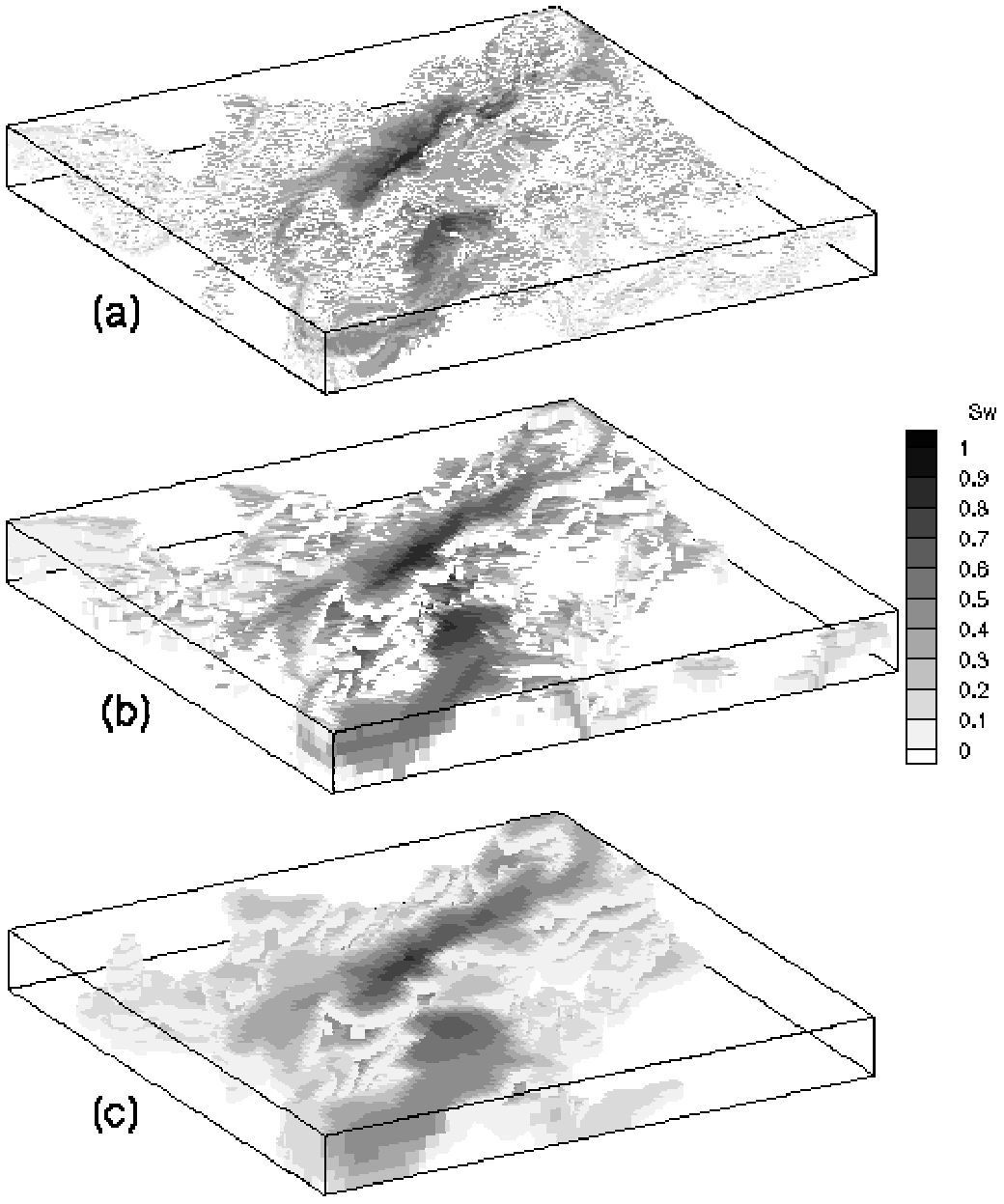
(a)
(b)
(c)
Sw
1
0.9
0.8
0.7
0.6
0.5
0.4
0.3
0.2
0.1
0

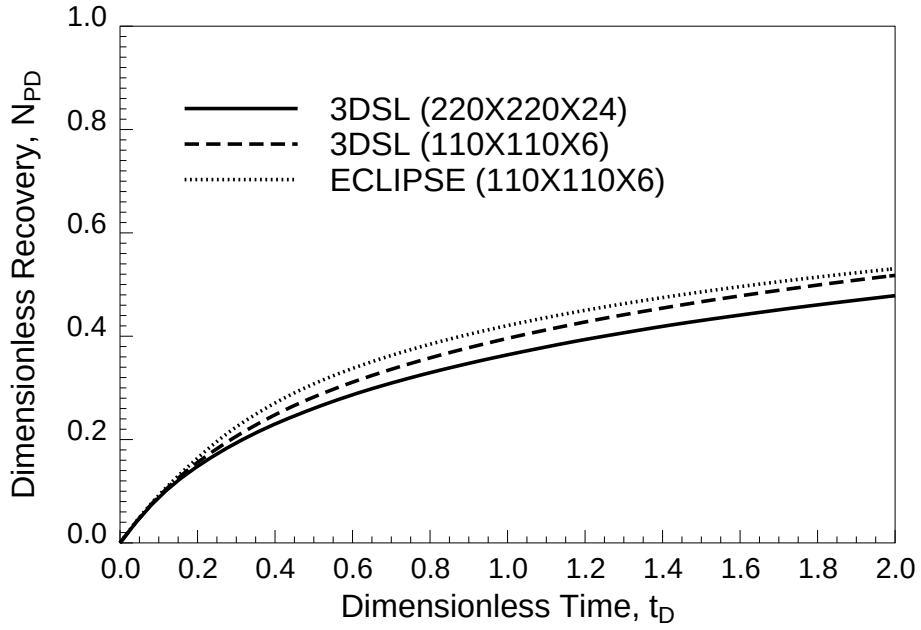


Figure 4.26: Waterflood recovery comparisons between the million gridblock model and an upscaled 72,600 gridblock model.

### 4.16.2 Screening Equiprobable Realizations

The streamline method is also ideally suited to screen multiple geostatistical realizations before resorting to a more conventional solution method [69]. As an example, consider a 100,000 gridblock waterflood model with 8 producers, 9 injectors, and one horizontal producer, completed in 5-spot patterns (Fig. 4.27). The injectors and vertical producers are full interval completions, while the horizontal producer is completed in layer five only. Thirty equiprobable realizations were created using sequential Gaussian simulation. First, the streamline method was used to generate the corresponding oil recovery curves for each permeability field. Next, the permeability fields resulting in the high and low recoveries were rerun using ECLIPSE. The oil recovery results are summarized in Fig. 4.28. Clearly, the range in recovery predicted by the streamline method is also predicted by the two ECLIPSE runs. Note however, that the ECLIPSE results are shifted consistently upward, which is attributed to numerical diffusion effects within ECLIPSE. For these multiwell field cases, 3DSL results

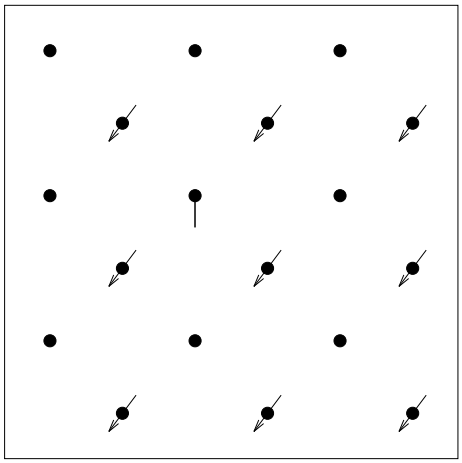

Figure 4.27: Well locations for 100×100×10 field model, 8 producers, 9 injectors, and 1 horizontal producer.

for a single image were generated in 1.5 hours, while ECLIPSE implicit results were generated in 140 hours for the low recovery case and 300 hours for the high recovery case. The speed up for this large waterflood problem is now 100-200 times, versus 50 times for the 3 smaller 50,000 gridblock waterfloods studied in Section 4.11.2.

For existing fields with large amounts of production data to honor, rather than using the streamline method to screen multiple images, the method can be used in the history matching process since multiple runs required to obtain a history match can be performed very quickly [55, 27, 28]. Once a reservoir model that satisfies historical data is built, either the streamline method or a conventional simulator could then be used for prediction purposes.

## 4.17 Chapter Summary

This chapter outlined the use of the streamline method to predict displacements when mapping analytical solutions to the streamlines. For tracer flow, the method is exact and can quantify the levels of numerical diffusion in conventional methods. Although mapping analytical solutions assumes that uniform initial conditions prevail along

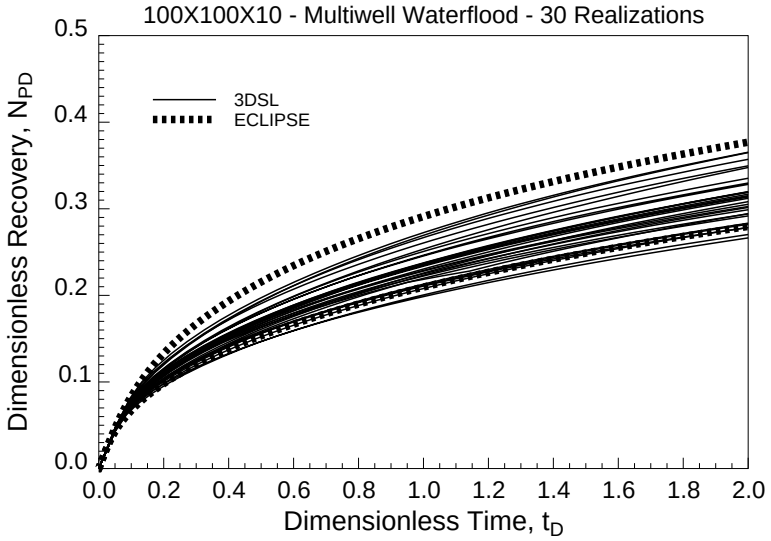


Figure 4.28: Application of the streamline method to screen realizations before running the high and low recovery models with ECLIPSE.

streamline paths, it was shown that this is a good assumption for flow dominated by heterogeneity. For nonlinear displacements like waterflood and FCM displacements, streamline paths are recalculated periodically to honor the changing mobility field. A key point is that the number of recalculations of the streamline paths (pressure field) required to reach a converged solution was 10 to 100 times less than conventional implicit finite difference methods giving speed-up factors between 1 and 2 orders of magnitude. Because of speed, the streamline method is also ideally suited to solving large problems ($10^6$ gridblocks) or screening geostatistical images. As shown, having the ability to model permeability fields with greater resolution did result is more pessimistic recovery predictions.

Mapping analytical 1D solutions is a very fast and accurate method with no numerical diffusion or mixing. However, mapping 1D analytical solutions also restricts the range of displacements that can be properly modeled. Any case that results in nonuniform initial conditions along streamlines cannot be modeled. Examples include reservoirs with nonuniform initial saturations, or changing well patterns. Additionally, only limited gravity effects can be accounted for in FCM displacements.

Multiphase gravity effects cannot be modeled. Accounting for gravity and nonuniform initial conditions are requirements to extend the streamline method to real field problems. Methods to overcome these limitations are discussed in Chapters 5 and 6.

# Chapter 5

# Mapping 1D Numerical Solutions

## 5.1 Introduction

This chapter describes mapping numerically generated solutions along streamlines. This idea was first proposed by *Bommer & Schecter* [11] to model uranium leaching in 2D porous media. The advantage of mapping numerical solutions is that a uniform initial condition along a streamline is no longer required. The method involves taking the conditions that exist along a recalculated streamline path and moving them forward in space and time within a 1D numerical solver. The new conditions are then mapped back to the underlying gridblocks which the streamline passes through. Because the workings of the 1D solver are completely decoupled from the full 3D problem, the numerical method is straight forward to implement into a 3D model.[1]

The process of moving the existing grid saturations forward along updated streamlines at each time step is equivalent to moving saturations along pathlines. *Bear* [8] describes a pathline for a fluid particle as the locus of its positions in space as time passes. For displacements where the streamline paths do not change with time, pathlines and streamlines are equivalent. However, for nonlinear displacements or cases with changing boundary conditions, the true motion of fluids is along pathlines. In Chapter 4, fluid pathlines were ignored. This was a valid assumption for heterogeneity dominated displacements with constant boundary conditions. In this chapter, fluid

[1]Some results from chapters 4 and 5 have been published in *Batycky et al.* [6, 5].

pathlines are approximated by piecing together the multiple streamlines that a fluid element will intersect over its lifetime. In other words, a fluid element is moved along the current streamlines for a small time and then the streamline paths are updated and the movement continued. Chapters 5 and 6 will show that moving fluids along pathlines extends the streamline method to a greater range of displacement problems.

## 5.2 Mapping a 1D Numerical Solution to a Streamline

If the multiphase gravity term in Eq. 3.13 is assumed to be $G_i = 0$, then Eq. 3.13 reduces to the following one-dimensional equation along a streamline,

$$\frac{\partial S_j}{\partial t} + \frac{\partial f_j}{\partial \tau} = 0, \tag{5.1}$$

implying that saturations are only a function of the total convective velocity field. Eq. 5.1 is a first-order hyperbolic PDE with the following initial condition at time $t^n$,

$$S_j = S_j(\tau, t^n), \tag{5.2}$$

and a constant flux boundary condition at $\tau$=0 (injection well location) of,

$$f_j = f_j(0, t^n). \tag{5.3}$$

$\tau$ represents the coordinate along a particular streamline in 3D space. These are the same equations that are solved in Chapter 4. However, the key advantage of a numerical method is that the initial condition is no longer required to be uniform but can vary along the streamline. The trade-off is that additional CPU time is required to calculate new solutions to Eq. 5.1 as opposed to the simple scaling rule used for analytical solutions.

### 5.2.1 Picking Up Initial Conditions From Streamlines

Once the pressure field and streamline paths are recalculated (Fig. 5.1.b), the first step is to define the saturation distribution present along a recalculated streamline

path. Saturation versus time-of-flight information is recorded for each streamline traced from injector to producer. Figure 5.1.c is a simple picture of this recording process. A new saturation value is recorded over a $\Delta\tau_{blk}$ each time the streamline enters a new gridblock. Because $\Delta\tau_{blk}$ can vary between gridblocks, the $S$ versus $\tau$ information is defined on an irregular $\tau$ grid. This behavior is obvious if one considers a streamline being traced in a quarter five-spot pattern on a regular Cartesian grid. $\Delta\tau_{blk}$ will be very small near the producer and injector but quite large in the middle of the domain. Thus, in $\tau$ space there will be greater resolution where flow velocities are high than where flow velocities are low. The solution in $\tau$ space results in a natural grid refinement of the 1D solution.

Before the $S$ versus $\tau$ profile can be passed to the 1D numerical solver, the information is transformed onto a regularly spaced $\tau$ grid (Fig. 5.1.d). Transforming onto a regular 1D grid simplifies the calculation of internode fluxes within the 1D solver. The number of nodes to use for the regularly spaced $\tau$ grid is based on the number of gridblocks that a streamline passes through multiplied by a factor of two. Naturally, longer streamlines will contain more nodes, while shorter streamlines will contain less nodes. For each streamline, saturation values are assigned to the regular $\tau$ grid such that,

$$\int_0^s S_j d\tau|_{regular} = \int_0^s S_j d\tau|_{irregular}. \tag{5.4}$$

By honoring Eq. 5.4, mass is always conserved in the transformation process.

Transforming onto a regular 1D grid results in averaging of saturations, and represents one source of numerical diffusion in the streamline method. As an example, the effect of the transformation method can be seen by differences in saturation profiles between Fig. 5.1.c and Fig. 5.1.d, where the magnitude of local high saturation values have been reduced.

### 5.2.2 The 1D Numerical Solver

With the initial information along a streamline defined on a regularly spaced $\tau$ grid, the next step is to move the saturations forward in time by $\Delta t$. For simplicity, Eq. 5.1 is solved using a standard single-point upstream (SPU) weighting method

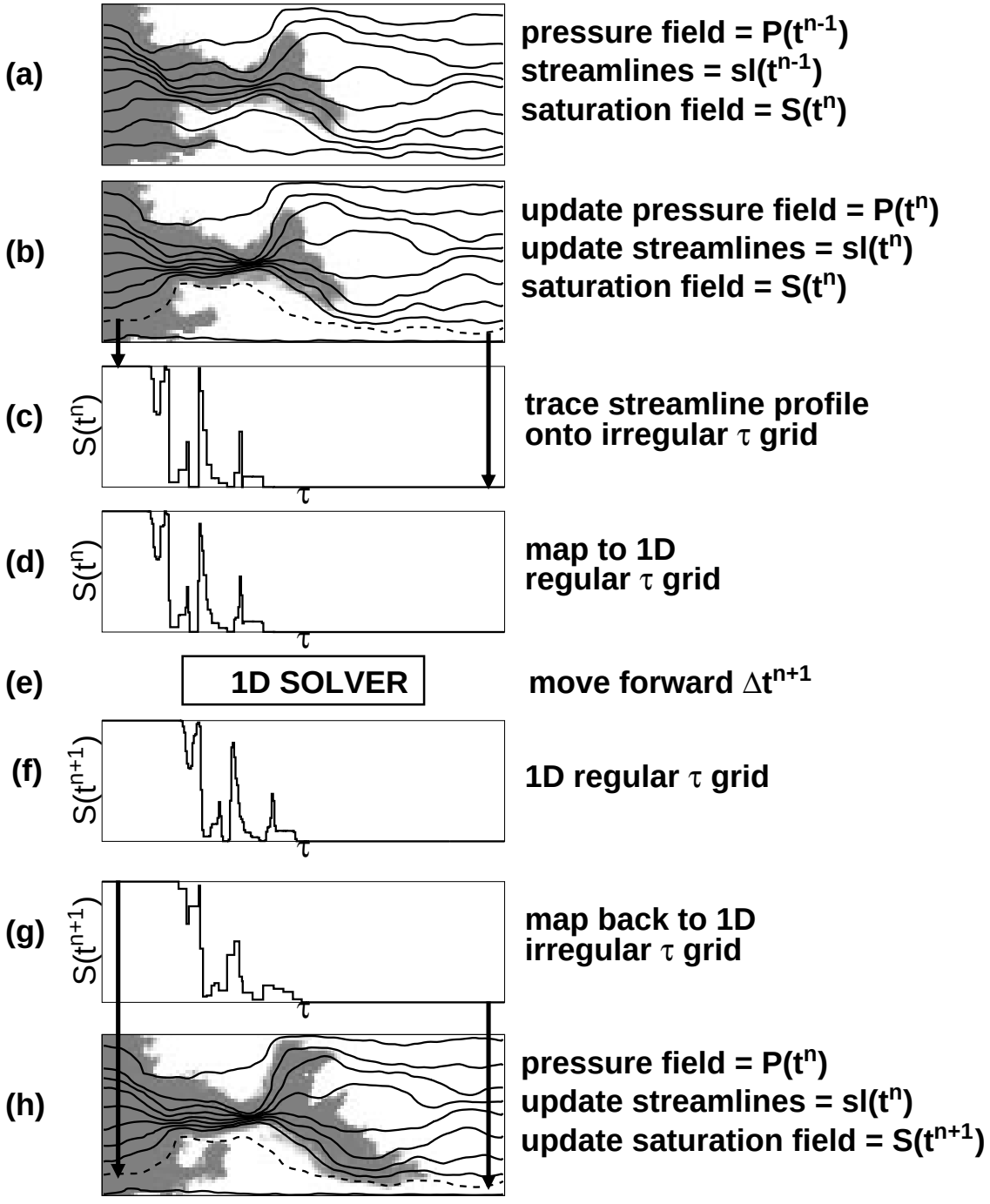


Figure 5.1: Pictorial of picking up a solution from the saturation grid, moving it forward, then mapping to a new saturation grid.

that is explicit in time. Discretization of Eq. 5.1 gives the saturation at the end of the $n^{th}$ time step for node $i$ as,

$$S_i^{n+1} = S_i^n - \frac{\Delta t_{sl}^{n+1}}{\Delta \tau_{sl}}(f_i^n - f_{i-1}^n) \tag{5.5}$$

where $\Delta t_{sl}^{n+1}$ is the current time step size along a streamline and $\Delta \tau_{sl}$ is the time-of-flight distance between nodes for a given streamline.

A stable solution to Eq. 5.5 is governed by the value of the Courant Number along a streamline,

$$N_c^{sl} = \frac{\Delta t_{sl}\, v_{max}}{\Delta \tau_{sl}}, \tag{5.6}$$

where $v_{max}$ represents the maximum wave speed of all the saturations present along the streamline. For an explicit in time method, the maximum stable time step size allowable for solving Eq. 5.5 is determined by the Courant-Fredrich-Lewy stability criterion, $N_c^{sl} \leq 1$. The fastest saturation velocity cannot travel more than one $\tau$ node per time step. Using Eq. 5.6, the maximum time step size for Eq. 5.5 is defined as,

$$\Delta t_{sl} \leq \frac{N_c\, \Delta \tau_{sl}}{v_{max}}, \tag{5.7}$$

where $v_{max}$ typically represents the leading shock speed. For each streamline traced in the domain, Eq. 5.5 is solved multiple times until,

$$\Delta t = \sum_{n=1} \Delta t_{sl}^n. \tag{5.8}$$

The numerical solution of Eq. 5.1 does result in numerical diffusion. *Lantz* [50] quantified the level of numerical diffusion for a SPU scheme in terms of a numerical Peclet Number ($N_{pe}$). The Peclet Number for each streamline is given by,

$$N_{pe}^{sl} = \frac{2}{1 - N_c^{sl}}. \tag{5.9}$$

Since $N_c^{sl}$ is defined based on the leading shock speed, $N_{pe}^{sl}$ characterizes the level of numerical diffusion at the leading shock along each streamline. For tracer and FCM displacements, $N_c^{sl}$=0.9999, giving a Peclet number for the leading front of $N_{pe}$=20,000. Thus, for tracer and FCM displacements, there is minimal numerical diffusion associated with the 1D solver.

### 5.2.3 Mapping Updated Solution Back to Grid

After a streamline solution has been moved forward by $\Delta t$ on the regularly $\tau$ spaced nodes, it is transfered back to the original irregular $\tau$ grid. Again, this transfer is a source of numerical diffusion as seen by the differences between the saturation profiles in Fig. 5.1.f and Fig. 5.1.g. Local high and low saturation values are averaged out over certain locations along the $\tau$ coordinate. This transformation has a greater averaging effect on changing the saturation profile than any numerical diffusion associated with the 1D solver.

Once the saturation variables are transformed to the irregular $\tau$ grid they can then be mapped onto a *new* saturation grid. Within the new grid, saturation properties for each gridblock are accumulated until all streamlines have been traced in the domain. After all streamlines have been traced and mapped to the new grid, average gridblock saturations are calculated using the time-of-flight weighting method discussed in Section 4.3 (Eq. 4.12). This latter averaging process represents the major source of numerical mixing in the streamline method and is discussed in detail in Section 5.6. Rather than using Eq. 4.13, the gridblock average total mobility is now determined using,

$$\bar{\lambda}_{t,gb} = \sum_{j=1}^{n_p} \frac{k_{rj}(\bar{S}_{gb})}{\mu_j}. \tag{5.10}$$

With all grid fluid properties now defined at the new time level, the properties are copied back to the original saturation grid.

## 5.3 Missed Gridblocks

Not all gridblocks will contain a streamline when tracing from injectors to producers. These missed gridblocks are assigned properties in a different manner than the method discussed in Section 4.4, when analytical solutions were mapped to streamlines. The key difference when mapping numerical solutions is the requirement of an injection boundary condition for the numerical solution. The injection conditions is defined by tracing from missed gridblocks back until an injector is reached. The properties along the streamline are then moved forward in the manner discussed in the above

section. However, when mapping properties back to the underlying saturation grid, only those gridblocks that did not have a streamline (missed gridblocks) are assigned updated saturations.

Missed gridblocks typically have very low flow rates associated with them and thus very large $\tau$'s. When mapping to and from the refined 1D $\tau$ grid, these large $\tau$'s tend to under weight the saturation values of upstream gridblocks and would result in unusually low saturation values being reassigned to upstream gridblocks that already carry streamlines in them. This is why in the remapping, only the missed gridblocks are assigned properties.

## 5.4 Time Stepping

As when mapping analytical solutions, an underlying idea is that the streamline paths are allowed to change in time to honor the changing total mobility field. Unlike mapping analytical solutions, the requirement of uniform initial conditions along recalculated streamline paths is no longer necessary. The method is completely general when mapping numerical solutions.

To move a 3D solution forward in time from $t^n$ to $t^{n+1} = t^n + \Delta t_p^{n+1}$ the following steps are:

1. At the start of a new time step, $t^{n+1}$, solve for the pressure field $P$ using Eq. 3.7. Recall that rate or pressure constraints are defined for the new time step $t^{n+1}$ whereas the mobility field is defined from the mapping at the previous time step $t^n$ (an IMPES method).

2. Apply Darcy's Law (Eq. 3.5) to determine the total velocity at gridblock faces.

3. Trace streamlines from injectors to producers as outlined in Chapter 3. While tracing a streamline do the following:

   (a) Pick up the current saturation information from each gridblock that the streamline passes through. In this manner, a profile of saturation versus

$\tau$ is generated for the streamline at time $t^n$ (Fig. 5.1.c). Transform to a regular fine spaced $\tau$ grid (Fig. 5.1.d).

(b) Pass the saturation profile into a 1D numerical solver and move the saturations forward by $\Delta t_p^{n+1}$ by solving Eq. 5.1 (Fig. 5.1.e).

(c) Map the new saturation profile back to the original streamline $\tau$ grid (Fig. 5.1.g), then to a new saturation grid.

4. Average all the streamline properties within each gridblock of the new grid to determine the saturation distribution at $t^{n+1}$ (Fig. 5.1.h).

5. Return to step 1.

The time step size between pressure solves is defined as $\Delta t_p$. The time step size between saturation remappings to the underlying grid (convective step along streamlines) is defined at $\Delta t_c$ and is limited by the CFL constraint for an explicit scheme. This constraint requires that fluid cannot move more than one gridblock per convective time step.

In a conventional IMPES scheme, the value of $\Delta t_c$ is based on the global grid CFL constraint which is determined by the largest flow velocity in the domain – typically near a well.[2] This leads to very small values of $\Delta t_c$. Fronts far from wells are moved at less than the optimal one gridblock per convective step.[3] Moreover, the pressure field is typically recomputed at each $\Delta t_c$. This means that $\Delta t_p = \Delta t_c$ in a conventional method and the pressure field is recomputed an unnecessarily large number of times.

In a conventional implicit scheme there is no constraint on the time step size, but the trade-off is convergence problems and increased numerical diffusion over the IMPES scheme.

For the streamline method, $\Delta t_c$ and $\Delta t_p$ are completely decoupled by moving fluids along streamlines. There is no longer a global grid CFL constraint, and typically $\Delta t_p >> \Delta t_c$. Furthermore, $\Delta t_c$ in the streamline method is much greater than $\Delta t_c$ in a

[2]Grid refinement around wells can actually make the maximum size of $\Delta t_c$ even smaller.

[3]An adaptive implicit finite-difference method, whereby a fully implicit scheme is used near wells while an IMPES scheme is used away from wells, can overcome this problem.

conventional finite-difference method. The constraint on the convective time step size is now within the 1D solver giving a local streamline CFL constraint (Section 5.2.2). Thus for each streamline, many small time steps are taken within the 1D solver to move a solution forward by $\Delta t_c$. Solving multiple 1D equations along streamlines is much faster than solving the full 3D equation multiple times to reach a desired $\Delta t_c$. Additionally, for each streamline the fastest front is moved at the optimal local CFL number. Thus for tracer and FCM displacements where the front velocity is 1 for all saturations, all fronts are moved at a CFL number of 1 along streamlines. That is, the front moves one $\tau$ interval per $\Delta t_{sl}$.

By removing the global grid CFL constraint the issue of converged solutions is still present, as was discussed in Chapter 4. Convergence of the numerical method is discussed in Section 6.5.

## 5.5 Volume Balance Errors

With the numerical mapping method, gridblock saturations are picked up from the underlying grid, moved forward, and then mapped back down. Because grid information is explicitly moved forward, there should be no need for a time correction, as was required when mapping analytical solutions (Section 4.7). However, the process of mapping back to the underlying grid and then determining average gridblock saturations using the $\Delta\tau$ weighting method (Section 4.3), does not ensure that volume is conserved. The volume balance problem occurs because saturations rather than explict volumes are moved along streamlines. Thus a time correction is still required after each remapping step to conserve volume exactly. For displacements studied here, the time correction is on the order 0.01% – 0.1% of the true time increment.

## 5.6 Mixing Due to Remapping

After all streamlines and missed gridblocks have been traced, average gridblock saturations are calculated as described in Section 4.3. For any gridblock with two or more streamlines, the gridblock property is an average based on the properties of all the

streamlines. Streamlines communicate with each other on a gridblock scale each time this averaging process occurs. In the numerical mapping technique, these average properties become the new initial conditions that are moved forward at the next time step. The more times that mapping back to the underlying grid occurs, the more mixing that results. This mixing process represents the main source of numerical diffusion when mapping numerical solutions to streamlines. The mixing effect occurs because saturation information is only known to within a single gridblock scale.

To illustrate the mixing effect due to remapping, consider the tracer displacement shown in Fig. 5.2. Recall that with a tracer displacement, the exact solution (diffusion free) can be obtained using the method discussed in Chapter 4. The exact solution is shown in column 1. Column 2 represents the saturation profile by mapping to the underlying grid only once to reach $t_D$=0.6. The entire time step is taken within the 1D solver and the final solution is almost identical to the reference answer. For the third column of saturation profiles, three remapping steps were taken to reach $t_D$=0.6. There is now more mixing present at $t_D$=0.4 and $t_D$=0.6 than compared with the analytical results. Finally, in column 4 are the resulting saturation profiles when taking 6 time steps to reach $t_D$=0.6. Clearly, the amount of mixing increases at each time step, and at $t_D$=0.6 mixing in the column 4 picture is greater than in the previous columns at $t_D$=0.6. Figure 5.2 illustrates that when mapping 1D numerical profiles, the solution at a new time step is dependent on the solution at the previous time step. Any previously mixed saturations are moved forward and remixed at the end of the next time step. On the other hand, when mapping analytical solutions, the underlying saturation profile was always ignored and a new analytical solution scaled to the new time was mapped, resulting in diffusion-free solutions.

Notice in Fig. 5.2 that there is essentially no difference between the saturation profiles at $t_D$=0.6 for the analytical method (column 1) and the numerical method with only one mapping step (column 2). Any minor differences are due to diffusion effects within the 1D solver and the transformation process from irregular to regular $\tau$ grids. These diffusion effects are smaller than the diffusion effects simply due to the number of mapping steps, as noted by increased mixing in the $t_D$=0.6 profiles from columns 2-4. Clearly the SPU scheme is sufficiently accurate. The accuracy is a result

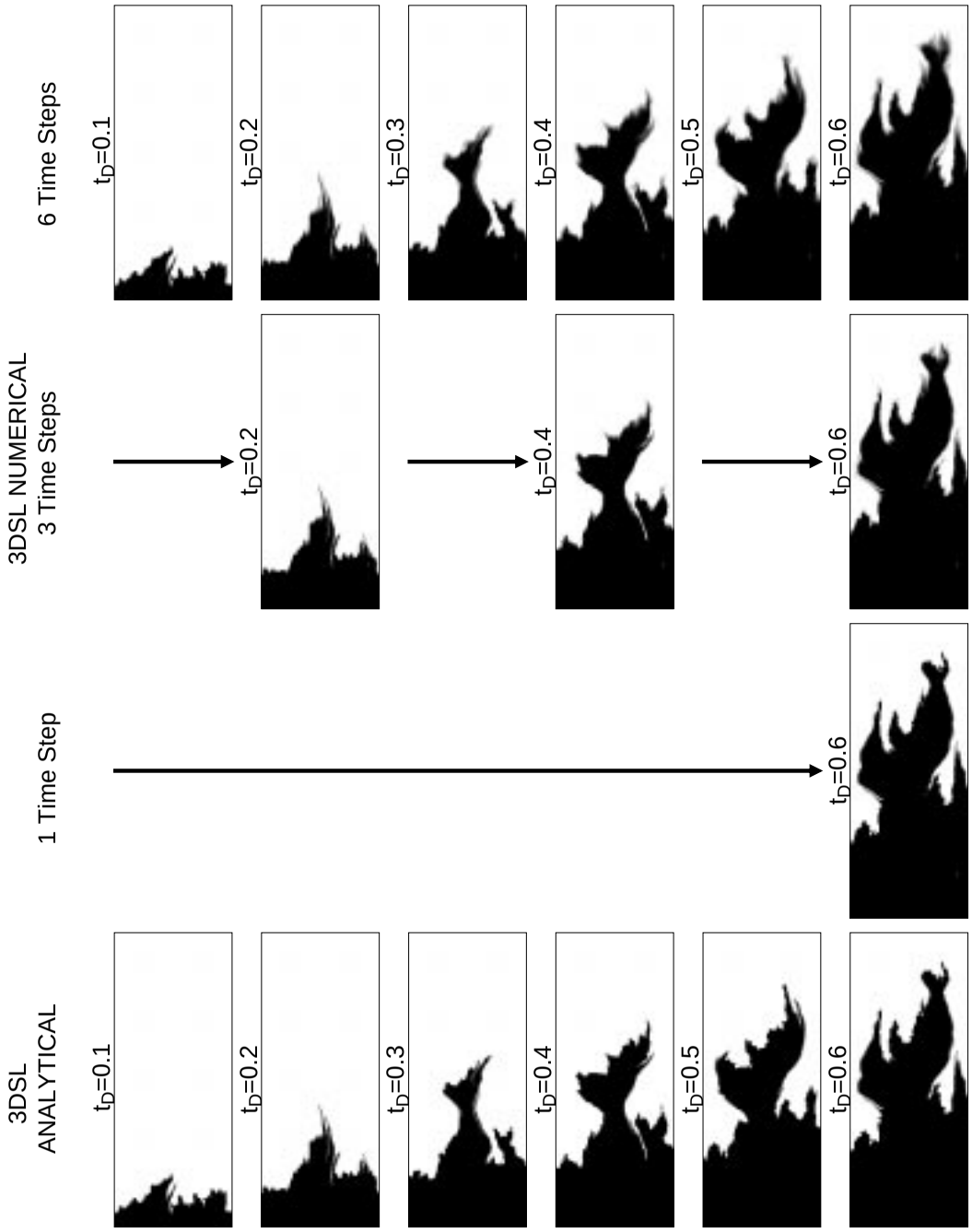


Figure 5.2: Effect of number of time steps on mixing when mapping 1D numerical solutions. Column 1 represents the mixing free solutions generated using the method of Chapter 4.

of being able to maintain very large numerical Peclet numbers for each streamline, within the 1D solver. A more accurate TVD scheme was also implemented for the 1D solver [9]. However, the TVD scheme did not reduce the level of numerical diffusion of the final 2D solutions. Again, this implies that diffusion associated with mapping solutions to and from the underlying grid is greater than numerical diffusion associated with the 1D solver.

It is also worth comparing the level of mixing present in the streamline simulator against ECLIPSE. The tracer profiles for the ECLIPSE fully implicit scheme and the corresponding 3DSL results are shown in Fig. 5.3. The ECLIPSE implicit method required 43 time steps to reach $t_D$=0.3. By contrast, forcing 3DSL to take 43 time steps produces superior results with less numerical diffusion. The ECLIPSE-IMPES solution is shown in Fig. 5.4, which requires 296 time steps and has reduced numerical diffusion compared with the implicit results. Taking 296 time steps with 3DSL gives a similar tracer distribution to the ECLIPSE IMPES results. Note that there is more mixing now present in the 3DSL solutions compared to those in Fig. 5.2 column 4 which is due to the greater number of remappings.

Another key point for Fig. 5.4 is that, because of the global CFL condition ECLIPSE takes an excessive number of convective time steps to reach $t_D$=0.3 (very small $\Delta t_c$), while the streamline method gives a more accurate and faster result in one mapping step (Fig. 5.2, column 2). The ability to take large time steps is why the streamline method exhibits such large speed-up factors. This example also highlights that, using the optimal global CFL condition (ECLIPSE) gives result that are less accurate than the results obtained by using the optimal local CFL condition along each streamline. Increased accuracy is important for FCM displacements where large levels of numerical diffusion can alter simulation results, as will be shown in Section 5.8.

## 5.7 Immiscible Two-Phase Displacements

To model a waterflood, a numerical solution can be mapped along streamlines instead of mapping an analytical 1D Buckley-Leverett profile as was done in the previous


Figure 5.3: Comparison of tracer profiles at $t_D$=0.3 in a 250×100 heterogeneous domain showing the level of numerical diffusion between (a) ECLIPSE implicit and (b) streamline results for the same number of time steps.

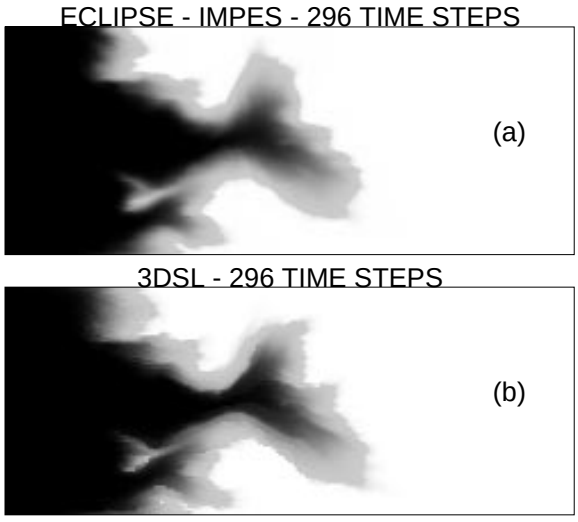


Figure 5.4: Comparison of tracer profiles at $t_D$=0.3 in a 250×100 heterogeneous domain showing the level of numerical diffusion between (a) ECLIPSE-IMPES and (b) streamline results for the same number of time steps.

chapter. The same 1D solver used for tracer and FCM displacements is used here. However, appropriate two-phase relative permeability curves and fluid viscosities are now required. For waterflood displacements, the maximum wave speed is greater than 1 and is associated with the velocity of the Buckley-Leverett shock. For stability reasons within the 1D solver $N_c \neq 1$ until the shock has developed. Fortunately, a 1D waterflood displacement is self-sharpening and rather insensitive to numerical diffusion. Thus, the value of $N_c$ has only a small effect on smearing of the leading shock.

The three 50×50×20 permeability fields shown in Fig. 4.13 are again used here. For comparison with the results of Section 4.11.2, well and fluid properties as well as the number of time steps are kept the same. The well geometry is a 5-spot pattern with a producer in the upper 10 gridblocks of each corner and an injector in the lower 10 central gridblocks. The fluid viscosity ratio is $\mu_o/\mu_w$=10. A comparison of results between the streamline method and ECLIPSE - IMPLICIT for each permeability model is shown in Fig. 5.5. Individual well response and total field recoveries between the two methods are in agreement.

Note that for each permeability model, the recovery produced by 3DSL and ECLIPSE are now almost identical. Recall that when analytical solutions were mapped along the streamlines, there was a slight difference between the two methods (Fig. 4.14). The difference was attributed to numerical diffusion within ECLIPSE since the analytical method is diffusion-free. Thus for waterflood displacements, when mapping numerical solutions to the streamlines, the mixing that results from mapping to the underlying saturation grid appears to replicate the mixing within ECLIPSE. Runtime performance for each simulation method is summarized in Table 5.1. For these cases, the streamline method was approximately 20 times faster than ECLIPSE.

## 5.8 First-Contact Miscible Displacements

First-contact miscible displacements can be modeled with the numerical solver used for the two-phase immiscible displacements. The difference lies in the form of the

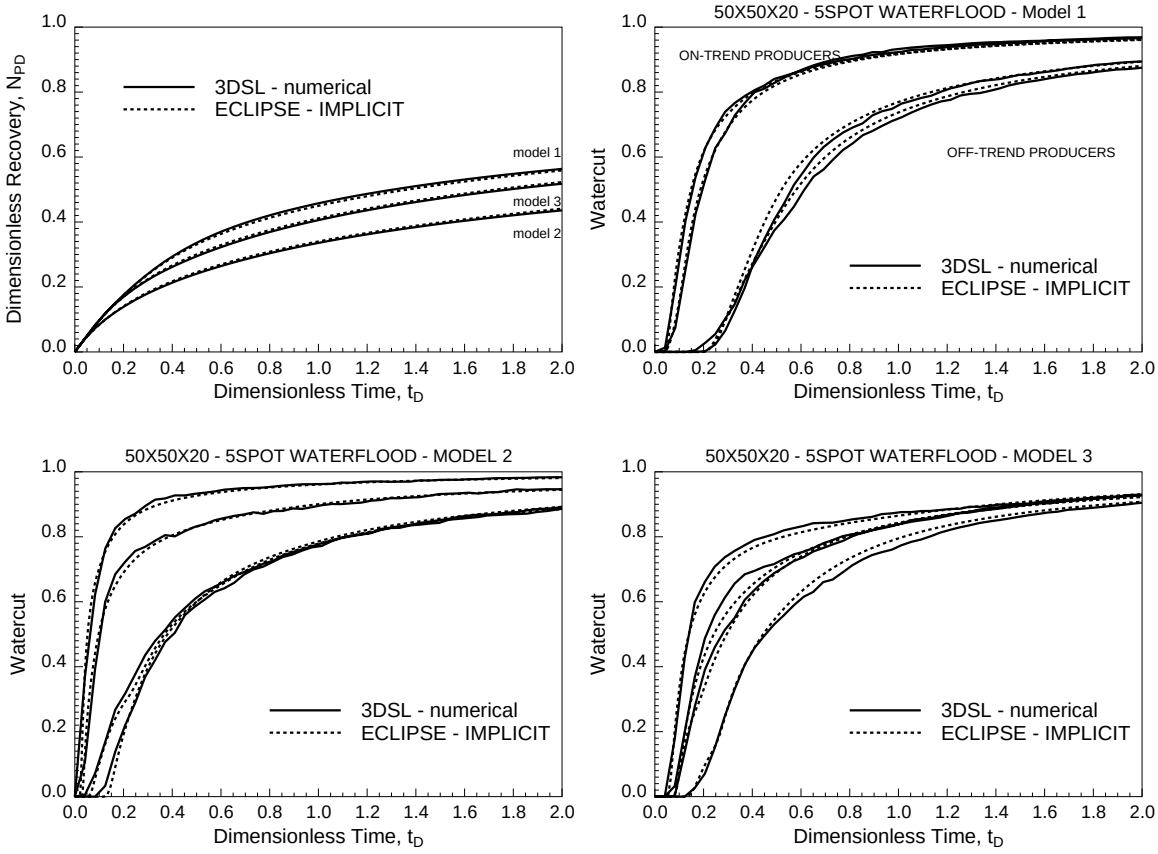


Figure 5.5: Comparison of recovery and individual producer watercuts between 3DSL (numerical) and ECLIPSE - IMPLICIT, for three different permeability models. Compare with Fig. 4.14 showing 3DSL analytical results.

| | 3DSL | | | ECLIPSE - implicit | | | |
|---|---|---|---|---|---|---|---|
| Case | CPU (min) | Time Steps | Pressure Solves | CPU (min) | Time Steps | Matrix Solves | Speed-up Factors |
| 1 | 36 | 50 | 25 | 1062 | 206 | 663 | 30 |
| 2 | 48 | 50 | 25 | 600 | 182 | 340 | 13 |
| 3 | 32 | 50 | 25 | 951 | 187 | 599 | 30 |

Table 5.1: Comparison of simulator performance parameters between the streamline method and ECLIPSE for 3 different waterflood 5-spot models.

fractional flow function. Within the streamline simulator the fraction flow function is given by the Todd & Longstaff model (see Section 4.12.1).

### 5.8.1 Modeling Viscous Fingering

As the level of heterogeneity for a FCM displacement is reduced, fluid movement becomes less dominated by heterogeneity and more dominated by the fluid distribution. An unstable first-contact miscible displacement in a mildly heterogeneous porous media will lead to viscous fingering of the injected fluid through the in place fluid. Viscous fingering problems are difficult to model for any simulation method. See *Araktingi & Orr* [1, 2], *Tchelepi & Orr* [67], or *Christie* [17] for a thorough discussion of numerical simulation techniques for viscous fingering in porous media.

Recall in Chapter 4 that the streamline technique coupled with the correct analytical 1D solution (Koval's model) could model FCM displacements provided the flow was dominated by heterogeneity. It was assumed that viscous fingering was captured in an average sense along each streamline. However, for less heterogeneous systems the displacement method could not reproduce explicit viscous fingering. *Thiele* [68] presents FCM displacements where the analytical streamline method failed because recovery was dominated by explicit fingering patterns. Viscous fingering problems are highly unstable and nonlinear. Component pathlines are far different than instantaneous streamlines. The numerical streamline method has the advantage over the analytical method of correctly moving components along pathlines.

As an example consider a mildly heterogeneous $250\times100$ cross sectional model FCM displacement [68]. The fluid viscosity ratio is $\mu_o/\mu_g$=10 and a Todd & Longstaff mixing parameter of $\omega$=1 is used, which assumes complete mixing of the solvent and oil at the gridblock scale. Figure 5.6 compares the solvent profiles at $t_D$=0.3 for the numerical streamline method, the BP FCT research code, ECLIPSE IMPES two-point upstream method, and ECLIPSE - IMPES single point upstream method. Also included for reference is the result from mapping Koval's analytical solution along streamlines.

Figure 5.6 demonstrates that by mapping numerical solutions, the streamline

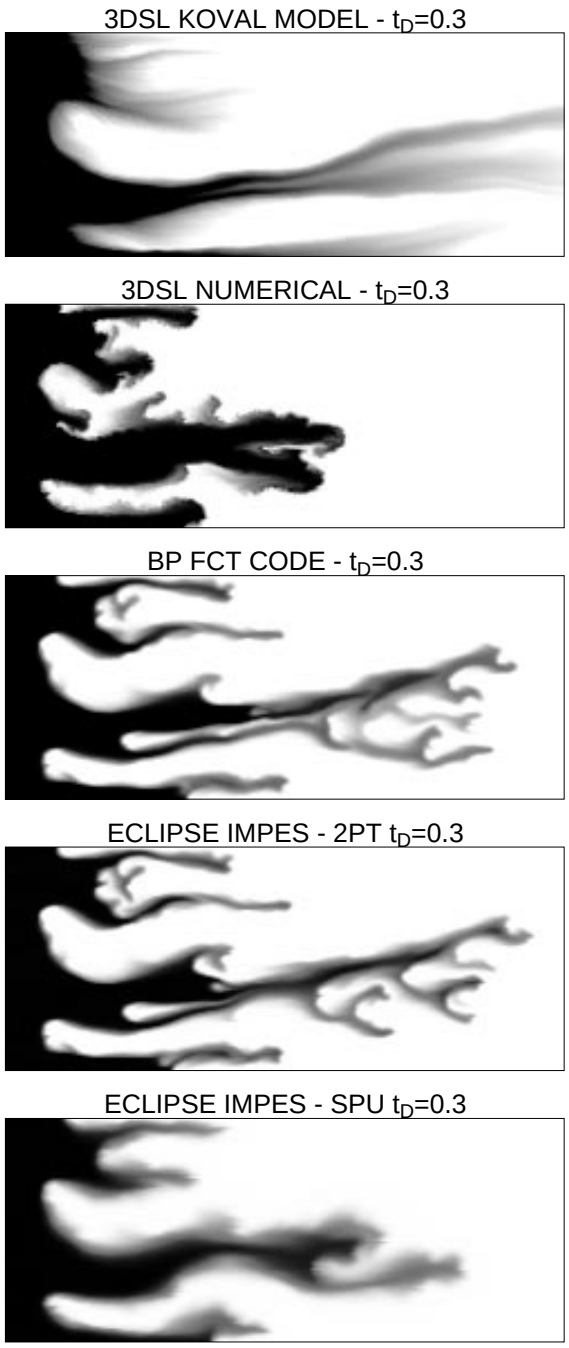


Figure 5.6: FCM displacement in a mildly heterogeneous 250×100 porous media. Comparison of finger profiles at $t_D$=0.3 for 5 different methods.

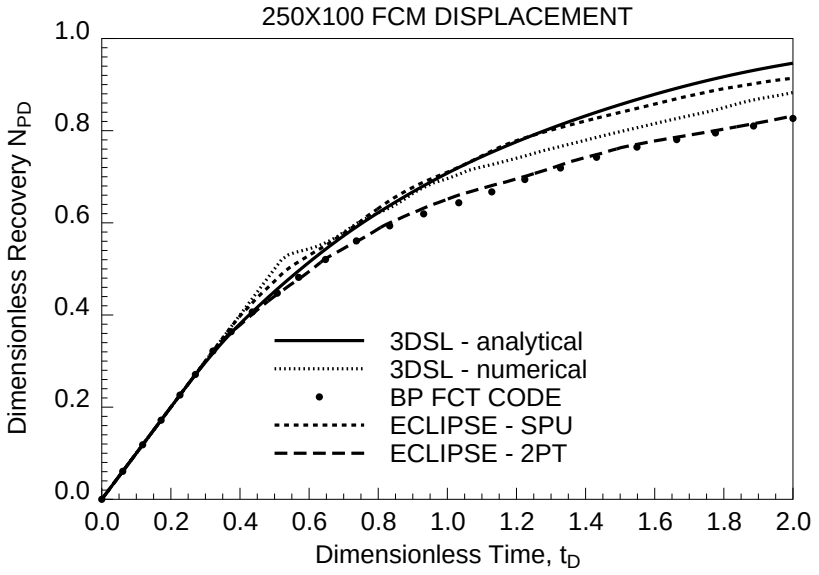


Figure 5.7: FCM recovery comparisons for four numerical methods. Results using the anaytical streamline method are included for reference.

method does produce viscous fingering, though finger width and locations differ from results obtained with more conventional numerical methods. However, because there is some correlated heterogeneity, each method identifies a central high permeability region. It is unclear what the reference solution is since the level of numerical diffusion present in each method does effect the results of this unstable displacement. This example demonstrates that differences in the numerical method can lead to large differences in finger patterns. Certainly, comparing the difference using single-point upstream weighting versus two-point upstream weighting within ECLIPSE illustrates this fact. The BP FCT code which also uses a two-point upstream method produces results similar to the high-order ECLIPSE results. One key difference in the four numerical methods is that the leading edges of all the fingers in the conventional methods are diffuse with concentrations less than one. However, the streamline results retain the sharp fluid contrast at the finger tips. To reach $t_D$=0.3, the streamline method required 100 times fewer time steps than the other methods and as the preceeding section demonstrated, there is considerably less mixing due to numerical effects in

the streamline method than conventional methods. Furthermore, the maximum front speed is far less than the optimal one gridblock per time step in the conventional methods – another source of numerical diffusion. It is possible that the thinner more diffuse fingers in the conventional numerical methods are a result of increased mixing due to numerical diffusion.

It is worth noting that the streamline results shown here are somewhat unrealistic since they do not account for physical diffusion. The results approach the limiting case of no diffusion. Both *Tchelepi & Orr* [67] and *Christie et al.* [20] note the importance of including a physical diffusion tensor in order to match experimental results.

A comparison of the recovery curves for the different methods is shown in Fig. 5.7. The high-order ECLIPSE results agree very well with the BP FCT results, much more so than the single-point upstream ECLIPSE results. The fatter, less diffuse finger pattern in the streamline method gives higher recovery results than the high-order numerical methods.

### 5.8.2 Effect of $\omega$ on Field Scale Displacements

For FCM displacements, the only adjustable parameter in the Todd & Longstaff model, and hence the streamline simulator, is the mixing parameter $\omega$. The mixing parameter attempts to capture fingering between solvent and oil at a sub-gridblock scale due to heterogeneities that exist at a sub-gridblock scale. *Todd & Longstaff* [73] found that $\omega$=2/3 worked well to forecast recovery in laboratory sand packs, while $\omega$=1/3 was more appropriate for field scale displacements. Their conclusions are dependent on the gridblock sizes they used. In general, their results indicate that improved mixing of the solvent and oil occured at the smaller scale.

The value of $\omega$ can have a large impact on displacement performance. However, quantitatively determining the correct value of $\omega$ based on a desired physical process is difficult. It is quite easy to illustrate the sensitivity of displacement results on $\omega$ using the streamline method, because of its speed. Figure 5.8 illustrates the effect that $\omega$ has on recovery predictions for the numerical streamline method in heterogeneity

dominated displacements.[4] Figures 5.9 – 5.12 provide a visual comparison of solvent profiles at $t_D$=0.5 for various values of $\omega$. For all cases, as $\omega$ increases, breakthrough time increases. In general, recovery also increases as $\omega$ increases. This behavior can be explained by studying the limiting cases of $\omega$. When $\omega$=0, the displacement contains a long rarefaction wave with no displacement front, resulting in very poor recovery efficiency at the gridblock scale. In the limit of $\omega$=1, a sharp displacement front is preserved and local recovery efficiency is very high for invaded gridblocks. However, overall recovery is now also a function of heterogeneity and the total mobility field. For homogeneous media, as expected, recovery is highest at $\omega = 1$. As heterogeneity begins to dominate, there is competition between efficiently displacing fluid from high flow channels versus cross-flow into low permeability regions. Thus, $\omega = 1$ may not always result in the highest recovery as heterogeneity becomes more dominant.

ECLIPSE results for $\omega = 1$ are also included for each permeability field. Each ECLIPSE run required 150 times more CPU than the equivalent streamline run. Using ECLIPSE for this type of sensitivity study on $\omega$ would require an impractical amount of CPU time. Comparing streamline results with ECLIPSE results (Fig. 5.8) indicates that there is no unique value of $\omega$ in the streamline method that can be used to obtain agreement with ECLIPSE. Within ECLIPSE numerical diffusion has a strong influence on the properties of the solution. The $\omega$ parameter in the streamline method has a linear scaling effect on recovery and cannot be expected to replicate the diffusion effects in ECLIPSE. Agreement may be improved by including physical diffusion in the streamline model as outlined by *Blunt et al.* [10].

As discussed in Chapter 4, *Thiele* [68] noted for heterogeneity dominated systems that $\omega$ determined by Koval's model gave good agreement with conventional methods when mapping analytical solutions to streamlines. Koval's model captured viscous fingering effects in an average sense along each streamline. However, mapping numerical solutions along streamlines captures viscous fingering effects explicitly, as was shown in the previous section. For all displacements in this thesis, sub-gridblock scale

[4]Heterogeneity is characterized using the heterogeneity index, $HI = \sigma^2_{\ln k}\lambda_c$, as defined by *Gelhar & Axness* [31].

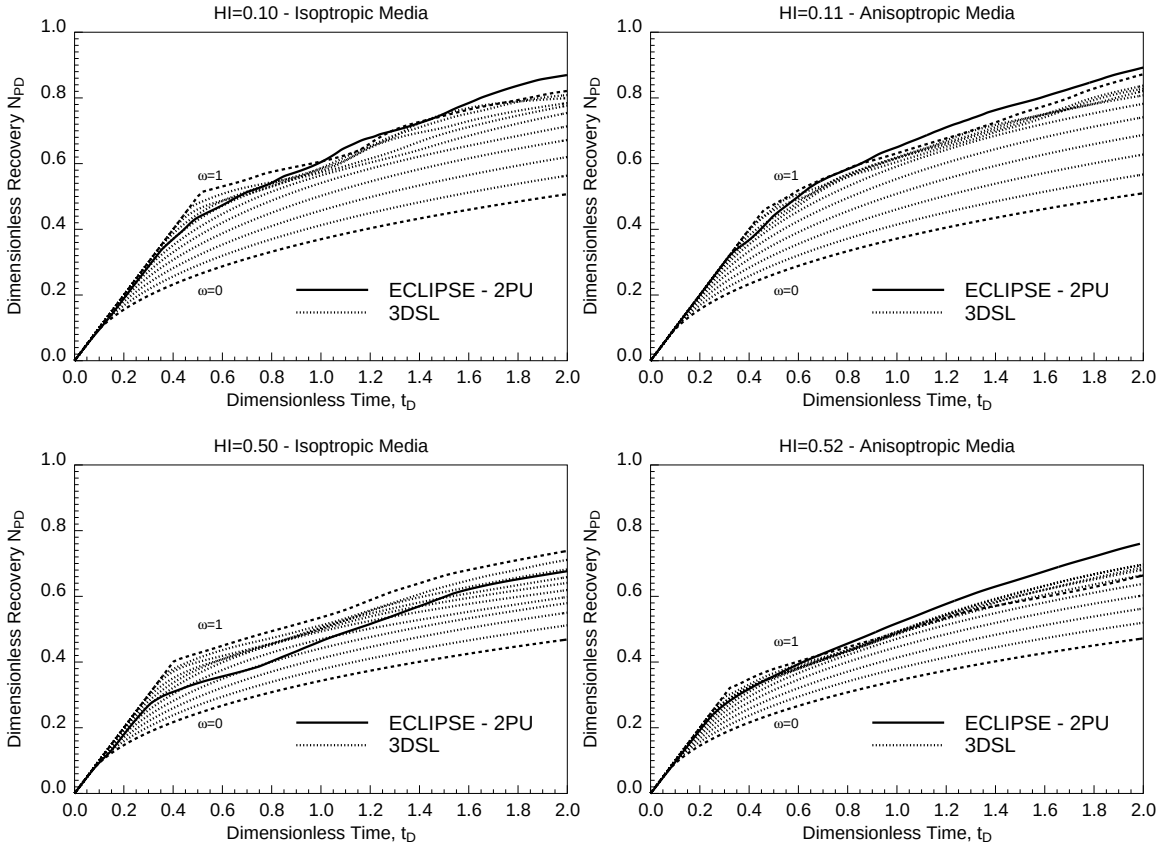


Figure 5.8: Effect of $\omega$ on streamline FCM recoveries for different levels of heterogeneity (isotropic and anisotropic).

heterogeneities are unknown and assumed not to exist. As a result, the most appropriate value for the mixing parameter, when mapping numerical solutions, is $\omega$=1. However, for comparisons between 3DSL and ECLIPSE, Fig. 5.8 suggests that a value of $0.7 < \omega < 1.0$ within the streamline method will result in some agreement between the two methods, but the exact value is dependent on the level of heterogenity.

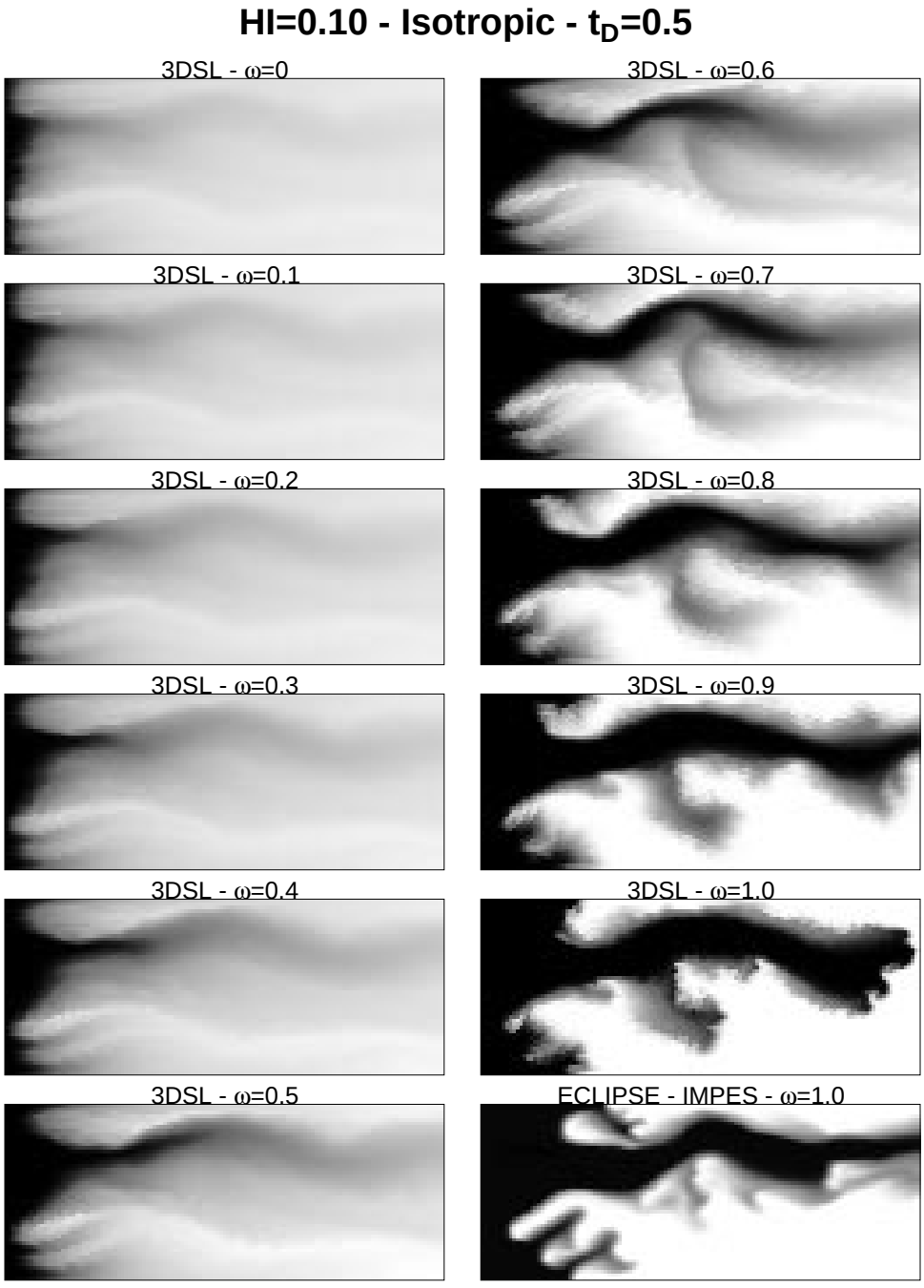


Figure 5.9: Comparison of saturation profiles in a heterogeneous FCM displacement for different values of $\omega$, HI=0.1, isotropic media.

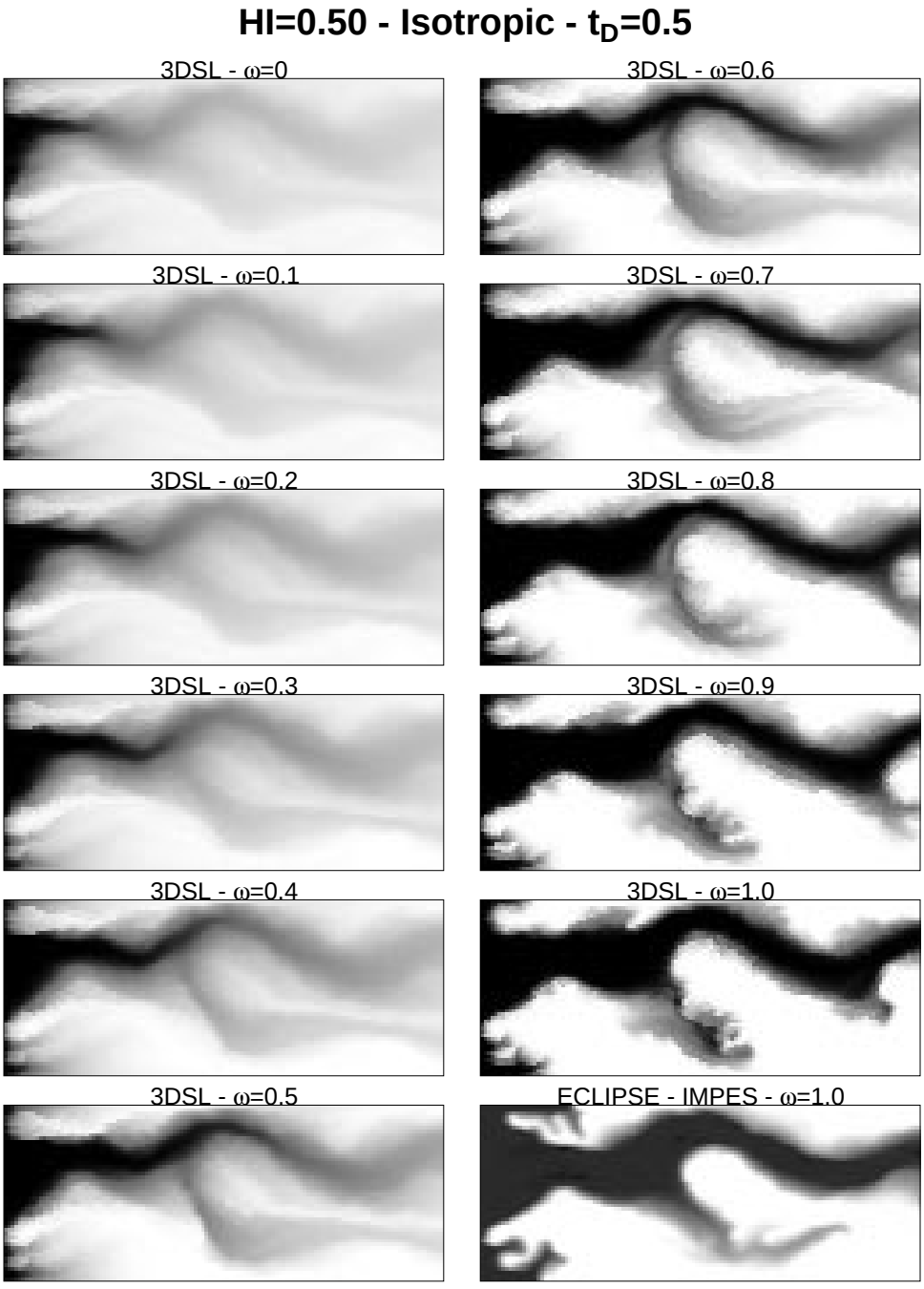


Figure 5.10: Comparison of saturation profiles in a heterogeneous FCM displacement for different values of $\omega$, HI=0.5, isotropic media.

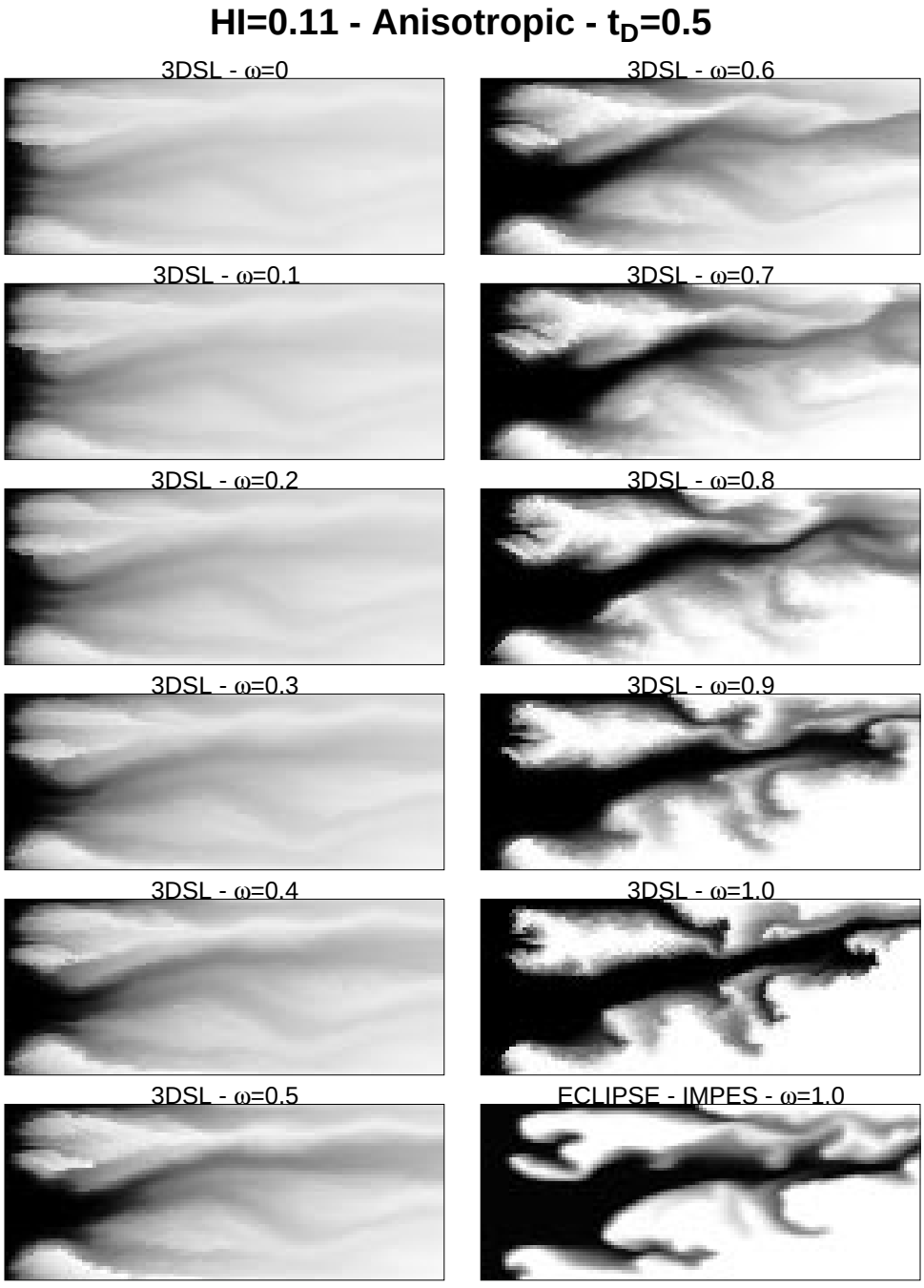


Figure 5.11: Comparison of saturation profiles in a heterogeneous FCM displacement for different values of $\omega$, HI=0.1, anisotropic media.

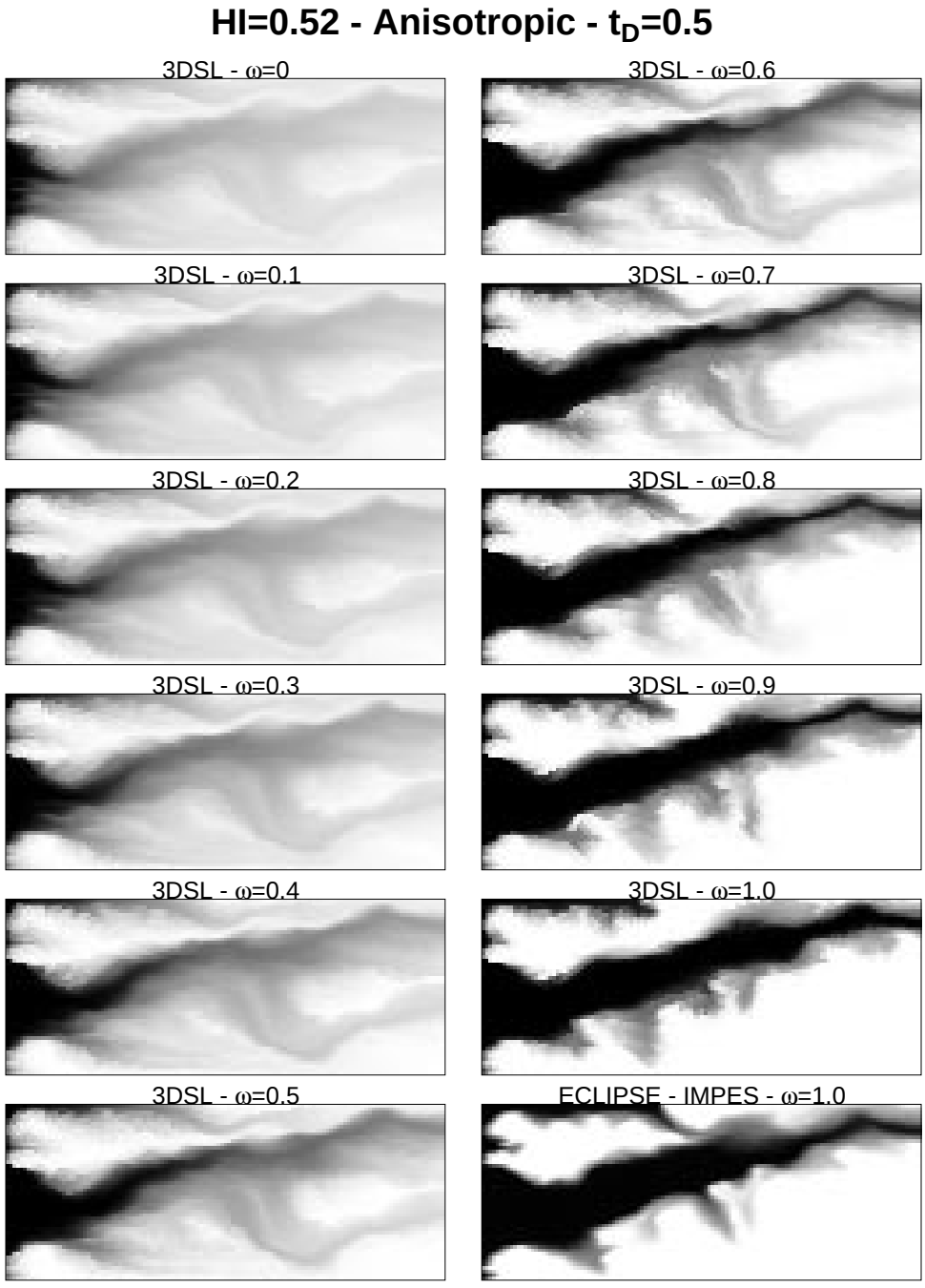


Figure 5.12: Comparison of saturation profiles in a heterogeneous FCM displacement for different values of $\omega$, HI=0.52, anisotropic media.

### 5.8.3 3D Displacements

The three 50×50×20 permeability fields shown in Fig. 4.13 are again used here. For comparison with the results of Section 4.12.3, well and fluid properties as well as the number of time steps remain the same. The well geometry is a 5-spot pattern with a producer in the upper 10 gridblocks of each corner and an injector in the lower 10 central gridblocks. The fluid viscosity ratio is $\mu_o/\mu_w$=10. For both ECLIPSE and the numerical streamline method, a value of $\omega$=1 is the most appropriate value since it is assumed that sub-gridblock scale heterogeneities do not exist. Additionally, to compare results here with those in Section 4.12.3, Koval's model giving $\omega = 0.725$ will also be used for the streamline results.

A comparison of results between the streamline method ($\omega = 0.725$) and ECLIPSE - IMPLICIT two-point upstream method ($\omega = 1.0$) for each permeability model are shown in Fig. 5.13. Individual well GOR responses agree well. Again, the mixing due to remapping back to the underlying saturation grid gives improved total field recovery matches, as compared to the match in Fig. 4.18 generated using the analytical mapping method of Chapter 4.

A second set of displacements was performed on the same three models using the streamline method, but now with $\omega$=1. The results between the streamline model and ECLIPSE ($\omega$=1) are shown in Fig. 5.14. Again individual well GOR responses agree well between the two methods, however, the streamline recoveries are consistently higher than the ECLIPSE recoveries. Reducing mixing of the displacement front in the streamline method has resulted in improved recoveries. On the other hand, the greater amount of numerical diffusion within ECLIPSE tends to underestimate recovery.

## 5.9 Field Applications

Mapping numerical solutions along streamlines has only marginally reduced the speed of the method. However, the requirement of uniform initial conditions has been removed. The streamline method is now capable of modeling infill drilling situations,

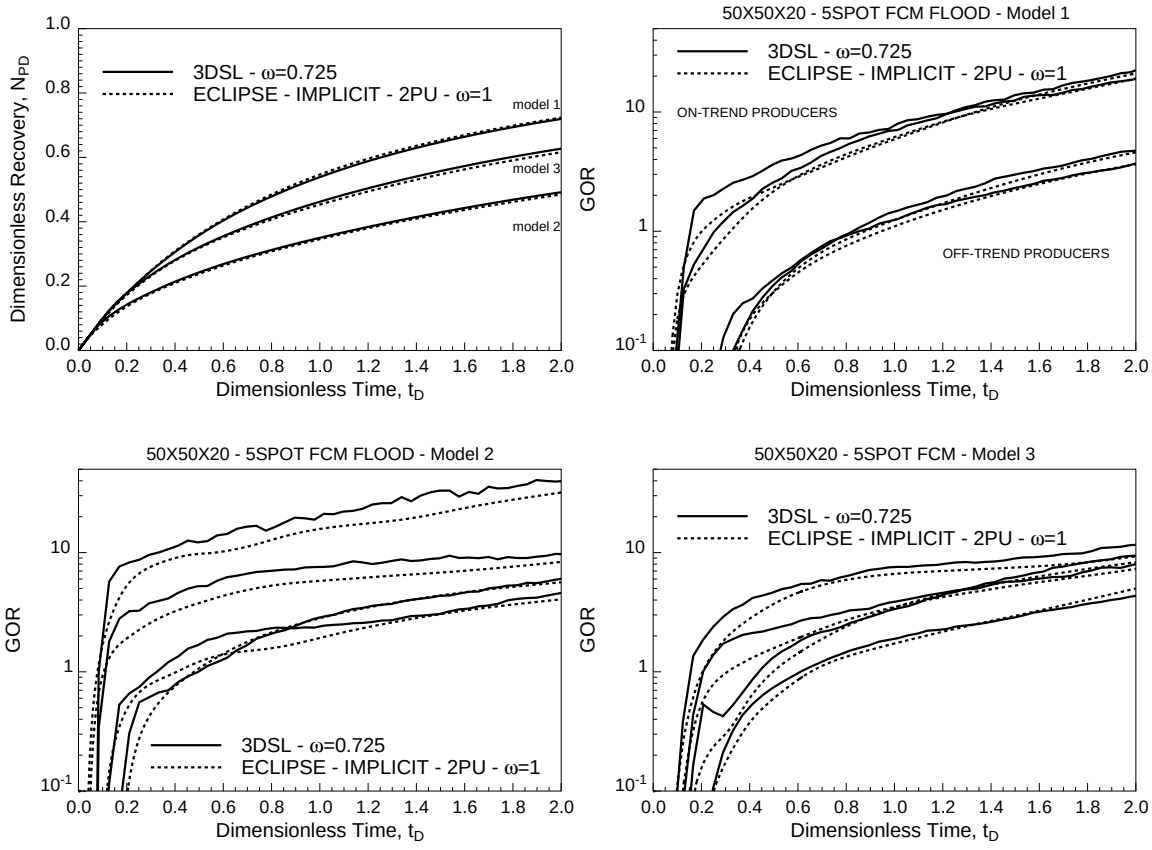


Figure 5.13: Comparison of recovery and individual producer GOR's between 3DSL $\omega$=0.725 (numerical) and ECLIPSE - IMPLICIT $\omega$=1, for three different permeability models.

| Model | 3DSL | | | ECLIPSE - implicit | | | |
|---|---|---|---|---|---|---|---|
| | CPU (min) | Time Steps | Pressure Solves | CPU (min) | Time Steps | Matrix Solves | Speed-up Factors |
| 1 | 58 | 50 | 50 | 3980 | 326 | 1327 | 69 |
| 2 | 43 | 50 | 50 | 2361 | 336 | 860 | 55 |
| 3 | 55 | 50 | 50 | 4370 | 362 | 1085 | 80 |

Table 5.2: Comparison of simulator performance parameters between the streamline method (numerical) and ECLIPSE for 3 different FCM 5-spot models.

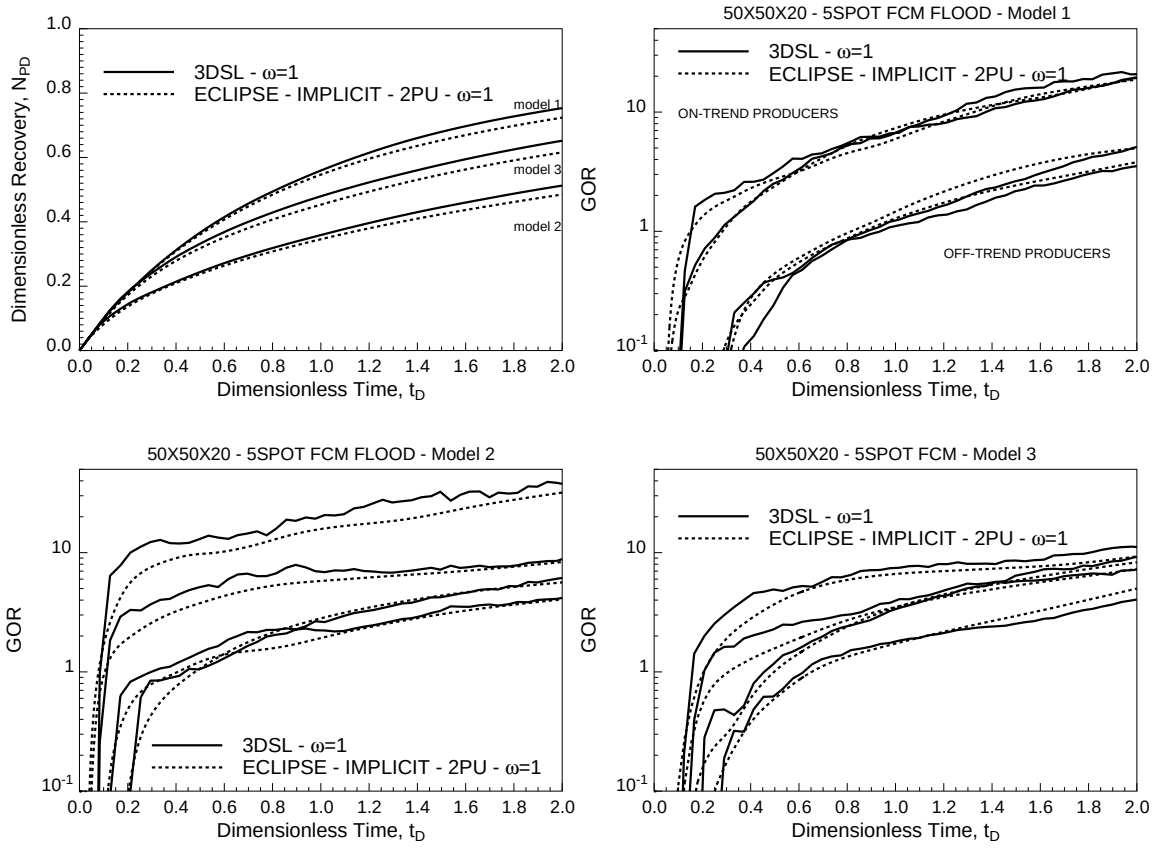


Figure 5.14: Comparison of recovery and individual producer GOR's between 3DSL $\omega$=1 (numerical) and ECLIPSE - IMPLICIT $\omega$=1, for three different permeability models.

producer/injector conversions, and fields with water/oil or gas/oil contacts.

### 5.9.1 Screening Multiple Images

Even when mapping numerical solutions, the streamline method is still orders of magnitude faster than conventional methods. The speed of the method makes it ideally suited to evaluating reservoir uncertainty. The thirty permeability fields studied in Section 4.16.2 under waterflood production are again used here. In this case, numerical rather than analytical solutions are mapped to the streamlines. On

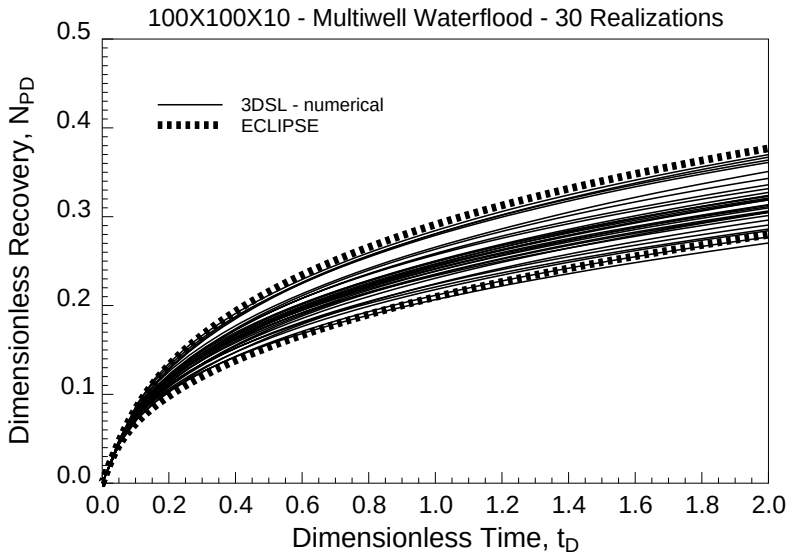


Figure 5.15: Waterflood recovery for 30 equiprobable realizations as predicted by the streamline method. ECLIPSE results are only shown for the permeability fields resulting in the high and low recoveries as predicted by the streamline method.

average, each 100,000 gridblock model required 2.3 hours CPU time.[5] It was also observed that the permeability fields predicted to give the high and low recoveries using the analytical streamline method were the same fields predicted using the numerical method. In fact, the ranking of all 30 permeability fields predicted by the two streamline methods did not change. Figure 5.15 is a summary of the recovery curves for the 30 realizations generated using the numerical streamline method. Note that the ECLIPSE results no longer appear to be shifted up relative to the streamline results, as was seen in Fig. 4.28. The improved agreement is a result of the mixing now present in the streamline method when mapping numerical solutions.

### 5.9.2 Field Scale Infill Drilling

As an example of the flexibility of the streamline method, a field scale well conversion problem is studied. A 1.16 million gridblock model ($220\times220\times24$) permeability field

[5]When mapping analytical solutions, each streamline model required an average CPU time of 1.5 hours.

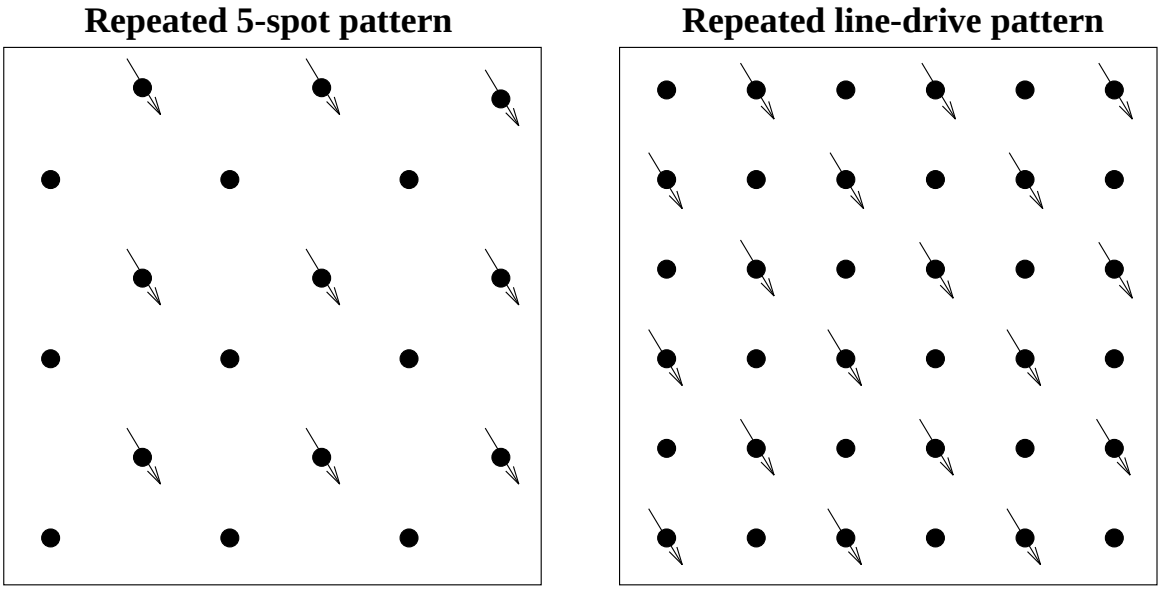


Figure 5.16: Well patterns for infill drilling waterflood example.

was generated using sequential Gaussian simulation. The permeability correlation lengths are $\lambda_c$=0.25 in the on-trend direction, $\lambda_c$=0.03 in the off-trend direction, and $\lambda_c$=0.17 in the vertical direction. This fine scale permeability field was run directly with 3DSL.

Initially, the field is completed in repeated five-spot patterns, as shown in Fig. 5.16. Figure 5.17 is an areal view of the waterflood at $t_D$=1.0. Due to the diagonal orientation of the permeability field, the sweep efficiency is quite poor. Realistically, this type of sweep pattern can occur in waterfloods where injection pressures exceed fracture pressure. A preferential fracture orientation results in a fracture induced permeability anisotropy. The solution to the poor sweep efficiency is to convert the patterns to line-drive by converting the watered out producers to injectors and infill drilling additional producers (Fig. 5.16). Due to the changing well boundary conditions and the nonuniform water saturation now present, this problem can only be modeled by mapping numerical solutions along streamlines. Figure 5.18 is an areal view of the line-drive waterflood at $t_D$=1.0 assuming that the pattern conversions

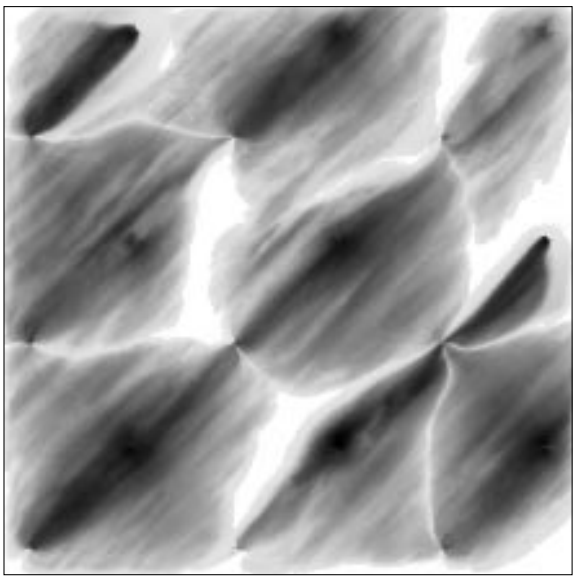

Figure 5.17: Areal averaged waterflood map for a 220×220×24 repeated 5-spot waterflood pattern at $t_D$=1.0, as predicted by the streamline method.

occurred at $t_D$=0.4. There is considerably improved sweep in Fig. 5.18 over that in Fig. 5.17.

The fine scale model was run using 3DSL and required 50 hours for the base case recovery curve, and 40 hours for the incremental results. The base case and incremental recovery due to the pattern modifications are shown in Fig. 5.19. The million gridblock model could not be run with ECLIPSE using available computer resources. To compare with ECLIPSE, the model was upscaled by a factor of 16 to 72,000 gridblocks (110×110×6) using geometric averaging of absolute permeability. Relative permeabilities were not altered for the coarse scale model. The oil recovery results for ECLIPSE-IMPES are also shown in Fig. 5.19. For this model, the ECLIPSE base case recovery curve required 55 hours run time, while the incremental results required 13 hours run time. An ECLIPSE fully implicit solution for the base case model required 120 hours run time. The large run time was due to time step convergence problems for this size model. Included for reference are 3DSL upscaled results, which required 28 minutes run time for the base case and 22 minutes run

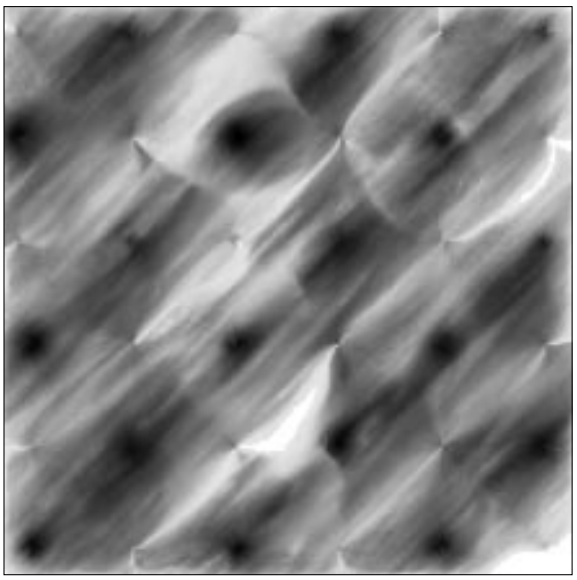

Figure 5.18: Areal averaged waterflood map for a 220×220×24 repeated line-drive waterflood pattern at $t_D$=1.0, as predicted by the streamline method.

time for the incremental case. The upscaled streamline results agree very well with the upscale ECLIPSE results, but were generated 300 times faster.

As seen in Fig. 5.19, incremental oil recovery due to infill drilling is underestimated in the upscaled models. This is because upscaling leads to a higher prediction of oil recovery for the base case 5-spot model than for the line-drive model. The reason upscaling does not affect each model the same is that the interwell permeability correlation lengths are 50% smaller in the line-drive pattern model than the 5-spot pattern model. This comparison highlights two points: (1) the ECLIPSE base case model was 16 times smaller than the 3DSL model, yet both required approximately the same run time; (2) ignoring fine-scale heterogeneity can lead to an overly optimistic prediction of field performance. The streamline model is a new tool that can capture increased reservoir heterogeneity in field scale multiwell models.

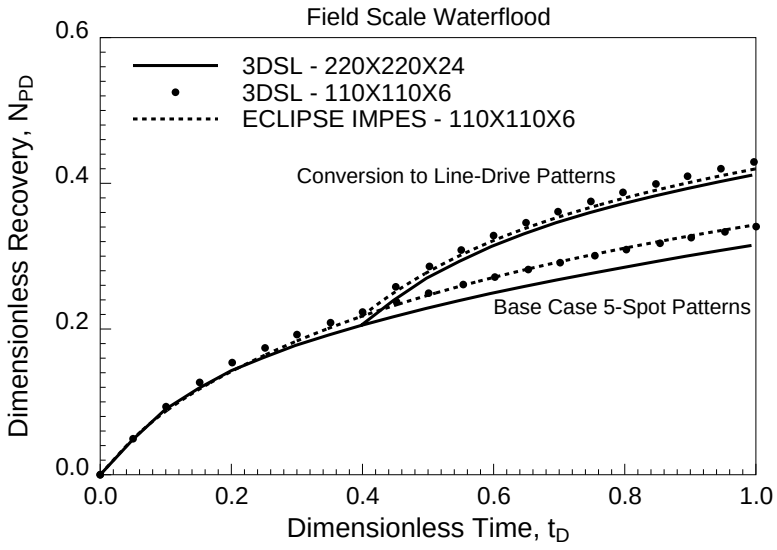


Figure 5.19: Waterflood oil recovery comparisons between 3DSL million gridblock model and upscaled ECLIPSE - IMPES and 3DSL models.

## 5.10 Chapter Summary

This chapter demonstrates that mapping numerical solutions to streamlines extends the method to account for the more general situations present in field scale simulations. For example, changing well conditions or nonuniform initial fluid saturations can now be modeled. However, the large speedup factors of the method are still retained even with the added expense of evaluating numerical, rather than analytical solutions. As Section 5.4 emphasized, the maximum time step size in conventional IMPES methods is governed by the grid stability constraint (a global CFL condition). However, with the streamline method, the convection equation is effectively decoupled from the underlying grid. Therefore, grid stability constraints are also decoupled from the solution to the convection equation. This decoupling allows for very large time step sizes between convective steps and pressure solves in the streamline method.

This chapter also showed that mixing between streamlines at the gridblock scale now occurs each time the streamlines are mapped to the underlying grid. The mixing is a result of only knowing gridblock saturations to within a single gridblock scale.

The mixing improved the agreement between the streamline method and ECLIPSE for waterflood displacements, though it is quite possible that the level of mixing present in the numerical solutions is still larger than the physical mixing that occurs in field scale displacements. In any case, the streamline method is no less accurate than conventional finite-difference methods. However, it is much faster.

For first-contact miscible displacements, agreement between the streamline method and ECLIPSE varied depending on the level of heterogeneity. The difference was mainly due to the magnitude of numerical diffusion within ECLIPSE, which is not present in the streamline results. It was also shown that adjusting the mixing parameter $\omega$ in the streamline method, may replicate the numerical diffusion in ECLIPSE and produce good agreement between the two methods.

In Chapter 4, the assumption that flow was dominated by heterogeneity was required to preserve the uniform initial conditions along recalculated streamline paths. In this chapter, this assumption has been eliminated. Displacements controlled by fluid mobility can also be modeled, as was illustrated by the viscous fingering examples.

# Chapter 6

# Gravity Results With 1D Numerical Solutions

## 6.1 Introduction

The influences of gravity effects on displacements are well known. For miscible displacements, *Stalkup* [65] notes that gravity segregation of fluids can result in reduced recoveries, while *Whillhite* [79] noted similar effects in immiscible displacements. Clearly, to extend the streamline method to three-dimensional field scale displacements the method must be able to account for gravity. In fact, *Tchelepi & Orr* [67] noted accounting for gravity is more important in three-dimensional displacements than in two-dimensional displacements.

This chapter describes how gravity effects are accounted for in single and multiphase 3D displacements with the streamline method. To account for multiphase gravity effects, one possibility is to trace general phase streamlines, as discussed by *Blunt et al.*[10]. A second choice is to continue to trace a single set of streamlines along the total velocity vector and then use an operator splitting method to correct for multiphase gravity effects. A similar operator splitting method applied to front-tracking is used by *Bratvedt et al.* [14]

Historically, streamline methods have been unable to account for gravity effects. This is a result of mapping analytical solutions along streamlines which implies that

the fluid path follows the streamline path. However with gravity, a fluid pathline is different than a fluid streamline.[1] The fluid pathline can be properly modeled by mapping numerical solutions along streamlines and updating the streamline paths periodically. In the case of multiphase flow, an explicit gravity step (operator splitting) is also added.

## 6.2 Definition of Gravity Number

The magnitude of the gravity forces in a displacement are characterized by the time required for fluids to move up or down versus the time required for fluids to move across a domain. Using Darcy's law to determine the travel times, a dimensionless gravity number is defined as [4] [67],

$$N_g = \frac{\overline{K}_v \Delta\rho g L^2}{\overline{K}_h (\Delta P_h) H}, \tag{6.1}$$

where $\overline{K}_v$ and $\overline{K}_h$ are average vertical and horizontal permeabilities respectively, $\Delta\rho$ is the fluid density difference, $\Delta P_h$ is the pressure drop in the horizontal direction, $L$ is the distance between wells, and $H$ is the model height. Thus, as density differences or model length increase, the gravity number increases, while if model height or horizontal flow rate increase (horizontal pressure drop increases), the gravity number decreases.

The above definition of $N_g$ in Eq. 6.1 is rigorous only for strictly two-dimensional homogeneous permeability fields. For more complex displacements, all the parameters in Eq. 6.1 can vary in space, and the pressure drop can vary in time due to changes in the mobility field. Thus, a single value of $N_g$ cannot characterize a displacement. However, since the interest is in relative comparisons of $N_g$ for different displacements, an average value of $N_g$ will be consistently applied and quoted. Thus, $\Delta P_h$ will be the average pressure drop between an injector and surrounding producers, throughout the displacement life. For simple 2D models $\overline{K}_v$ and $\overline{K}_h$ were determined from pressure solves using constant pressure and no-flow boundary conditions in each coordinate

[1] A fluid pathline represent the locus of a particle's position in space through time [8].

direction. For 3D permeability fields with general well locations it is difficult to define a related $\overline{K}_v/\overline{K}_h$ ratio. Instead, for 3D cases it is assumed that $\overline{K}_v/\overline{K}_h$ is equivalent to the square root of the variogram anisotropy ratio used to construct a permeability field. *Wen* [78] found that this method of approximating $\overline{K}_v/\overline{K}_h$ is satisfactory for $\lambda_c < 0.2$.

## 6.3 First Contact Miscible Displacements

For FCM displacements when the Todd & Longstaff mixing parameter is $\omega = 1$, the fluids are completely mixed at the gridblock scale and have identical properties. As a result, there is no density difference within a given gridblock and the last term in Eq. 3.36 becomes $G_j = 0$. The phase velocity and the total velocity are aligned at all times and gravity effects are accounted for in equation Eq. 3.7 only.

Figure 6.1 is an illustration of an FCM gravity dominated displacement in a homogeneous cross-section. The fluid mobility ratio is 10 and $N_g = 40$. The streamlines that fluids are moved along for a given time step have been overlaid on the resulting saturation profile. Based on solving Eq. 3.7, and tracing the subsequent velocity field, the streamlines paths rise where they contain "light" fluid and sink again where they contain "heavy" fluid.

Every gridblock in the domain must contain a streamline. The complication of gravity is that some gridblocks will contain circulation streamlines, rather than streamlines passing from injectors to producers. As gravity forces are increased, this occurs in a greater percentage of gridblocks. When mapping analytical solutions to the streamlines, circulation cells cannot be properly modeled. Thus, only low gravity numbers or displacements dominated by heterogeneity can be modeled (*Blunt et al.* [10]). However, with the numerical mapping technique of this chapter, mapping a numerical solution along a circulation cell is no more difficult than mapping a solution along a streamline that passes from an injector to producer.

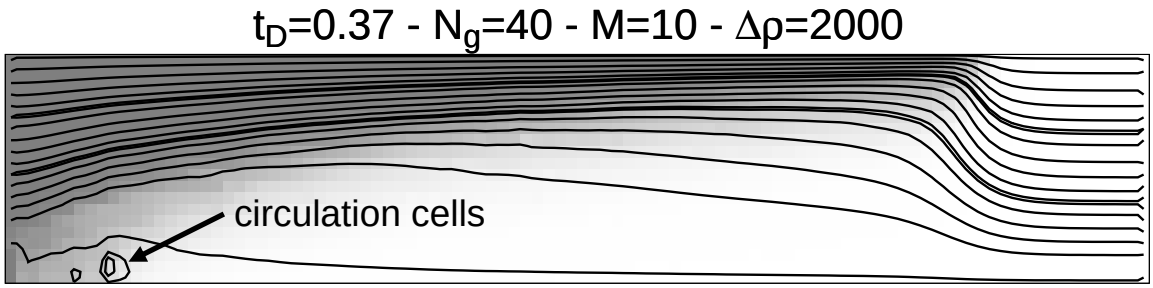


Figure 6.1: FCM gravity dominated displacement in homogeneous cross-section.

### 6.3.1 2D Displacements

In this section, careful comparisons of 2D gravity dominated FCM displacements are considered. The 125×50 permeability field used in this study is shown in Fig. 6.2. To emphasize the effects of gravity as $N_g$ increases, rather than have full cross-section completions, the injection well is located in the lower left 10 gridblocks of the model, while the production well is located in the lower right 10 gridblocks. The fluid viscosity ratio is $\mu_o/\mu_g$=10 and $\omega$=1. Fluid densities were changed to alter the gravity number for successive runs. All streamline results presented in this section are converged solutions. Sensitivity of convergence due to gravity effects is summarized in Section 6.5.

A comparison of solvent profiles between ECLIPSE - IMPES and 3DSL are shown in Figs. 6.3, 6.4, and 6.5. Clearly the numerical streamline method can model gravity dominated displacements as can be seen by the increased amount of solvent rising in the model as the gravity number is increased. In comparison with the ECLIPSE results, the profiles appear to be similar although there is more detail in the 3DSL results. It is also worth noting that because of greater numerical diffusion, ECLIPSE predicts earlier breakthrough for the $N_g$=0 case.

A summary of the oil recovery curves for each method and gravity number are shown in Fig. 6.6. In general, ECLIPSE tends to under-predict recovery compared with the streamline method. The increased amount of numerical diffusion within ECLIPSE results in more mixing of the solvent and the oil which in turn reduces the

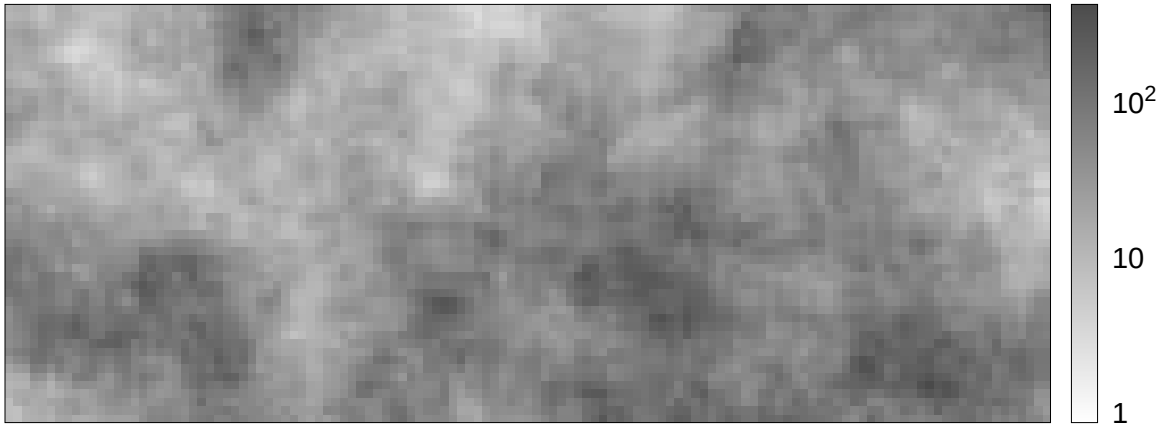


Figure 6.2: 125×50 heterogeneous permeability field, $\lambda_c$=0.4, $\sigma^2_{\ln} = 0.83$, $HI$=0.332.

| | 3DSL | | ECLIPSE - IMPES | | |
|---|---|---|---|---|---|
| $N_g$ | Cpu (min) | Pressure Solves | CPU (min) | Time Steps | Speed-up Factor |
| 0 | 2.2 | 50 | 616 | 1742 | 280 |
| 2 | 4.5 | 122 | 2268 | 8641 | 504 |
| 10 | 10.3 | 306 | 9010 | 32767 | 875 |

Table 6.1: Comparison of simulator performance parameters between the streamline method and ECLIPSE for 2D model at three different gravity numbers.

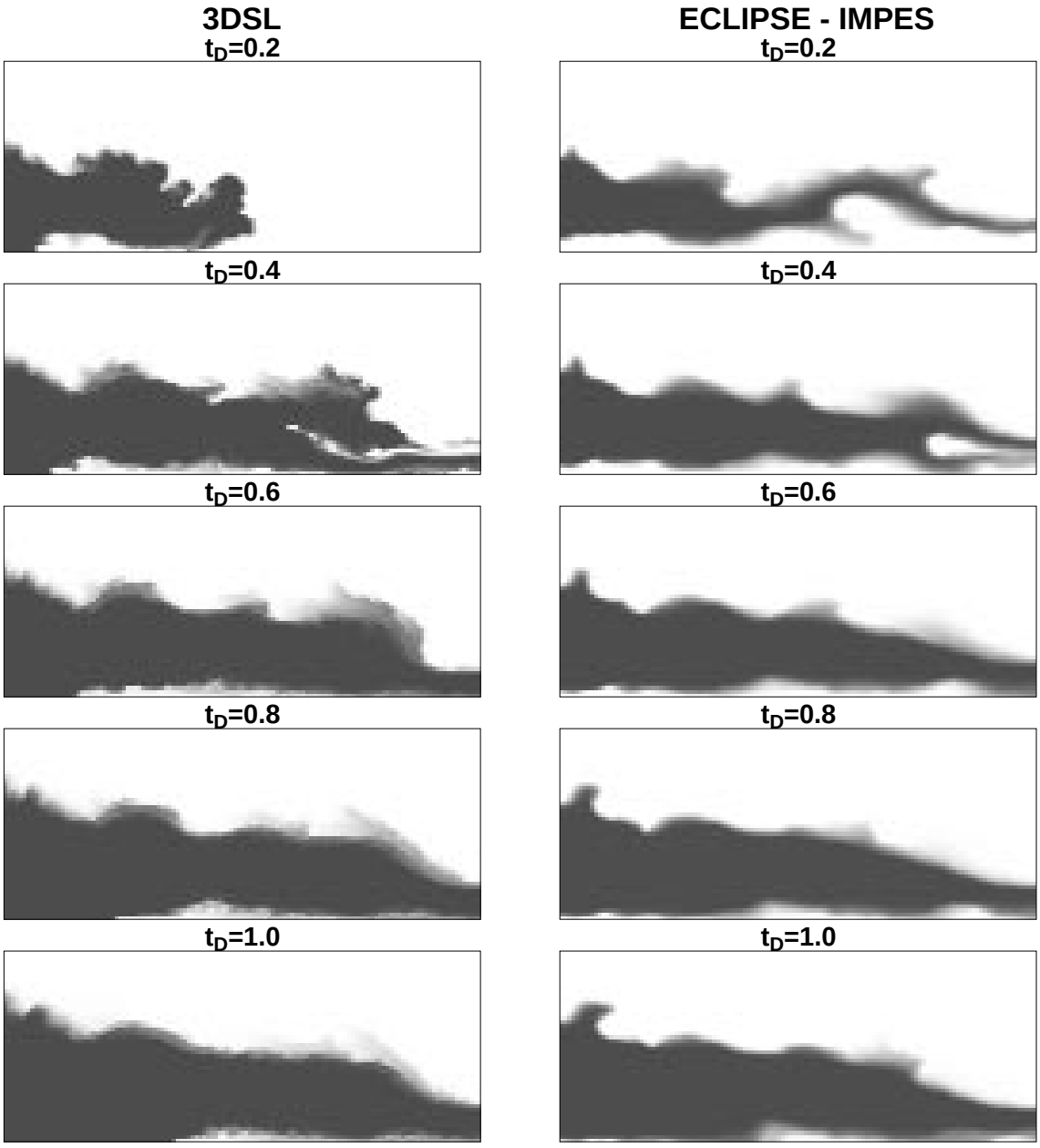


Figure 6.3: FCM displacement comparisons between 3DSL and ECLIPSE - IMPES. 125×50 domain, $N_g$=0, injection is into the lower left 10 gridblocks and production is from the lower right 10 gridblocks.

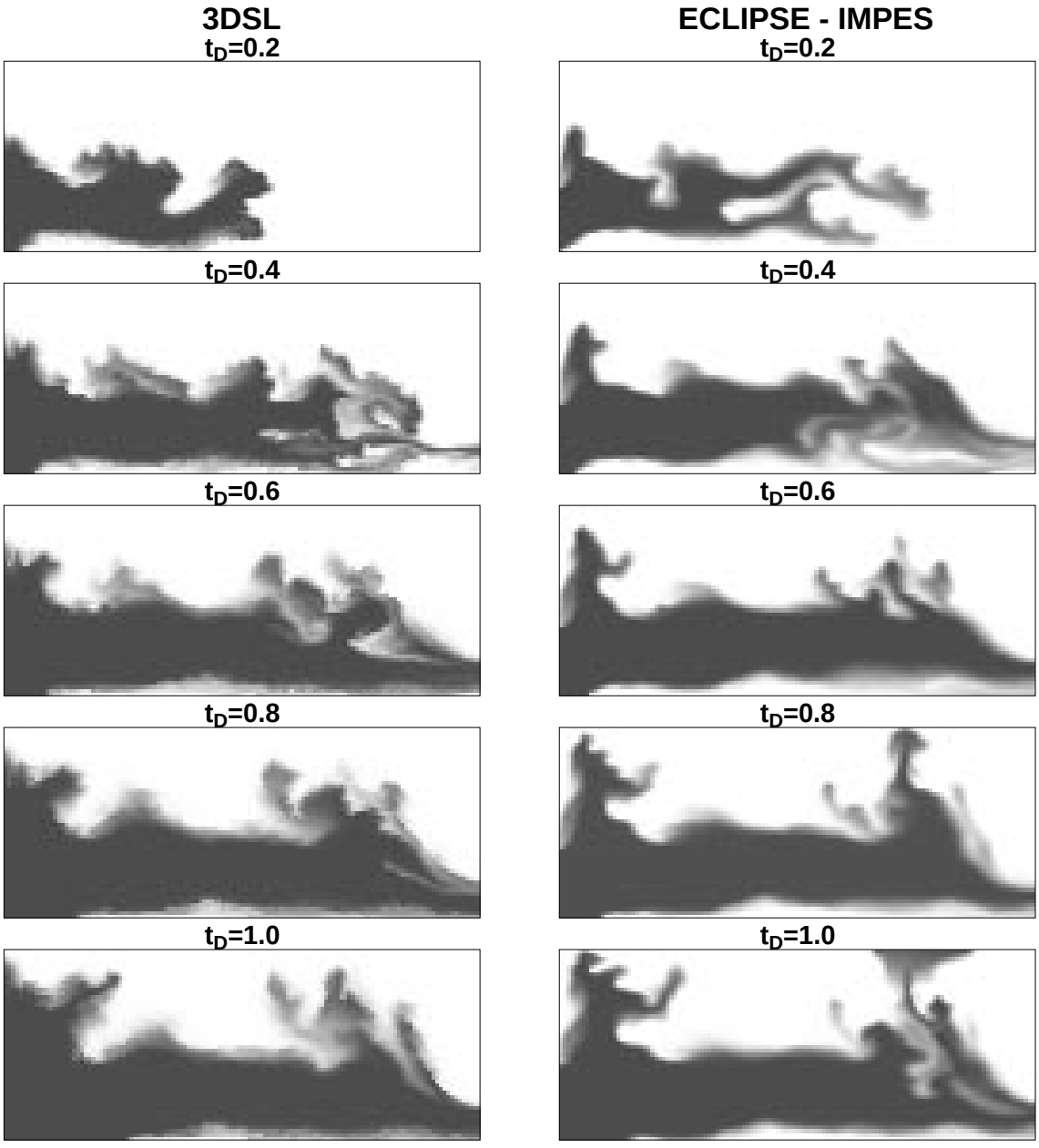


Figure 6.4: FCM displacement comparisons between 3DSL and ECLIPSE - IMPES. 125×50 domain, $N_g$=2, injection is into the lower left 10 gridblocks and production is from the lower right 10 gridblocks.

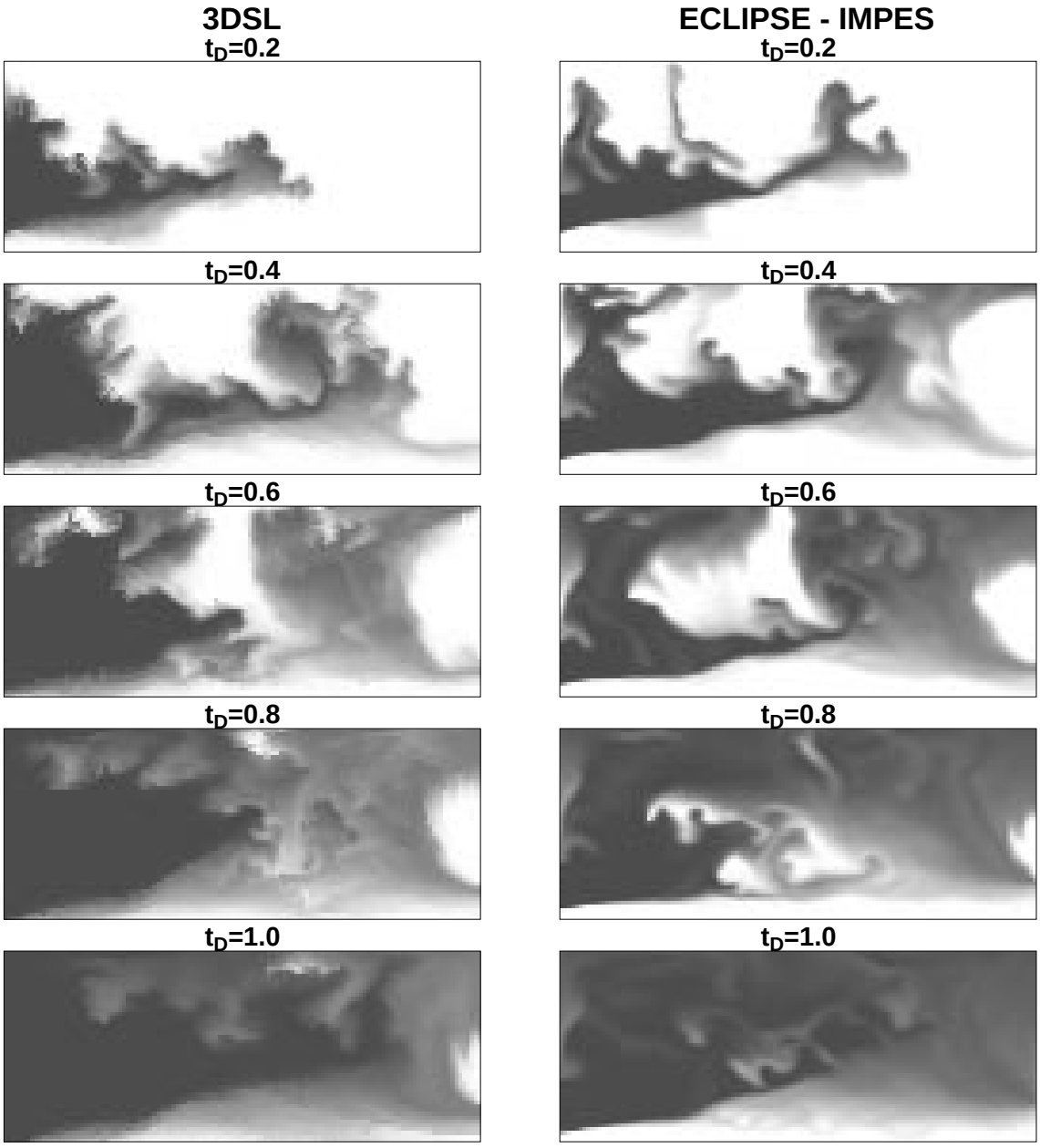


Figure 6.5: FCM displacement comparisons between 3DSL and ECLIPSE - IMPES. 125×50 domain, $N_g$=10, injection is into the lower left 10 gridblocks and production is from the lower right 10 gridblocks.

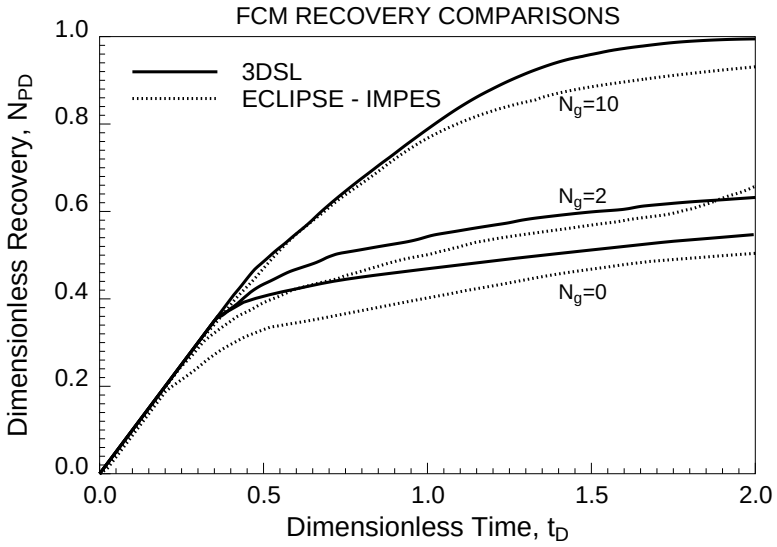


Figure 6.6: FCM recovery comparisons between 3DSL and ECLIPSE - IMPES.

effective density between the two fluids. Thus, the ability of the solvent to rise up and displace oil is reduced.

The power of the streamline method in this case is that it gives more accurate answers and does so in a fraction of the time compared to conventional results. Streamline simulator performance compared with ECLIPSE is summarized in Table 6.1. Note that although the streamline method required additional pressure solves to reach a converged solution as gravity effects were increased, speed-up factors over ECLIPSE still increased. Running on a standard UNIX workstation, ECLIPSE results for this small problem with $N_g$=10 required over 32,000 time steps and 6 days of CPU time to reach $t_D$=2. Whereas, the streamline method only required 306 time steps and 10 minutes of CPU time. This translates into a speed-up factor of 875. For the $N_g$=2 problem, the speed-up factor was 504. For $N_g$=0, the speed-up factor was 280. Although not shown here, ECLIPSE fully implicit results were also calculated at the three gravity numbers. CPU usage was reduced, however the fully implicit results suffered from considerable amounts of numerical diffusion and showed even poorer agreement with the streamline solutions.

### 6.3.2 3D Displacements

Three dimensional FCM gravity dominated displacements are very difficult and CPU intensive to perform. Recent notable works include *Christie et al.* [21] and *Tchelepi & Orr* [67]. *Tchelepi & Orr* studied 2D and 3D FCM displacements and noted that 3D flows were always more affected by buoyancy differences than were 2D flows. This is due to additional pathways for fluid to move vertically in 3D compared with 2D.

As a 3D example, consider a 50,000 gridblock ($50\times50\times20$) FCM displacement with and without gravity. An injection well is located in the top two central gridblocks, and a production well is located in the lower two gridblocks of the model in each corner. With this well configuration, gravity effects should improve recovery by improving vertical conformance. The solvent distributions for $N_g$=0 and $N_g$=0.1 are shown in Fig. 6.7 at $t_D$=0.52. Figure 6.8 clearly shows that adding gravity to this 3D model increases the amount of solvent in the top of the model and results in a large impact on oil recovery efficiency. Each streamline model required 2 CPU hours, translating to approximately 50 days for each ECLIPSE result if they were obtained using our current computer resources.

## 6.4 Two-Phase Immiscible Displacements

Multiphase gravity effects are particularly difficult to model using streamline methods since the gravity vector in Eq. 3.13 is seldom aligned with a streamline trajectory. For practical reservoir field simulations, it is important to account for multiphase gravity effects. To solve,

$$\frac{\partial S_j}{\partial t} + \frac{\partial f_j}{\partial \tau} + \frac{\nabla \cdot \vec{G}_j}{\phi} = \frac{q_s f_{j,s}}{\phi}, \tag{6.2}$$

the equation is split into two parts based on operator splitting. *Bratvedt et al.* [14] presented a similar operator splitting technique applied to front tracking along streamlines. The convective portion of Eq. 3.13 has already been solved and is,

$$\frac{\partial S_j^c}{\partial t} + \frac{\partial f_j}{\partial \tau} = \frac{q_s f_{j,s}}{\phi}, \tag{6.3}$$

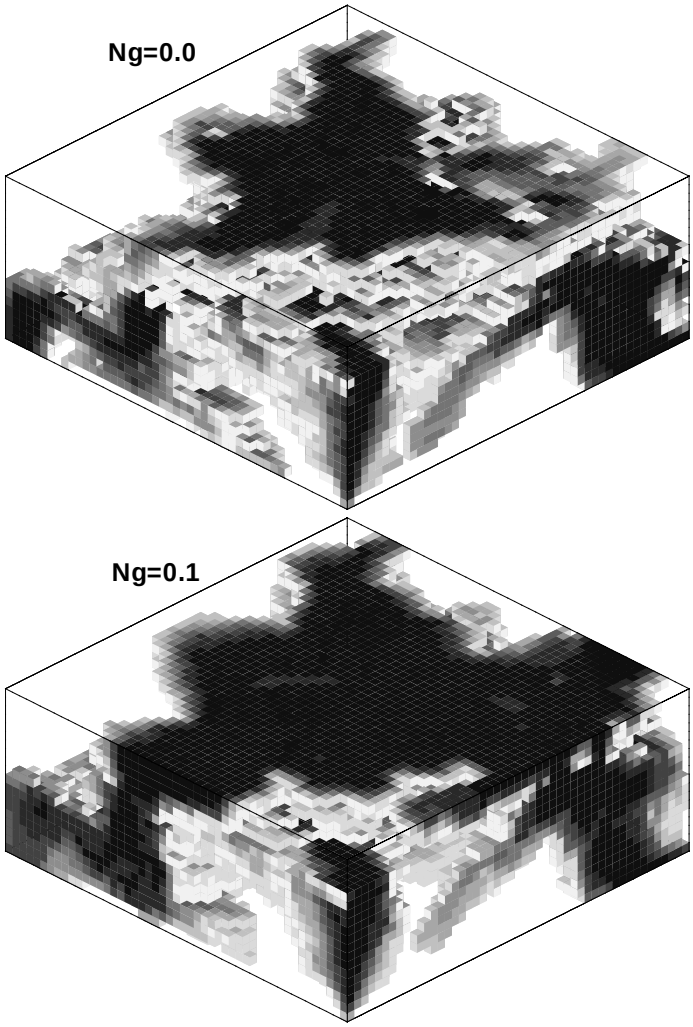


Figure 6.7: Solvent distribution in a heterogeneous media at $t_D$=0.52, without gravity and with gravity, as predicted by the streamline model. An injection well is located in the top two gridblocks in the model center, production wells are located in the lower two gridblocks in each corner of the model.

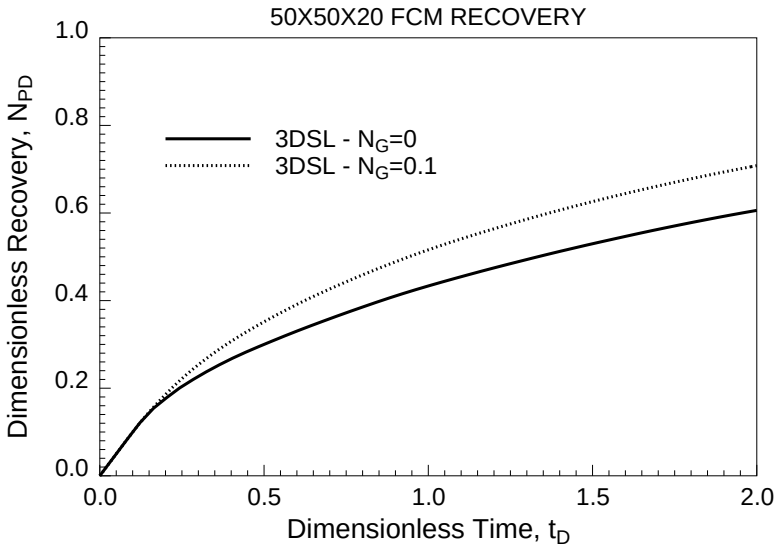


Figure 6.8: FCM displacement recovery comparison results from 3DSL for a 3D model with two different gravity numbers.

where $S_j^c$ is a temporary saturation distribution at the end of the convective step. The gravity portion of Eq. 6.2 is the one dimensional equation,

$$\frac{\partial S_j}{\partial t} + \frac{\nabla \cdot \vec{G}_j}{\phi} = 0, \tag{6.4}$$

solved along gravity lines oriented along the $\vec{g}$ vector. The initial condition to Eq. 6.4 is $S_j^c$ determined at the end of the convective step. For simplicity the Cartesian grid is assumed to be horizontal with the $z$ axis aligned along $\vec{g}$. Thus Eq. 6.5 becomes,

$$\frac{\partial S_j}{\partial t} + \frac{1}{\phi}\frac{\partial G_j}{\partial z} = 0, \tag{6.5}$$

and is a 1D first-order hyperbolic PDE. The advantage of decoupling Eq. 3.13 in this way is that Eq. 6.5 is only solved in flow regions where gravity effects are important. For example, in locations where fluids are already completely segregated $G_j$ becomes zero, as discussed in the next section, and Eq. 6.5 will not be solved.

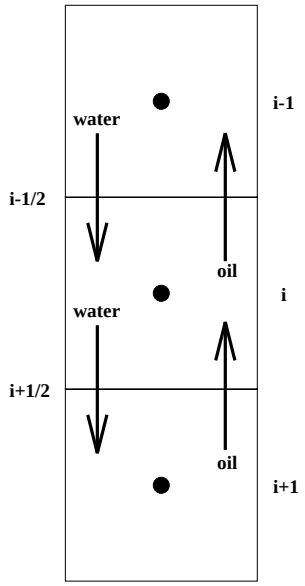


Figure 6.9: A 1D vertical discretization of an oil/water problem.

### 6.4.1 Numerical Solution along Gravity Lines

The numerical solution to Eq. 6.5 is similar to the method outlined in Section 5.5. The discretization in space and time of Eq. 6.5 is given by,

$$S_i^{n+1} = S_i^n - \frac{\Delta t_g}{\phi_i \Delta z_i}(G_{i+\frac{1}{2}} - G_{i+\frac{1}{2}}), \tag{6.6}$$

for node $i$, where $G$ is defined in Eq. 3.11, and $\Delta t_g$ is the local time step size along a gravity line. *Sammon* [63] and *Brenier & Jaffre* [15] point out that the upstream direction at which to evaluate $G$ is fluid dependent and is based on the flow direction. Consider Fig. 6.9 with three nodes of a vertical two-phase oil/water system where oil is less dense than water. The proper discretization of Eq. 3.11 about $G_{i+\frac{1}{2}}$ becomes,

$$G_{i+\frac{1}{2}} = \frac{(K_{z,i+1}k_{ro,i+1})(K_{z,i}k_{rw,i})(\rho_w - \rho_o)g}{(\mu_w K_{z,i+1}k_{ro,i+1}) + (\mu_o K_{z,i}k_{rw,i})}. \tag{6.7}$$

Note that the water properties are evaluated at the $i^{th}$ node while the oil properties are evaluated at the $i+1$ node. A similar equation is written for $G_{i-\frac{1}{2}}$. The above

equation can easily be rewritten for gas/oil systems where the gas properties are now determined at the $i+1$ node, while the oil properties are determined at the $i^{th}$ node.

For the case where gravity segregation has already occurred such that $S_{w,i} = S_{w,connate}$ and $S_{w,i+1} = 1 - S_{o,residual}$, Eq. 6.7 becomes $G_{i+\frac{1}{2}} = 0$. As expected, no flow occurs at the $i + \frac{1}{2}$ interface.

### 6.4.2 Time Stepping

The time stepping method is identical to that outlined in Section 5.4. Following the convective step taken along all streamlines, an updated saturation map exists ($S_j^c$), after which the following steps are appended:

6. If $G_j \neq 0$, include a gravity step that traces gravity lines from the top of the domain to the bottom of the domain along $\vec{g}$. For each gravity line do the following:

   (a) While tracing a gravity line, pick up the saturation distribution as a function of $z$ calculated in the convective step.

   (b) Pass the saturation profile into a 1D numerical solver and move the saturations forward by $\Delta t_p^{n+1}$ by solving Eq. 6.5. Map the new saturation profile back to the original gravity line.

7. If $G_i \neq 0$ average all gravity line properties within each gridblock to determine the final saturation distribution at $t^{n+1}$.

8. Return to Step 1 of Section 5.4.

### 6.4.3 2D Comparisons

In this section, careful 2D comparisons of gravity dominated waterflood displacements are considered. The permeability field shown in Fig. 6.10 is 250×75, and contains permeabilities that range over three-orders of magnitude. The fluid viscosity ratio is $\mu_o/\mu_w$=15. The oil and water densities were held constant but injection flow rate

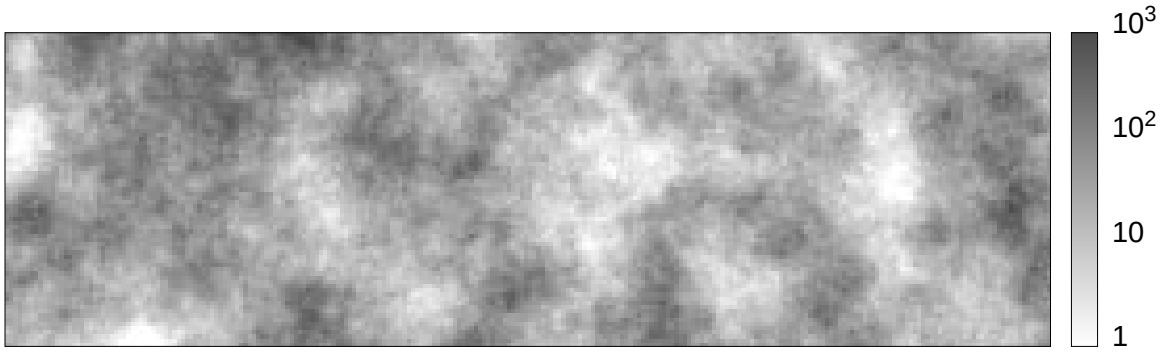


Figure 6.10: A 250×75 heterogeneous permeability field, $\lambda_{c,x}$=0.14 $\lambda_{c,z}$=0.47, $\sigma^2_{\ln}$ = 1.47, $HI$=0.21.

was varied to alter the gravity number. To magnify the effects of gravity, rather than model full interval completions, the injector was completed in the upper left 10 gridblocks of the model, while the producer was completed in the upper right 10 gridblocks of the model.

A comparison of saturation profiles between 3DSL and ECLIPSE - IMPES are shown in Figs 6.11, 6.12, and 6.13, for $N_g$=0, $N_g$=0.4, and $N_g$=10 respectively. Clearly, the new streamline method can account for gravity effects in two-phase flow as noted by the increased amount of water sinking in the model as gravity forces are increased. The streamline results show greater detail and less numerical diffusion than the ECLIPSE results, which would explain the slight difference in recoveries predicted by the two methods (Fig. 6.14).

Aside from reduced numerical artifact, a second important difference between the two methods is the speed-up factors. Compared with FCM displacements, ECLIPSE is much faster for two-phase immiscible flow calculations. Primarily, it is a result of not requiring ECLIPSE to use the two-point upstream method as was needed for FCM displacements. However, the streamline method is still faster and more accurate than ECLIPSE. For this model, the speedup factor for $N_g$=0 was 11, for $N_g$=0.4 was 4, and $N_g$=10 was 3. A summary of run performance parameters is shown in 6.2. For the waterflood example the speed-up factors decreased as gravity forces increased. This occurs because a large percentage of CPU time is now required in the 1D gravity

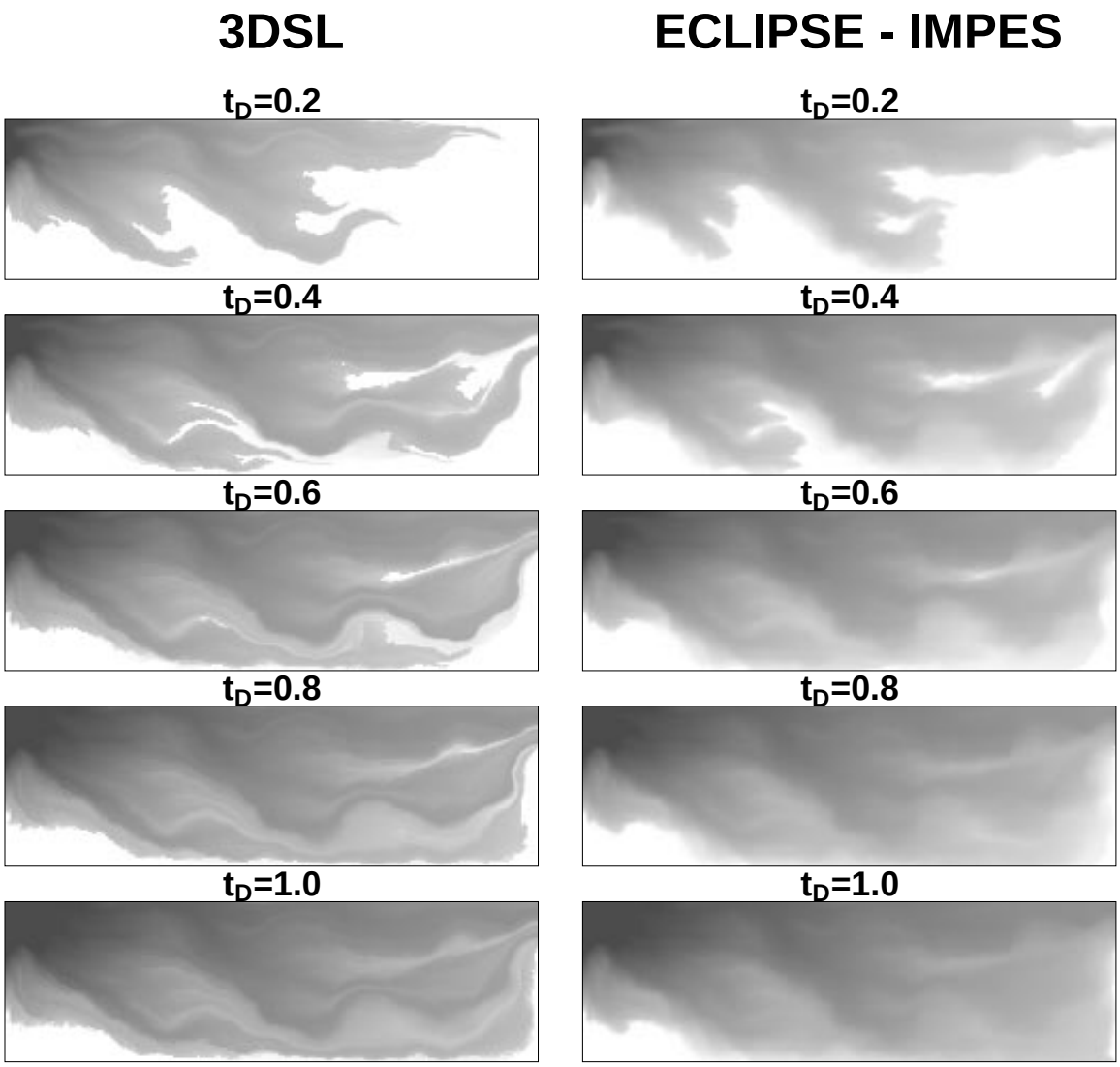


Figure 6.11: Water saturation comparisons between the streamline method and ECLIPSE - IMPES in a 250×75 heterogeneous domain for $N_g$=0. Water injection is in the upper 10 left gridblocks and production is from the upper 10 right gridblocks.

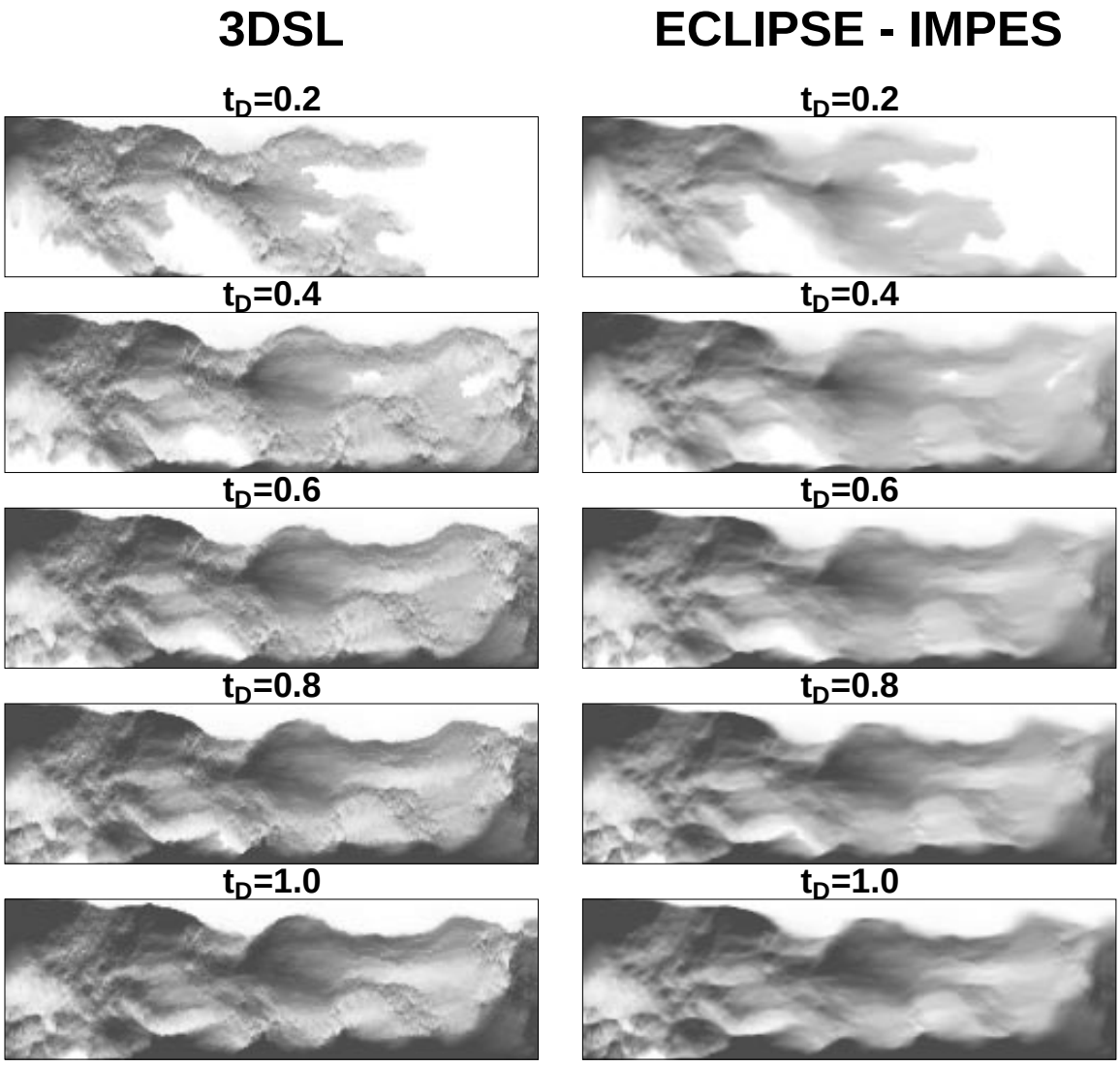


Figure 6.12: Water saturation comparisons between the streamline method and ECLIPSE - IMPES in a 250×75 heterogeneous domain for $N_g$=0.4. Water injection is in the upper 10 left gridblocks and production is from the upper 10 right gridblocks.

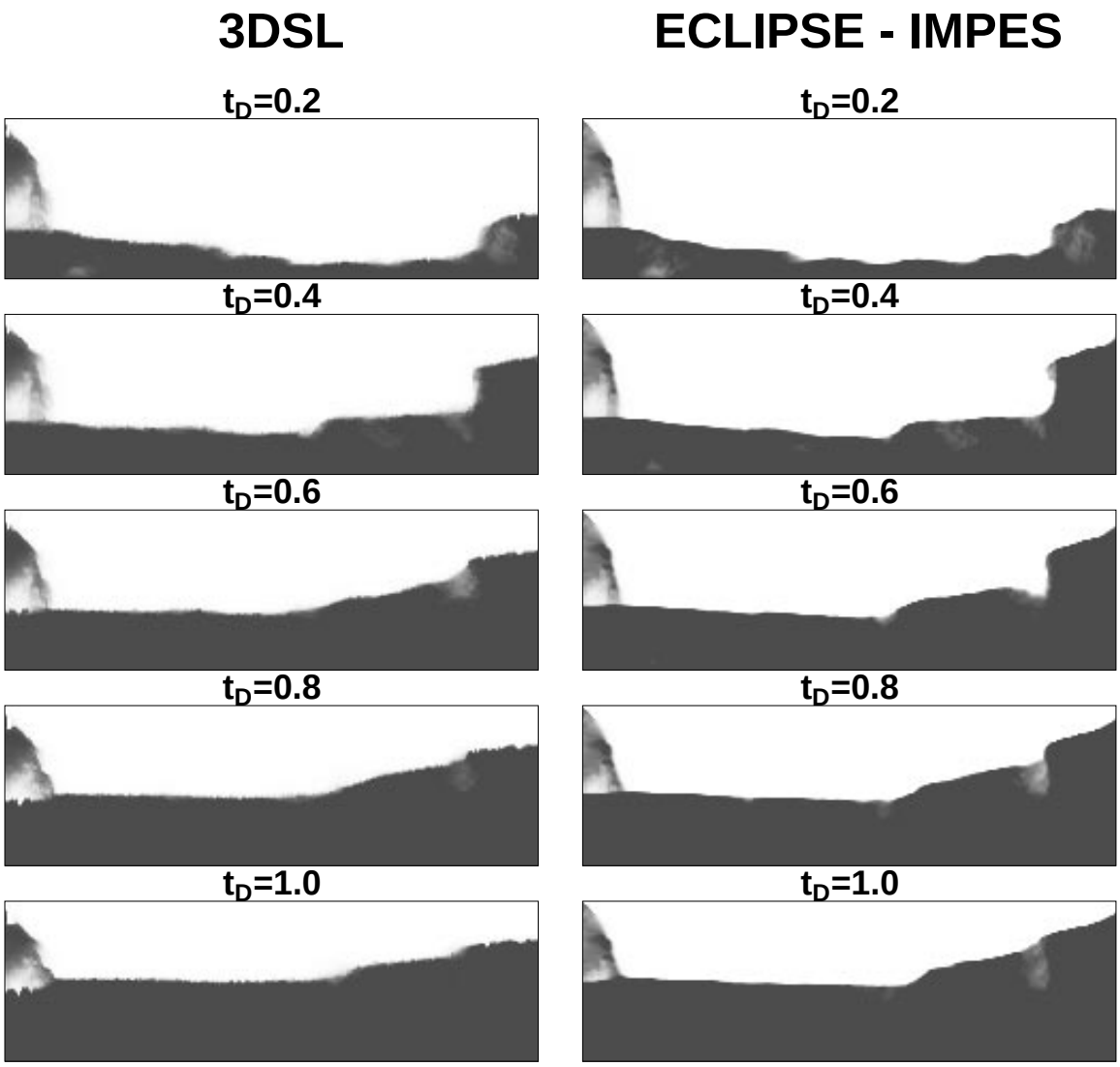


Figure 6.13: Water saturation comparisons between the streamline method and ECLIPSE - IMPES in a 250×75 heterogeneous domain for $N_g$=10. Water injection is in the upper 10 left gridblocks and production is from the upper 10 right gridblocks.

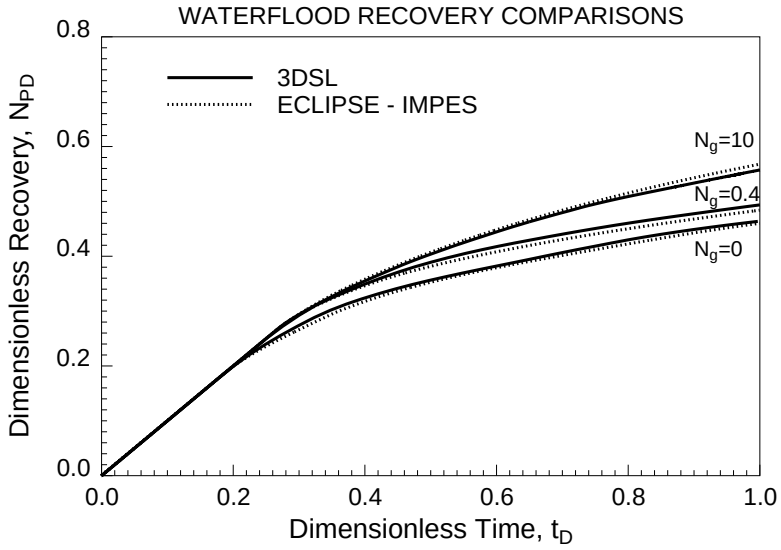


Figure 6.14: Comparison of waterflood recovery predictions in a 250×75 heterogeneous media for three different gravity numbers

solver. As $N_g$ increases the streamline simulator behaves more like a conventional method moving fluid vertically rather than moving fluid along streamlines.

### 6.4.4 3D Comparisons

In this section, a 100,000 gridblock (100×100×10) waterflood model with and without gravity is considered. An injection well is located in the lower two central gridblocks, and a production well is located in the upper two gridblocks of the model in each corner. The water saturation profile predicted by the streamline method is shown in Fig. 6.15 at $t_D$=0.5 for $N_g$=0 and $N_g$=1.0 ($\mu_o/\mu_w$=10). For this model gravity has the beneficial effect of improving the vertical conformance of the water front. With this large two-phase model it is possible to compare the streamline results against ECLIPSE in an acceptable amount of run time. The corresponding water saturation profiles for ECLIPSE are shown in Fig. 6.16. These profiles are similar to the streamline results in Fig. 6.15. Figure 6.17 is a comparison of oil recovery predicted by the two methods showing good agreement for $N_g$=0, but some differences

| | 3DSL | | ECLIPSE - IMPES | | |
|---|---|---|---|---|---|
| $N_g$ | CPU (min) | Pressure Solves | CPU (min) | Time Steps | Speed-up Factor |
| 0 | 14 | 40 | 149 | 2890 | 11 |
| 0.4 | 27 | 40 | 106 | 2013 | 4 |
| 10 | 263 | 1479 | 777 | 10651 | 3 |

Table 6.2: Comparison of simulator performance parameters between the streamline method (numerical) and ECLIPSE - IMPES for a 2D model.

for $N_g$=1.0. Again, changing the gravity number by a small amount can have a large effect on displacement performance in 3D. Although the location of oil recovery is significantly different with and without gravity, the impact on the recovery curve is not as pronounced for this waterflood as was the case for the FCM displacement of the previous section.

Recall that the speed-up factors for the small 2D model of the previous section were 10 or less. For this larger 100,000 gridblock model the streamline model required 50 minutes run time for $N_g$=0, while the equivalent ECLIPSE IMPES model required 101 hours run time – a speedup factor of 120. For the case $N_g$=1.0, the streamline model required 5.4 hours run time (100 pressure solves), while the ECLIPSE IMPES model required 297 hours run time (60,000 time steps) – a speedup factor of 55. This latter speed-up factor is largely influenced by inefficiencies in the 3DSL pressure solver.

For the $N_g$=1.0 case, using the default IMPES settings in ECLIPSE decreased the run time to 134 hours, but also resulted in an inaccurate solution. Several gridblocks containing negative saturations as high as -20% were observed. This indicated stability problems in the IMPES method. For the final run shown, the maximum time step size was a factor of 4 times smaller than the default size in order to avoid stability problems.

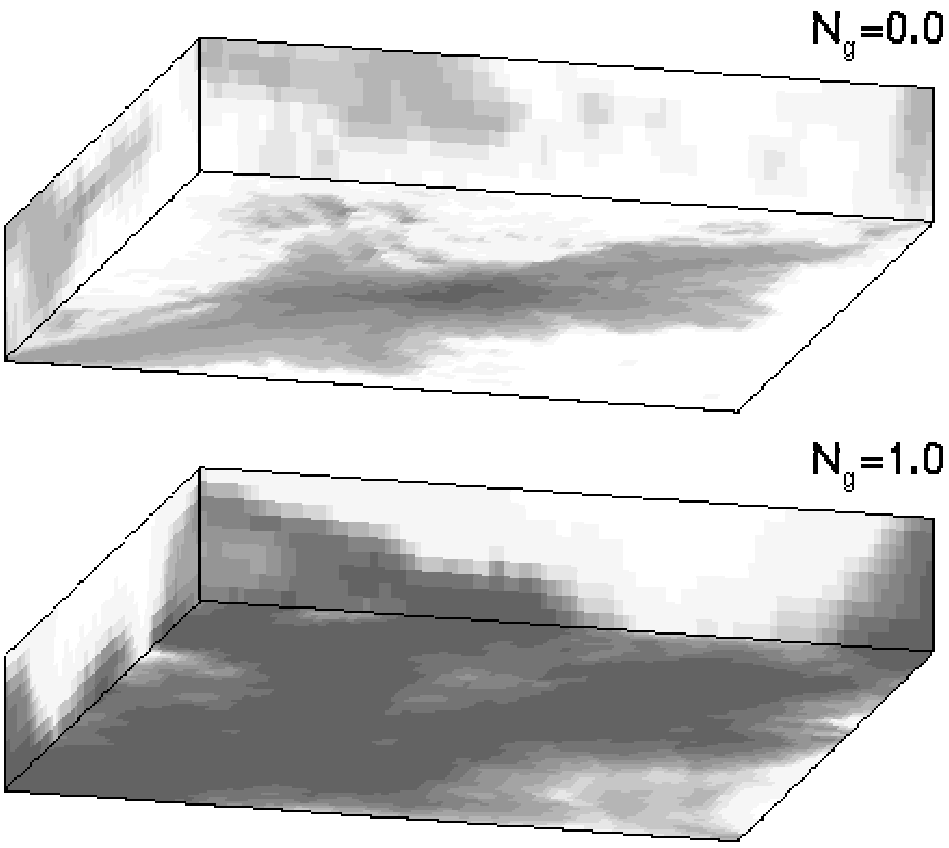


Figure 6.15: Water saturation distribution at $t_D$=0.6 in a 5-spot pattern as predicted by the streamline method for two different gravity numbers.

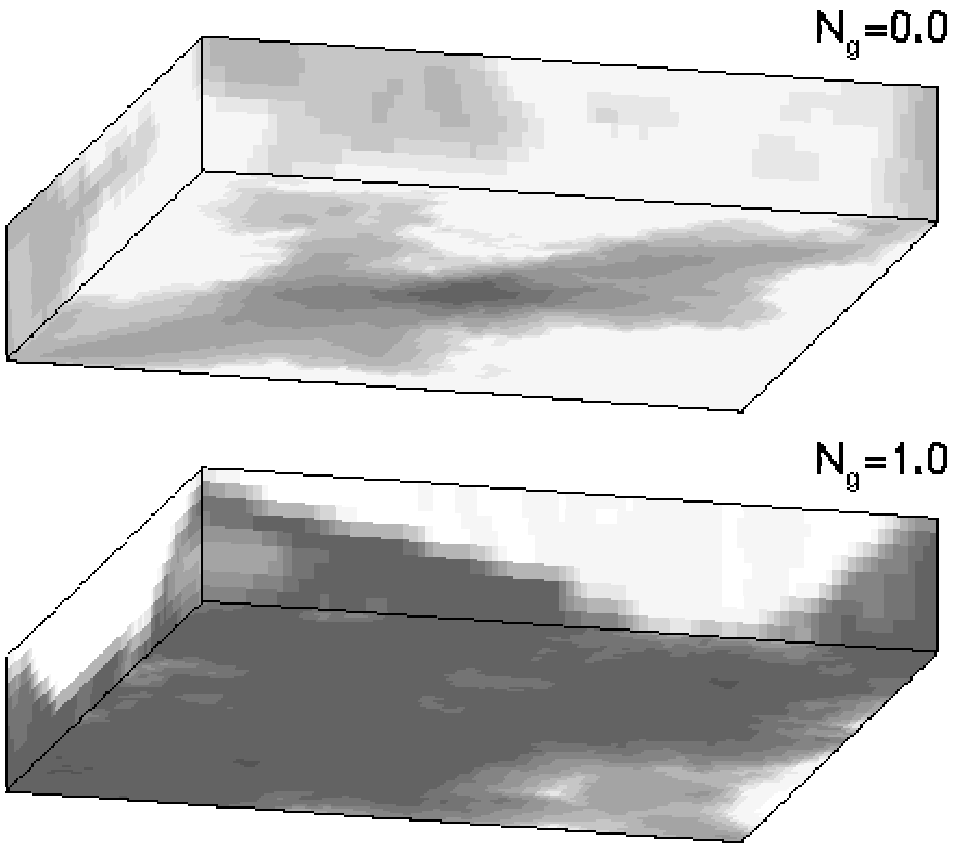


Figure 6.16: Water saturation distribution at $t_D$=0.6 in a 5-spot pattern as predicted by ECLIPSE - IMPES for two different gravity numbers.

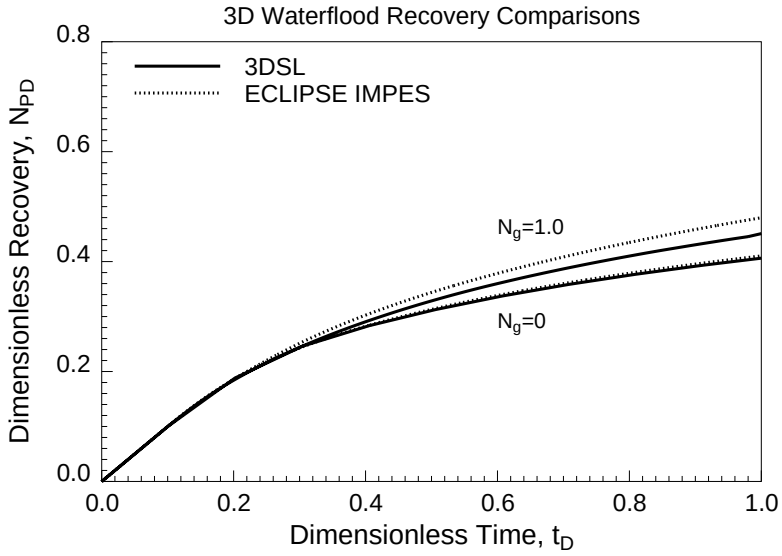


Figure 6.17: Waterflood displacement recovery comparison between the streamline method and ECLIPSE - IMPES for two different gravity numbers in a 100×100×10 gridblock model.

## 6.5 Convergence

The streamline method is an IMPES method, in that fluid saturations are moved forward in time based on the current velocity field (streamline paths). Because fluid movement is decoupled from the underlying grid, the streamline method is stable for any size time step between pressure solves ($\Delta t_p$). However, there is a maximum size for $\Delta t_p$, and it is dependent on how often the pressure field requires updating to capture nonlinearities accurately in the pressure solution due to changes in the total mobility ratio and gravity terms. These nonlinearities are a further function of the displacement type, the level of heterogeneity, and the fluid viscosity ratio. A displacement is considered converged when further reduction in $\Delta t_p$ yields no additional changes in the recovery curve for a given displacement.

Recall that when mapping analytical solutions to streamlines, convergence was only valid for flow dominated by heterogeneity (Section 4.13). In the numerical method, because fluid saturations are moved forward explicitly at each time step,

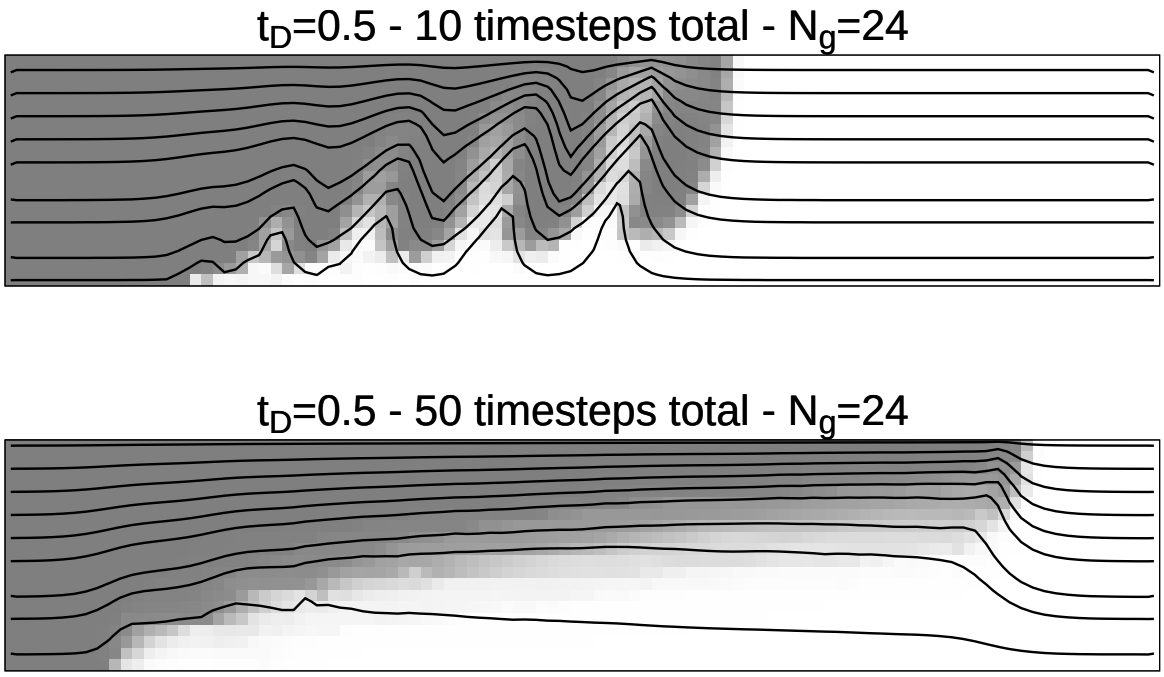


Figure 6.18: Effect of time step size on solvent profile for a gravity dominated FCM displacement in a homogeneous cross-section.

the converged solution is physically realistic and valid for any level of heterogeneity.

### 6.5.1 Effects due to Gravity

Gravity is an additional nonlinearity that alters the pressure field through time, and hence, the streamline paths. Figure 6.18 illustrates the effect of taking too large a time step between pressure solves. "Light" injected fluid will be moved along a downward portion of a streamline resulting in the swirl effect seen at the interface between the two fluids. This effect is eliminated by increasing the number of pressure solves over a given time interval (reducing $\Delta t_p$). Although the problem is magnified in a homogeneous system, this simple example illustrates that the presence of gravity does require additional pressure solves over a given time interval to reach a converged solution.

### 6.5.2 Convergence Based on Increasing Pressure Solves

Convergence of the 2D FCM displacements considered in Section 6.3.1 is shown in Fig. 6.19. For each gravity number, a series of displacements were run over the fixed total time of $t_D$=2. Also for each gravity number, the time step size between convective steps was held constant ($\Delta t_c$ constant) but the number of pressure solves was increased ($\Delta t_p$ reduced). Holding the number of convective steps constant amounts to fixing the number of remappings to the underlying grid, and thus the level of mixing between streamlines. Based on Fig. 6.19, convergence results were assigned to Table 6.1. To summarize, as the gravity number changed from 0 to 2 to 10 the number of pressure solves required to reach a converged solution changed from 100 to 100 to 250, respectively. Note that for $N_g$=10, although there is no change in predicted recovery after 50 pressure solves, a swirl effect between the solvent and oil interface was observed in the saturation profiles for all but the 250 pressure solves case.

Similar numerical experiments were carried out for the 2D waterflood example discussed in Section 6.4.3. As $N_g$ changed from 0 to 0.4 to 10, the number of pressure solves required for convergence increased from 40 to 40 to 1500. Again, for the $N_g$=10 case there is little difference between recovery curves after 100 pressure solves. Convergence was determined based on studying the associated saturation profiles for nonphysical features.

### 6.5.3 Convergence Based on Front Movement

Rather than having to run a displacement multiple times and analyze the recovery curves and saturation profiles for convergence, it would be useful to determine the time step size between pressure solves ($\Delta t_p$) *a priori*. For an IMPES method, the optimum time step size is such that the fastest front moves one gridblock per time step. Unfortunately, in a conventional finite-difference method, the maximum time step size is typically based on constraints dictated by high flow rate gridblocks near wells. Thus, as a displacement proceeds, front movement is considerably less than a single gridblock per time step. However, with the streamline method the fastest front can always be moved at a single gridblock per time step, regardless of the velocity

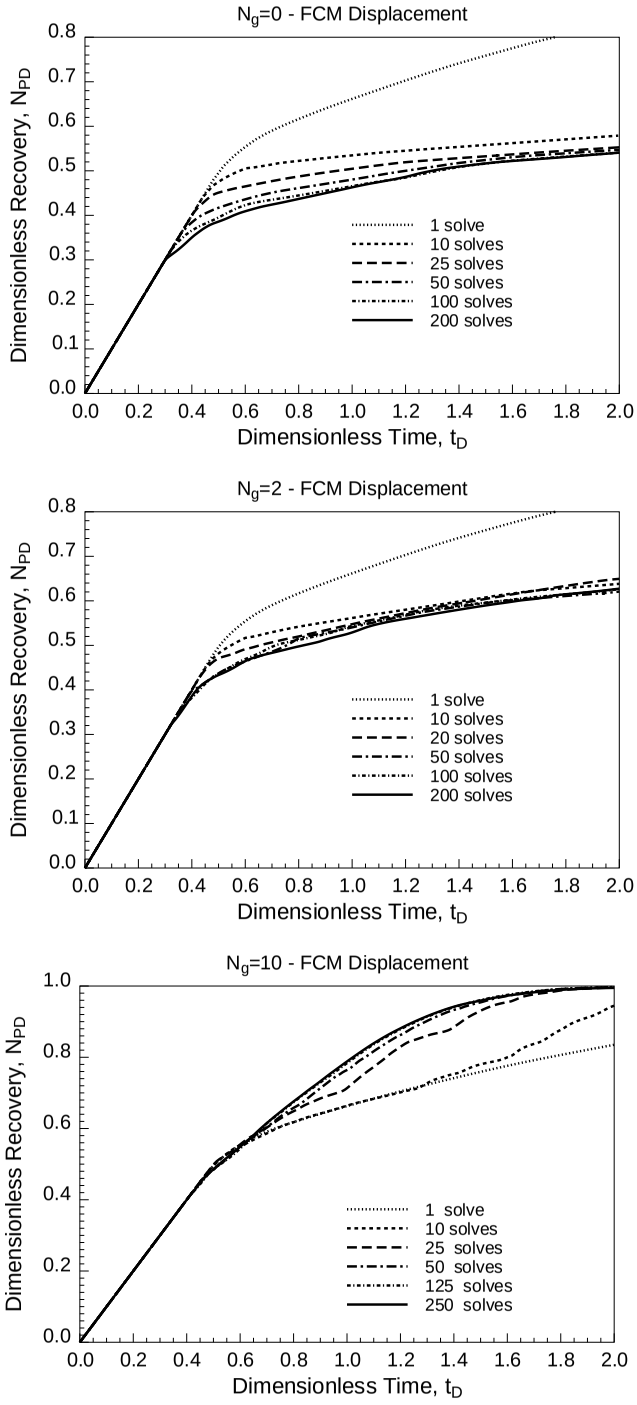


Figure 6.19: 3DSL convergence of recovery for 2D FCM displacements at three different gravity numbers as the number of pressure solves is increased ($M$=10).

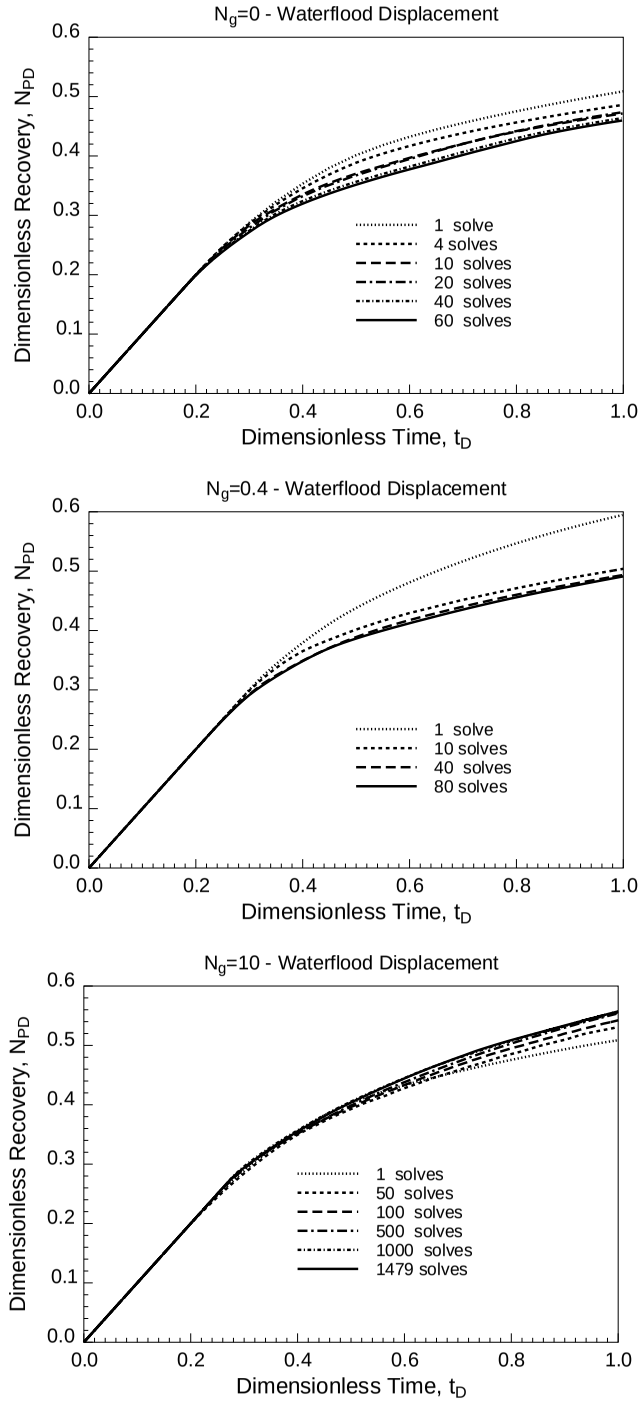


Figure 6.20: 3DSL convergence of recovery for 2D waterflood displacements at three different gravity numbers as the number of pressure solves is increased ($\mu_o/\mu_w$=15).

constraints near wells. Moreover, with the streamline method, fronts can be moved substantially further than a single gridblock per time step. Thus, the parameter of interest is the maximum number of gridblocks that the leading front can move yet still ensure convergence. This parameter remains a function of the nonlinearities in the pressure field. But, the limiting case of moving the fastest front 1 gridblock per time step will alway result in a converged solution. Smaller time steps simply result in saturation changes at a sub-gridblock level only and cannot be required to improve accuracy.

For the streamline method, a good estimate of the next time step size $\Delta t_p^{n+1}$ before a pressure solve is required is based on,

$$\Delta t_p^{n+1} = \frac{\tau_{min}^n}{n_{blks,\tau_{min}^n}} \frac{MAX_{blks}}{V_{blshock}}, \tag{6.8}$$

where $\tau_{min}^n$ is the minimum time-of-flight for all streamlines reaching producers at the $n^{th}$ time level that do not have fluid breakthrough, $n_{blks,\tau_{min}^n}$ is the number of blocks that the minimum time-of-flight streamline passes through, $MAX_{blks}$ is the desired maximum number of gridblocks the leading front can move per time step, and $V_{blshock}$ is the dimensionless Buckley-Leverett shock velocity for the displacement. Eq. 6.8 predicts that on average the maximum front speed obeys $MAX_{blks}$. An additional feature of the automatic time stepping using Eq. 6.8 is that $\Delta t_p$ will begin to increase after breakthrough.

Using Eq. 6.8, a sensitivity study on $MAX_{blks}$ was conducted for the three FCM displacements of Section 6.3.1 (125×75 gridblocks). Maximum front movement was varied between 1 and 20 gridblocks per time step. Recovery curves for the corresponding $N_g$ and $MAX_{blks}$ are shown in Fig. 6.21. Note for these comparisons a single remapping to the underlying grid occurred after each pressure solve. Thus, the number of remappings is no longer constant between runs. Based on Fig. 6.21, as $N_g$ changed from 0 to 0.4 to 10, the value of $MAX_{blks}$ was reduced from 5 to 2 to 1. As expected, for large gravity effects, front movement was reduced to a single gridblock per time step. Moving a front any faster increases the possibility of moving light fluids on downward portions of streamlines, as discussed in Section 6.5.1.

A similar convergence study was conducted for the three waterflood displacements

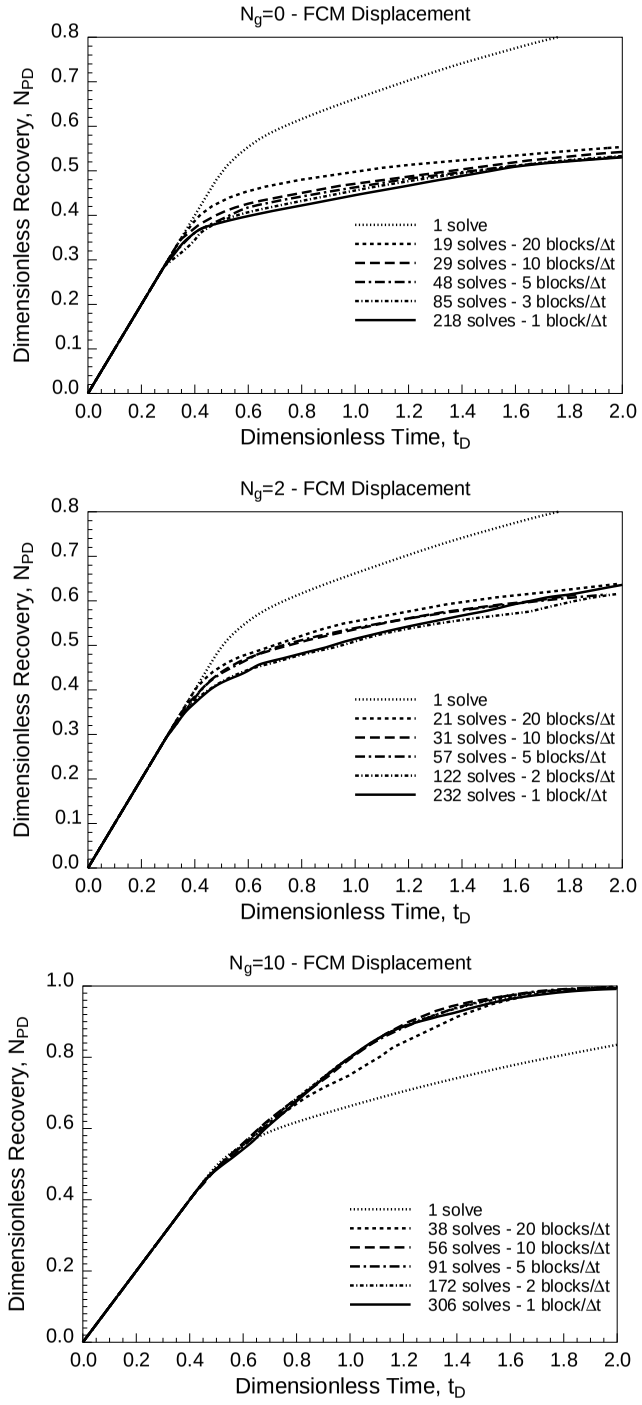


Figure 6.21: 3DSL convergence of recovery for 2D FCM displacements at three different gravity numbers as the number of pressure solves is increased ($M = 10$).

presented in Section 6.4.3 (250×75) gridblocks. Front movement was varied from 250 blocks per time step down to 15 blocks per time step for $N_g$=0 and $N_g$=0.4. Front movement was varied from 25 blocks per time step down to 1 block per time step for the $N_g$=10 case. Recovery curves for each case are summarized in Fig. 6.22. Based on Fig. 6.22, as $N_g$ changed from 0 to 0.4 to 10, the corresponding value of $MAX_{blks}$ required for convergence changed from 25 to 31 to 2. $MAX_{blks}$ does not decrease consistently as expected between $N_g$=0 and $N_g$=0.4. The addition of a small amount of gravity alters the water path (see Fig. 6.11 versus Fig. 6.12) and must result in a reduced $\tau_{min}$ for the breakthrough streamline. For the waterflood $N_g$=10 case a converged solution was reached at 2 gridblocks per time step, rather than 1 as in the FCM case. This is because there is now the operator splitting step that will adjust fluid positions after they are moved convectively along streamlines.

One key conclusion from this section is that the streamline method does exhibit convergence as the maximum front speed is reduced to the limiting case. However, for all but the gravity-dominated displacements, a front speed of one is not required. Table 6.3 summarizes the maximum number of gridblocks that a front must move in the 2D FCM displacements to result in a converged solution with the streamline method for each gravity number and the associated number of time steps. Also included are results from ECLIPSE – IMPES. A similar summary for the 2D waterflood displacements are shown in Table 6.4. For the streamline method, Tables 6.3 and 6.4 show that the greater the nonlinearity in the pressure field, the shorter distance that fronts must be moved in order to properly honor the nonlinearity. Note that in all cases, the maximum front speed within ECLIPSE was considerably less than 1 gridblock per time step. These small front speeds are a direct result of the time step size being dictated by global stability conditions in high flow rate gridblocks. Thus within ECLIPSE, the pressure field is recalculated each time step based on front movement at a sub-gridblock scale.

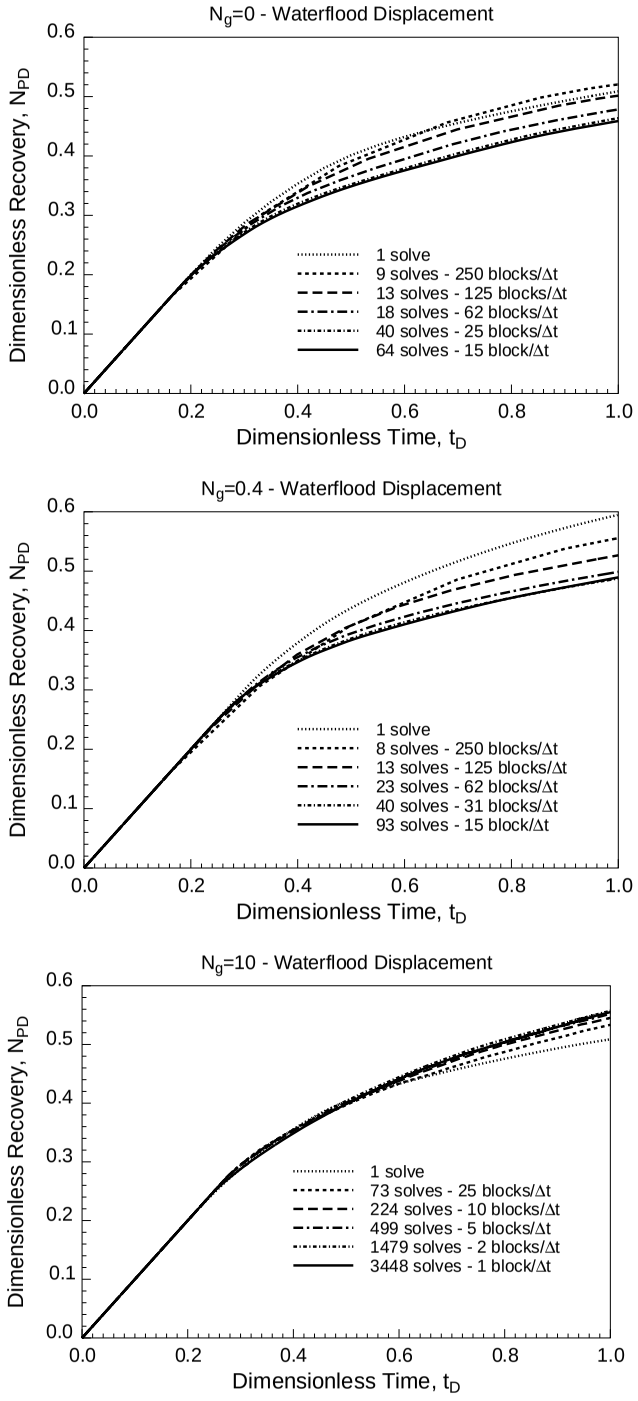


Figure 6.22: 3DSL convergence of recovery for 2D waterflood displacements at three different gravity numbers as the number of pressure solves is increased ($\mu_o/\mu_w$=15).

| | 3DSL | | ECLIPSE - IMPES | |
|---|---|---|---|---|
| $N_g$ | Time Steps | Maximum Front Speed | Time Steps | Maximum Front Speed |
| 0 | 48 | 5 | 1742 | 0.14 |
| 2 | 122 | 2 | 8641 | 0.03 |
| 10 | 306 | 1 | 32767 | 0.01 |

Table 6.3: Comparison of maximum front speeds (number of gridblocks per time step) required for convergence using 3DSL, and associated front speeds for ECLIPSE - IMPES, for 2D FCM model at three different gravity numbers.

| | 3DSL | | ECLIPSE - IMPES | |
|---|---|---|---|---|
| $N_g$ | Time Steps | Maximum Front Speed | Time Steps | Maximum Front Speed |
| 0 | 40 | 25 | 2890 | 0.35 |
| 0.4 | 40 | 31 | 2013 | 0.62 |
| 10 | 1479 | 2 | 10651 | 0.28 |

Table 6.4: Comparison of maximum front speeds (number of gridblocks per time step) required for convergence using 3DSL, and associated front speeds for ECLIPSE - IMPES, for 2D waterflood model at three different gravity numbers.

## 6.6 Chapter Summary

To model field scale displacements with the streamline model properly, gravity effects must be accounted for. Previous streamline/streamtube methods could not account for gravity effects since analytical solutions were mapped along streamlines. In this manner, there was no mechanism to move fluids along pathlines. However, by picking up the current saturations and moving them forward numerically along updated streamlines, fluid pathlines are honored. Gravity effects in FCM displacements could successfully be modeled over a large range of gravity numbers. Two-phase gravity problems are more difficult to model with the streamline method. However, by separating the governing equation into a convective step and a gravity step (operator-splitting) the streamline method now accounts for gravity effects in multiphase flow.

In comparisons with conventional simulation methods, the streamline method still retains orders-of-magnitude speed-ups and accuracy. The magnitude of the speed-up depends on the size of the gravity number, the model size, and the type of displacement process.

It was also shown that the streamline method converges as front movement is reduced to the limiting case of one gridblock per time step. However, by decoupling fluid movement from the underlying grid, maximum front speeds of much greater than one gridblock per time step were possible with the streamline method yet still resulted in converged solutions. For gravity-dominated displacements, front movement on the order of one gridblock per time step was required due to the additional nonlinearity of the displacement. In comparison, it was illustrated that the maximum front speeds in conventional IMPES methods are substantially less than one gridblock per time step. This is because time step size is governed by the global grid CFL constraint, which is typically defined by high flow velocities near wells.

# Chapter 7

# Recommendations

The streamline method has been extended to more general conditions by mapping one-dimensional numerical solutions along streamlines. The physics of the displacement is captured in the 1D solutions, while heterogeneity is captured by the streamline paths. The extensions include an investigation of gravity, changing well conditions, and even viscous fingering. It is fair to say however, that a vast set of problems still exist which conventional simulation methods can model that the current streamline method cannot. These are potential areas of future research. A second area of research would be based on applications that take advantage of the streamline simulator's speed. The method provides a useful tool to study problems where a flow simulation is only one component of a more complex modeling process such as, scale-up, history matching, or ranking of multiple images.

1. **Compositional Simulations**

   Compositional simulations with conventional methods have large CPU requirements, suffer from severe numerical diffusion and lack the large number of grid-blocks necessary to represent heterogeneity adequately or resolve displacement fronts between wells. *Thiele et al.* [71] mapped analytical compositional solutions to streamlines and quoted speed-up factors of 4-5 orders of magnitude.

A key result was that numerical diffusion in traditional methods almost completely eliminated mobility contrasts and gave overly optimistic recovery predictions compared with the streamline results. Mapping numerical compositional solutions to streamlines will introduced some numerical diffusion. However, as has been shown for tracer and FCM displacements, the numerical artifact is significantly less than the levels present in conventional methods. The added benefit of a numerical method will be that compositions will be moved along pathlines, more accurately capturing the nonlinearities in the solution.

Numerical compositional solutions can be mapped to streamlines in a very similar manner as miscible and two-phase solutions were. To extend the current method, the 1D solver will be modified to account for phase behavior effects to solve component conservation equations along streamlines.

2. **Black Oil Simulations**

Black oil simulations have not been investigated here, yet they are probably the second most common type of displacement modeled after waterflooding. The problem includes mass transfer between the oil and gas phase, compressibility effects, and the presence of a water phase. To extend the streamline method to this problem requires accounting for compressibility effects and three-phase flow. Certainly, 1D solutions of black oil models can be solved, but a valid question to ask is "What streamlines are the 1D solutions mapped along?" A total velocity can still be defined, but there is the added complication of streamlines originating in arbitrary gridblocks due to compressibility effects. There are also additional nonlinearities in the governing pressure equation since gridblock GOR's and oil and gas formation volume factors are now functions of pressure. Because of these nonlinearities, a greater number of pressure solves than the number required for incompressible problems may be required to minimize material balance errors.

3. **Additional Flow Mechanisms**

   The streamline method decouples each mechanism that influences flow, solving them separately then combining the results. This decoupling is attractive because it can be easier to implement and solve many simple problems as opposed to solving a single large problem at each time step. Gravity was treated as an additional correction to the convective step along streamlines by operator splitting. The result was a gravity step along gravity lines. Additional processes such as diffusion and capillary pressure can also be included in the streamline method. *Thiele et al.* [70] present a method to account for longitudinal diffusion by including a diffusion term in the 1D solution. *Blunt et al.* [10] present a method to account for transverse diffusion which amounts to adding a random component to the tracing of a streamline, an approach that is similar to particle tracking methods. Capillary effects can be modeled in the main direction of flow by modifying the one dimensional solution. However accounting for capillary effects in the transverse direction, which will typically have greater saturation gradients, may prove to be more difficult. A capillary step based on operator splitting could be included similarly to the representation of gravity effects, although the step will not be one-dimensional.

4. **Mixing Due to Remapping**

   The new method of mapping numerical solutions to streamlines has overcome many limitations of previous streamline methods. However discussed in Chapter 4, there is now mixing present at a gridblock scale between streamlines. The level of mixing is a function of the number of remappings taken during a simulation and is a result of only knowing saturation information to a gridblock scale detail. This work has not addressed how the mixing relates to a grid Peclet number for instance, or how longitudinal and transverse mixing are affected by the number of remappings.

5. **Volume Balance Errors**

   The remapping technique used in this work to assign gridblock average fluid properties did not guarantee volume conservation. A volume balance was performed after each remapping step to determine the required time correction to ensure conservation. An obvious improvement to the method would include a more rigorous mapping method which correctly picks up all of the fluid volume, moves it forward, and then correctly remaps the volume to the underlying grid. One possibility may be to store the saturation information on a finer grid than the grid on which the pressure field is solved.

6. **Contaminant Migration**

   A body of problems in the groundwater area exist with modeling flow of contaminant in porous media. Contaminant transport problems are typically modeled as single-phase flow, for which the streamline tracing is trivial. The difficulty of contaminant transport problems is accounting for the many reactions, adsorption and desorption of components that occur. Particle tracking methods are typically used but are slow and prone to mass-balance errors. Again, the streamline method is ideally suited to this class of problems because the 1D numerical solutions solved along streamlines can be easily modified to account for additional contaminant effects.

7. **Use as a Fast Flow Simulation Transfer Function**

   The speed of the streamline simulator makes it ideally suited to any process that requires a fast flow simulator embedded in a modeling loop. Such problems arise in automatic history matching, screening of geologic images, or estimating uncertainty in flow simulations based on uncertainty in permeability distributions.

   As this thesis demonstrates, the streamline simulator can solve million gridblock models on standard sized workstations. The method provides an easy way to increase resolution of heterogeneity by another order of magnitude. It would be interesting to examine what level of detail in modeling heterogeneity is required before no noticeable impact on recovery occurs.

8. **Improve Streamline Simulator Efficiency**

   The streamline simulator presented in this work (3DSL) is far from optimized. One area of improvement is the iterative solver. Currently 3DSL uses public domain solvers that are not specifically optimized for reservoir engineering problems. For example, the matrix inversion routine in ECLIPSE is roughly three times faster than that used in 3DSL.

   A second area that could be improved is the streamline tracing. Tracing streamline paths and time stepping along streamlines could be done in parallel on a shared memory machine.

# Chapter 8

# Conclusions

This work has presented an extension of previous streamline/streamtube methods to multiwell field scale displacements. Such field scale phenomena as heterogeneity, gravity, changing well conditions, and nonuniform initial conditions can now be modeled with the new streamline method.

The basic idea of the streamline method consists of decoupling the full 3D problem into multiple 1D problems solved along streamlines. This decoupling amounts to moving fluids along streamlines. Streamlines represent the natural grid on which to transport fluids. The method therefore reduces grid orientation effects, numerical diffusion, and most importantly it eliminates time step constraints due to stability. The ability to take large time steps has resulted in speed-up factors up to three orders of magnitude over conventional finite-difference methods.

The major conclusions of this work are:

1. **True 3D Multiwell Models**

   Use of streamlines rather than streamtubes allows straightforward modeling of true 3D domains.

2. **Fast Accurate Solutions**

   Tracer, waterflood, and first-contact miscible displacement comparisons indicate that the streamline method is faster than conventional finite difference

techniques by factors of 1 to 3 orders of magnitude. As displacement complexity and model size increase, the speed-up factors also increase. For FCM and tracer displacements, the streamline method produces more accurate results due to reduced levels of numerical diffusion. Waterflood displacements, which are very stable, are not as affected by numerical artifacts. For these latter cases the streamline method and conventional methods agree very well over a large range of field models.

3. **Fluid Movement Along Streamlines**

   Transporting fluid along the natural streamline grid, rather than between discrete gridblocks, offers several advantages. Most importantly, the underlying grid stability constraints that limit fluid movement in a conventional method are removed in the streamline method. There is no global grid CFL condition in the streamline method. Any size time step can be taken with the streamline method between saturation or pressure updates. Furthermore, grid orientation effects are substantially reduced in the streamline method.

4. **Converged Solutions**

   The ability to take very large time steps in the streamline method introduces a question of what maximum time step size can be taken before the pressure field needs to be updated. The answer is dependent on the nonlinearities of the displacement. For displacements dominated by heterogeneity, maximum front speeds of about 25 gridblocks per time step were satisfactory for waterfloods, while maximum front speeds of about 5 gridblocks per time step were satisfactory for FCM displacements. For gravity-dominated displacements, maximum front speed movement was reduced to 1–2 gridblocks per time step to properly account for the additional nonlinearity. It was also shown that the numerical streamline method does converge as the maximum front movement is reduced to the limiting case of a single gridblock per time step between pressure solutions.

5. **Accurate Representation of Heterogeneity Effects**

   Although the streamline method clearly has limitations, the most important

advantage is that the method can account for more detail in heterogeneity. Example cases in Chapters 4 and 5, demonstrated that the process of upscaling and reducing permeability detail can lead to over optimistic predictions of reservoir response.

6. **Solution to Million Gridblock Size Models**

   The speed of the streamline method makes it well suited to solutions of very large problems. Displacement results presented in Chapters 4 and 5 for multiwell million gridblock models illustrate that solutions can be obtained on a standard workstation. In contrast, the models were upscaled sixteen times in order to run on the same machine with a conventional finite-difference method. Thus, the streamline method makes more efficient use of fixed computer resources.

7. **Extension to Field Scale Conditions**

   Common situations present in field scale simulations include gravity effects, changing well conditions, and nonuniform saturation distributions present at the start of production. By mapping numerical solutions along streamlines the method can account for the above effects present in field scale displacements.

# Nomenclature

| | | |
|---|---|---|
| $A_{k+\frac{1}{2}}$ | = | gridblock cross-sectional area between $k$ and $k+1$ gridblocks |
| $\vec{B}$ | = | right hand side vector of pressure equation |
| $C$ | = | tracer concentration |
| $C_m$ | = | center of mass |
| $C_s$ | = | solvent concentration |
| $D_i$ | = | depth of gridblock $i$ from datum |
| $\vec{\vec{D}}_{ij}$ | = | dispersion coefficient of component $i$ in phase $j$ |
| $f_j$ | = | fractional flow of phase $j$ |
| $f_{j,s}$ | = | fractional flow of phase $j$ at source or sink |
| $f_p$ | = | fraction flow at a producer |
| $f^{sl}$ | = | fraction flow assigned to a streamline |
| $\vec{G}_j$ | = | gravity component of fraction flow of phase $j$ |
| $G_{z,k+\frac{1}{2}}$ | = | inter-block gravity transmissibility in $z$ direction |
| | | between $k$ and $k+1$ gridblocks |
| $g$ | = | gravitational acceleration constant |
| $H$ | = | height of 2D cross-sectional model |
| $HI$ | = | heterogeneity index |
| $\vec{\vec{K}}$ | = | absolute permeability tensor |
| $\overline{K}_h$ | = | average horizontal permeability |
| $\overline{K}_v$ | = | average vertical permeability |
| $k_{rj}$ | = | relative permeability of phase $j$ |
| $L$ | = | distance between producer and injector |
| $MAX_{blks}$ | = | maximum blocks that a front can move in a time step |
| $M$ | = | viscosity ratio |
| $m_x$ | = | velocity gradient across gridblock in $x$ direction |
| $N_c^{sl}$ | = | streamline Courant Number |
| $N_g$ | = | Gravity Number |
| $N_{PD}$ | = | dimensionless recovery |

| | | |
|---|---|---|
| $N_{pe}^{sl}$ | = | streamline Peclet Number |
| $n$ | = | number of pressure time steps |
| $n_p$ | = | number of phases |
| $n_{sl}^{face}$ | = | number of streamlines launched from an injection face |
| $P$ | = | pressure |
| $\vec{P}$ | = | pressure vector in pressure equation |
| $Q^n$ | = | total field injection rate at $n^{th}$ time step |
| $q_{face}$ | = | flux across injection block face |
| $q_s$ | = | source or sink flow rate |
| $q^{sl}$ | = | flux assigned to a streamline |
| $q_s^{sl}$ | = | source/sink flow rate based on sum of streamline fluxes |
| $r_{o,k}$ | = | Peaceman's radius of wellbore in layer $k$ |
| $r_{w,k}$ | = | wellbore radius in layer $k$ |
| $S_j$ | = | saturation of phase $j$ |
| $\bar{S}_{gb}$ | = | average saturation of a gridblock |
| $\bar{S}^{sl}$ | = | average saturation of a streamline within a gridblock |
| $s$ | = | spatial distance coordinate along a streamline |
| $s_k$ | = | wellbore skin in layer $k$ |
| $\mathbf{T}$ | = | transmissibility matrix |
| $T^n$ | = | true time after $n^{th}$ time step |
| $T_k^w$ | = | wellbore transmissibility of layer $k$ |
| $T_{z,k+\frac{1}{2}}$ | = | inter-block transmissibility in $z$ direction between $k$ and $k+1$ gridblocks |
| $t$ | = | time |
| $t_D$ | = | dimensionless time |
| $\vec{u}_j$ | = | Darcy velocity of phase $j$ |
| $\vec{u}_t$ | = | total Darcy velocity |
| $V$ | = | interstitial velocity |
| $V_{blshock}$ | = | Buckley-Leverett shock velocity |
| $\bar{V}_p$ | = | average porevolume of a streamtube |
| $V_{st}$ | = | volume of a streamtube |
| $v_D$ | = | dimensionless velocity |
| $W_I^n$ | = | cumulative volume of injection phase injected at $n^{th}$ time step |
| $W_P^n$ | = | cumulative volume of injection phase produced at $n^{th}$ time step |
| $x_D$ | = | dimensionless distance |
| $x_e$ | = | $x$ position of streamline exit location |
| $x_i$ | = | $x$ position of streamline inlet location |
| $x_o$ | = | $x$ position of origin in a gridblock |

| | | |
|---|---|---|
| $x, y, z$ | = | spatial coordinates |
| $\alpha$ | = | reservoir dip angle |
| $\gamma_i$ | = | mobility weighted wellbore specific gravity of layer $i$ |
| $\Delta P_h$ | = | average pressure drop in horizontal direction |
| $\Delta\rho$ | = | fluid density difference |
| $\Delta t_c$ | = | time step size between convective steps |
| $\Delta t_{e,x}$ | = | time-of-flight required to reach an $x$ exit face |
| $\Delta t_g$ | = | time step size along gravity line |
| $\Delta t_p$ | = | time step size between pressure steps |
| $\Delta t_{sl}$ | = | time step size along a streamline |
| $\Delta x$ | = | gridblock dimension in $x$ direction |
| $\Delta y$ | = | gridblock dimension in $y$ direction |
| $\Delta z$ | = | gridblock dimension in $z$ direction |
| $\Delta\tau_{sl}$ | = | time-of-flight increment along a streamline |
| $\zeta$ | = | local streamline coordinate |
| $\lambda_c$ | = | permeability correlation length |
| $\lambda_g$ | = | total gravity mobility |
| $\lambda_t$ | = | total mobility |
| $\mu_j$ | = | viscosity of phase $j$ |
| $\pi$ | = | Archimedes number |
| $\rho_j$ | = | density of phase $j$ |
| $\tau$ | = | time of flight |
| $\Phi$ | = | potential function |
| $\phi$ | = | porosity |
| $\Psi$ | = | stream function |
| $\omega$ | = | Todd & Longstaff mixing parameter |
| $\omega_i$ | = | weighting factor for a streamline in a gridblock |
| $\omega_{ij}$ | = | mass fraction of component $i$ in phase $j$ |

# Bibliography


[1] Araktingi, U.G. and Orr, F.M., Jr.: "Viscous Fingering, Gravity Segregation and Reservoir Heterogeneity in Miscible Displacements in Vertical Cross Section," paper SPE 20176 in proceedings of the 1990 SPE/DOE Seventh Symposium on Enhanced Oil Recovery, Tulsa, OK.

[2] Araktingi, U.G. and Orr, F.M., Jr.: "Viscous Fingering in Heterogeneous Porous Media," *SPE Advanced Technology Series* (October 1993) **1**, No. 1, 71–80.

[3] Aziz, K. and Settari, A.: *Petroleum Reservoir Simulation*, Applied Science Publishers, Essex, England (1979).

[4] Baker, R.O.: "Effect of Reservoir Heterogeneities and Flow Mechanisms on Numerical Simulation Requirements," Master's thesis, University of Calgary (July 1994).

[5] Batycky, R.P., Blunt, M.J., and Thiele, M.R.: "A 3D Field Scale Streamline Simulator With Gravity and Changing Well Conditions," paper SPE 36726 in proceedings of the 1996 Annual Technical Conference and Exhibition, Denver, Co, October.

[6] Batycky, R.P., Blunt, M.J., and Thiele, M.R.: "A 3D Multi-Phase Streamline Simulator with Gravity and Changing Well Conditions," Proceedings of the 17th International Energy Agency Collaborative Project on Enhanced Oil Recovery, Sydney, Australia (September 1996).

[7] Batycky, R.P., Thiele, M.R., and Blunt, M.J.: "A Streamline Simulator to Model

Field Scale Three-Dimensional Flow," in proceedings of the 1996 5th European Conference on the Mathematics of Oil Recovery, Leoben, Austria, September.

[8] Bear, J.: *Dynamics of Fluids in Porous Media*, American Elsevier, New York (1972).

[9] Blunt M.J. and Rubin R.: "Implicit Flux Limiting Schemes for Petroleum Reservoir Simulation," *Journal of Computational Physics* (Sept. 1992) **102**, No. 1, 194–210.

[10] Blunt, M.J., Lui, K., Thiele, M.R.: "A Generalized Streamline Method to Predict Reservoir Flow," *Petroleum Geoscience* (1996) **2**, 259–269.

[11] Bommer, M.P. and Schechter, R.S.: "Mathematical Modeling of In-Situ Uranium Leaching," *Society of Petroleum Engineers Journal* (December 1979) **19**, 393–400.

[12] Bratvedt, F., Bratvedt, K., Buchholz, C.F., Holden, L., Holden, H., and Risebro, N.H.: "A New Front-Tracking Method for Reservoir Simulation," *SPE Reservoir Engineering* (February 1992) **7**, 107–116.

[13] Bratvedt, F., Bratvedt, K., Buchholz, F., Gimse, T., Holden, H., Holden, L., and Risebro, N.: "Frontline and Frontsim: Two Full Scale, Two-Phase, Black Oil Reservoir Simulators Based on Front Tracking," *Surv. Math. Ind.* (1993) No. 3, 185–215.

[14] Bratvedt, F., Gimse, T., Tegnander, C.: "Streamline Computations for Porous Media Flow Including Gravity," *Transport In Porous Media* (October 1996) **25**, No. 1, 63–78.

[15] Brenier, Y., and Jaffre, J.: "Upstream Differencing for Multiphase Flow in Reservoir Simulation," *SIAM J. Numer. Anal.* (June 1991) **28**, No. 3, 685–696.

[16] Buckley, S.E. and Leverett, M.C.: "Mechanism of Fluid Displacement in Sands," *Trans., AIME* (1941) **249**, 107–116.

[17] Christie, M.: "High Resolution Simulation of Unstable Flows in Porous Media," *SPE Reservoir Engineering* (1989) **4**, No. 3, 297–303.

[18] Christie, M. and Bond, D.: "Multidimensional Flux–Corrected Transport for Reservoir Simulation," paper SPE 13505 in proceedings of the 1985 Reservoir Simulation Symposium, Dallas, TX.

[19] Christie, M. and Bond, D.: "Detailed Simulation of Unstable Processes in Miscible Flooding," *SPE Reservoir Engineering* (November 1987) **2**, No. 4, 514–522.

[20] Christie, M.A., Jones, A.D.W., and Muggeridge, A.H.: "Comparison Between Laboratory Experiments and Detailed Simulations of Unstable Miscible Displacements Influenced by Gravity," Proc, 2nd Norwegian Int. of Technology North Sea Oil and Gas Reservoirs Conference, Trondheim (May 1989).

[21] Christie, M.A., Muggeridge, A.H., and Barley, J.J.: "A Model Study of Viscous Fingering," *SPE Reservoir Engineering* (February 1993) **8**, 19–26.

[22] Colella, P., Concus, P., Sethian, J.: "Some Numerical Methods for Discontinuous Flows in Porous Media," *The Mathematics of Reservoir Simulation* (1983) 161–186.

[23] Corey, A.T.: "The Interrelation Between Gas and Oil Relative Permeabilities," *Producer's Monthly* (1954) **19**, No. 1, 38–41.

[24] Datta–Gupta, A. and King, M.J.: "A Semianalytic Approach to Tracer Flow Modeling in Heterogeneous Permeable Media," *Advances in Water Resources* (1995) **18**, 9–24.

[25] Datta-Gupta A., Lake, L.W., Pope, G.A., and King, M.J.: "A Type-Curve Approach to Analyzing Two-Well Tracer Tests," *SPE Formation Evaluation* (March 1995) **10**, 40–48.

[26] Deutsch, C.V. and Journel, A.G.: *GSLIB Geostatistical Software Library and User's Guide*, Oxford University Press, New York, NY (1992).

[27] Emanuel, A.S., Alameda, G.K., Behrens, R.A., and Hewett, T.A.: "Reservoir Performance Prediction Methods Based on Fractal Geostatistics," *SPE Reservoir Engineering* (August 1989) **4**, 311–318.

[28] Emanuel, A.S. and Milliken, W.J.: "The Application of Streamtube Techniques to Full Field Waterflood Simulation," paper SPE 30758 in proceedings of the 1995 Annual Meeting, Dallas, TX, October.

[29] Fay, C.H. and Prats. M.: "The Application of Numerical Methods to Cycling and Flooding Problems," Proceedings of the 3rd World Petroleum Congress (1951).

[30] Fayers, F.J., and Sheldon, J.W.: "The Effect of Capillary Pressure and Gravity on Two-Phase Fluid Flow in a Porous Medium," *Trans., AIME* (1959) **216**, 147–155.

[31] Gelhar, L.W. and Axness, C.L.: "Three-Dimensional Stochastic Analysis of Macrodispersion in Aquifers," *Water Resources Research* (1983) **19**, No. 1, 161–180.

[32] Glimm, J., Isaacson, E., Marchesin, D., McBryan, O.: "Front Tracking for Hyperbolic Systems," *Advances in Applied Mathematics* (1981) **2**, 91–119.

[33] Glimm, J., Lindquist, B., McBryan O., Padmanabhan, L.: "A Front Tracking Reservoir Simulator, Five-Spot Validation Studies and the Water Coning Problem," *The Mathematics of Reservoir Simulation* (1983) 107–136.

[34] Goode, D.J.: "Particle Velocity Interpolation in Block-Centered Finite Difference Groundwater Flow Models," *Water Resources Research* (May 1990) **26**, No. 5, 925–940.

[35] Hewett, T. and Behrens, R.: "Scaling Laws in Reservoir Simulation and Their Use in a Hybrid Finite Difference/Streamtube Approach to Simulation the Effects of Permeability Heterogeneity," *Reservoir Characterization, II*, L. Lake and J. Carroll, H.B. (eds.), Academic Press, Inc., London (1991) 402–441.

[36] Hewett, T. and Yamada, T.: "Theory of the Semi-Analytical Calculation of Oil Recovery and Effective Relative Permeabilities Using Streamtubes," Stanford Center for Reservoir Forecasting (SCRF) Annual Report, Stanford U. (1995).

[37] Hewett, T.A. and Behrens, R.A.: "Conditional Simulation of Reservoir Heterogeneity With Fractals," *SPE Formation Evaluation* (September 1990) **8**, 217–225.

[38] Hewett, T.A. and Behrens, R.A.: "Considerations Affecting the Scaling of Displacements in Heterogeneous Permeability Distributions," *SPE Formation Evaluation* (December 1993) **5**, 258–266.

[39] Higgins R.V. and Leighton, A.J.: "A Computer Method to Calculate Two–Phase Flow in Any Irregularly Bounded Porous Medium," *Journal of Petroleum Technology* (June 1962) **14**, 679–683.

[40] Higgins R.V. and Leighton, A.J.: "Computer Prediction of Water Drive of Oil and Gas Mixtures Through Irregularly Bounded Pororus Media — Three-Phase Flow," *Journal of Petroleum Technology* (September 1962) **14**, 1048–1054.

[41] Intera Information Technologies Limited: *Eclipse 100 Reference Manual*, Intera, Henly–on–Thames, Oxfordshire RG9 4PS, England (1993).

[42] Khataniar S. and Peters E.J.: "The Effect of Reservoir Heterogeneity on the Performance of Unstable Displacements," *J. of Petr. Science and Eng.* (May 1992) **7**, 263–281.

[43] Kincaid, D.R., Respess, J.R., Young, D.M., and Grimes, R.G.: "ITPACK 2C: A Fortran Package for Solving Large Sparse Linear Systems by Adaptive Accelerated Iterative Methods," (1995).

[44] King, M.J., Blunt, M.J., Mansfield, M., and Christie, M.A.: "Rapid Evaluation of the Impact of Heterogeneity on Miscible Gas Injection," paper SPE 26079 in proceedings of the 1993 Western Regional Meeting, Anchorage, AK, May 26–28.

[45] Kinzelbach, W.: "The Random Walk Method in Pollutant Transport," *Groundwater Flow and Quality Modelling*, E. Custodio, A. Gurgui , and J.P. Lobo Ferreira (ed.), D. Reidel Publishing Company (1988) 227–246.

[46] Kocberber, S., and Miller, M.: "Front-Tracking of Three-Dimensional Piston-Like Displacements in Porous Media," paper SPE 15598 in proceedings of the 1986 , New Orleans, LA, October.

[47] Koval, E.J.: "A Method for Predicting the Performance of Unstable Miscible Displacements in Heterogeneous Media," *Society of Petroleum Engineers Journal* (June 1963) **3**, 145–154.

[48] Lake, L.W., Johnston, J.R., and Stegemeier, G.L.: "Simulation and Performance Prediction of a Large-Scale Surfactant/Polymer Project," *Society of Petroleum Engineers Journal* (December 1981) **21**, 731–739.

[49] Lake, W.L.: *Enhanced Oil Recovery*, first edition, Prentice Hall, Englewood Cliffs, NJ (1989).

[50] Lantz, R.B.: "Quantitative Evaluation of Numerical Diffusion (Truncation Error)," *SPEJ* (September 1971) 315–319.

[51] Martin, J.C. and Wegner, R.E.: "Numerical Solution of Multiphase, Two-Dimensional Incompressible Flow Using Streamtube Relationships," *Society of Petroleum Engineers Journal* (October 1979) **19**, 313–323.

[52] Martin, J.C., Woo, P.T., and Wegner, R.E.: "Failure of Stream Tube Methods To Predict Waterflood Performance of an Isolated Inverted Five-Spot at Favorable Mobility Ratios," *Journal of Petroleum Technology* (February 1973) **25**, 151–153.

[53] Matanga, G.: "Stream Functions in Three-Dimensional Groundwater Flow," *Water Resources Research* (September 1993) **29**, No. 9, 3125–3133.

[54] Mathews, J.L., Emanuel, A.S., and Edwards, K.A.: "Fractal Methods Improve Mitsue Miscible Predictions," *Journal of Petroleum Technology* (November 1989) **41**, 1136–1989.

[55] Mathews,J.L., Emanuel,A.S., Edwards,K.A.: "A Modeling Study of the Mitsue Stage 1 Miscible Flood Using Fractal Geostatistics," paper SPE 18327 in proceedings of the 1988 63rd Annual Technical Conference and Exhibition of SPE, Houston, TX, October.

[56] Morel-Seytoux, H.: "Analytical-Numerical Method in Waterflooding Predictions," *Society of Petroleum Engineers Journal* (September 1965) 247–258.

[57] Muskat, M.: *Flow of Homogeneous Fluids*, International Human Resources Development Corporation, 137 Newbury Street, Boston MA 02116 (1937, 1982).

[58] Nelson, R.W.: "Stream Functions for Three-Dimensional Flow in Heterogeneous Porous Media," *Int. Assc. Sci. Hydrology* (1963) **64**, 290–300.

[59] Peaceman, D.W.: "Interpretation of Well-Block Pressures in Numerical Reservoir Simulation With Nonsquare Grid Blocks and Anisotropic Permeability," *SPEJ* (June 1983) 531–543.

[60] Peddibhotla, S., Cubillos, H., Datta-Gupta, A., and Wu, C.H.: "Rapid Simulation of Multiphase Flow Through Fine-Scale Geostatistical Realizations Using a New 3D Streamline Model: A Field Example," paper SPE 36008 in proceedings of the 1996 Petroleum Computer Conference, Dallas, TX, June, 2-5.

[61] Pollock, D.W.: "Semianalytical Computation of Path Lines for Finite-Difference Models," *Ground Water* (November-December 1988) **26**, No. 6, 743–750.

[62] Renard, G.: "A 2D Reservoir Streamtube EOR Model with Periodical Automatic Regeneration of Streamlines," *In Situ* (1990) **14**, No. 2, 175–200.

[63] Sammon, P.H.: "An Analysis of Upstream Differencing," *SPE Reservoir Engineering* (August 1988) **3**, 1053–1056.

[64] Shafer, J.M.: "Reverse Pathline Calculation of Time-Related Capture Zones in Nonuniform Flow," *Ground Water* (May-June 1987) **25**, No. 3, 283–289.

[65] Stalkup, F.I.: "Miscible Displacement," Monograph 8, Soc. Pet. Eng. of AIME, New York (1983).

[66] Stueben, K.: "Algebraic Multigrid (AMG): Experiences and Comparisons," Appl. Math. Comp, 13, Proceedings of the International Multigrid Conference (1983) 419–452.

[67] Tchelepi, H. and Orr Jr., F.: "Interaction of Viscous Fingering, Permeability Heterogeneity, and Gravity Segregation in Three Dimensions," *SPE Reservoir Engineering* (November 1994) **9**, 266–271.

[68] Thiele, M.R.: *Modeling Multiphase Flow in Heterogeneous Media Using Streamtubes*, PhD dissertation, Stanford University, Dept. of Petroleum Engineering, Stanford, CA (October 1994).

[69] Thiele, M.R., Batycky, R.P., Blunt, M.J., and Orr, F.M., Jr.: "Simulating Flow in Heterogeneous Media Using Streamtubes and Streamlines," *SPE Reservoir Engineering* (February 1996) **10**, No. 1, 5–12.

[70] Thiele, M.R., Blunt, M.J., and Orr, F.M., Jr.: "Modeling Flow in Heterogeneous Media Using Streamtubes — I. Miscible and Immiscible Displacements," *In Situ* (August 1995) **19**, No. 3, 299–339.

[71] Thiele, M.R., Blunt, M.J., and Orr, F.M., Jr.: "Modeling Flow in Heterogeneous Media Using Streamtubes — II. Compositional Displacements," *In Situ* (November 1995) **19**, No. 4, 367–391.

[72] Tijink, P., Gimse, T., Kaasschieter, E.,: "Streamline Computation for Front Tracking," *Computational Methods in Water Resources X* (1994) 1481–1488.

[73] Todd, M.R. and Longstaff, W.J.: "The Development, Testing and Application of a Numerical Simulator for Predicting Miscible Flood Performance," *Trans., AIME* (1972) **253**, 874–882.

[74] Tompson, A.F.B, and Gelhar, L.W.: "Numerical Simulation of Solute Transport in Three-Dimensional Randomly Heterogeneous Porous Media," *Water Resour. Res.* (Oct. 1990) **26**, No. 10, 2541–2562.

[75] Tompson, A.F.B, Schafer, A.L., and Smith, R.W.: "Impact of Physical and Chemical Heterogeneity on Cocontaminant Transport in a Sandy Porous Medium," *Water Resour. Res.* (April 1996) **32**, No. 4, 801–818.

[76] Uffink, G.: "Modeling Solute Transport With the Random Walk Method," *Groundwater Flow and Quality Modelling*, E. Custodio, A. Gurgui , and J.P. Lobo Ferreira (ed.), D. Reidel Publishing Company (1988) 247–265.

[77] Waggoner, J.R., Castillo, J.L., and Lake, L.W.: "Simulation of EOR Processes in Stochastically Generated Permeable Media," *SPE Formation Evaluation* (June 1992) **7**, 173–180.

[78] Wen, Xian-Huan: "Hydraulic Anisotropy Versus Geostatistic Anisotropy," to be published in Stanford Center for Reservoir Forecasting (SCRF) Annual Report, Stanford U. (1997).

[79] Whillhite, G.P: *Waterflooding*, Society of Petroleum Engineers (1986).

[80] Yih, C.: "Stream Functions in Three-Dimensional Flow," *La Houille Blanche* (1957) **3**, 445–450.

[81] Zijl, W.: "Numerical Simulations Based on Stream Functions and Velocities in Three-Dimensional Groundwater Flow," *J. Hydrol.* (1986) **85**, 349–365.